Climate forcings in Goddard Institute for Space Studies SI2000 simulations

Climate forcings in Goddard Institute for Space Studies SI2000 simulations

J. Hansen,[1] M. Sato,[1,2] L. Nazarenko,[1,2] R. Ruedy,[1,3] A. Lacis,[1] D. Koch,[1,4] I. Tegen,[5] T. Hall,[1,6] D. Shindell,[1] B. Santer,[7] P. Stone,[8] T. Novakov,[9] L. Thomason,[10] R. Wang,[11] Y. Wang,[12] D. Jacob,[13] S. Hollandsworth,[14] L. Bishop,[15] J. Logan,[13] A. Thompson,[14] R. Stolarski,[14] J. Lean,[16] R. Willson,[2] S. Levitus,[17] J. Antonov,[17] N. Rayner,[18] D. Parker,[18] and J. Christy[19]

Received 24 July 2001; revised 14 November 2001; accepted 27 November 2001; published 20 September 2002.

[1] We define the radiative forcings used in climate simulations with the SI2000 version of the Goddard Institute for Space Studies (GISS) global climate model. These include temporal variations of well-mixed greenhouse gases, stratospheric aerosols, solar irradiance, ozone, stratospheric water vapor, and tropospheric aerosols. Our illustrations focus on the period 1951–2050, but we make the full data sets available for those forcings for which we have earlier data. We illustrate the global response to these forcings for the SI2000 model with specified sea surface temperature and with a simple *Q*-flux ocean, thus helping to characterize the efficacy of each forcing. The model yields good agreement with observed global temperature change and heat storage in the ocean. This agreement does not yield an improved assessment of climate sensitivity or a confirmation of the net climate forcing because of possible compensations with opposite changes of these quantities. Nevertheless, the results imply that observed global temperature change during the past 50 years is primarily a response to radiative forcings. It is also inferred that the planet is now out of radiation balance by 0.5 to 1 W/m^2 and that additional global warming of about 0.5°C is already "in the pipeline." *INDEX TERMS:* 1620 Global Change: Climate dynamics (3309); 1635 Global Change: Oceans (4203); 1650 Global Change: Solar variability; *KEYWORDS:* climate forcings, climate models, greenhouse gases, aerosols, solar irradiance, ozone

Citation: Hansen, J., et al., Climate forcings in Goddard Institute for Space Studies SI2000 simulations, *J. Geophys. Res.*, *107*(D18), 4347, doi:10.1029/2001JD001143, 2002.

1. Introduction

[2] A fundamental challenge regarding climate is to determine how much of observed climate change is a response to climate forcings, as opposed to chaotic (unforced) variability. A climate forcing is an imposed perturbation of the Earth's energy balance with space. Forcings arise naturally, as with aerosols injected by volcanic eruptions, and from human activities, as with increasing greenhouse gases.

[3] Climate models provide a tool for investigating the effect of climate forcings. One obstacle to achieving the full potential of the models is the imperfect data for actual forcings. However, knowledge of forcings is improving as modern observations accumulate. Also, some estimated forcings for prior times are tending to become more

[1]NASA Goddard Institute for Space Studies, New York, New York, USA.
[2]Center for Climate Systems Research, Columbia University, New York, New York, USA.
[3]SGT Incorporated, New York, New York, USA.
[4]Department of Geology, Yale University, New Haven, Connecticut, USA.
[5]Max-Planck-Institute for Biogeochemistry, Jena, Germany.
[6]Department of Applied Physics and Applied Mathematics, Columbia University, New York, New York, USA.
[7]Lawrence Livermore National Laboratory, Livermore, California, USA.
[8]Center for Meteorology, Massachusetts Institute of Technology, Cambridge, Massachusetts, USA.
[9]Lawrence Berkeley National Laboratory, Berkeley, California, USA.
[10]NASA Langley Research Center, Hampton, Virginia, USA.
[11]School of Earth and Atmospheric Sciences, Georgia Institute of Technology, Atlanta, Georgia, USA.
[12]Department of Environmental Sciences, Rutgers University, New Brunswick, New Jersey, USA.
[13]Department of Earth and Planetary Sciences, Harvard University, Cambridge, Massachusetts, USA.
[14]NASA Goddard Space Flight Center, Greenbelt, Maryland, USA.
[15]Honeywell International, Buffalo, New York, USA.
[16]E. O. Hulbert Center for Space Research, Naval Research Laboratory, Washington, D. C., USA.
[17]National Oceanographic Data Center, NOAA, Silver Spring, Maryland, USA.
[18]Meteorological Office Hadley Centre, Bracknell, Berkshire, U.K.
[19]Earth System Science Center, University of Alabama, Huntsville, Alabama, USA.

0148-0227/02/2001JD001143

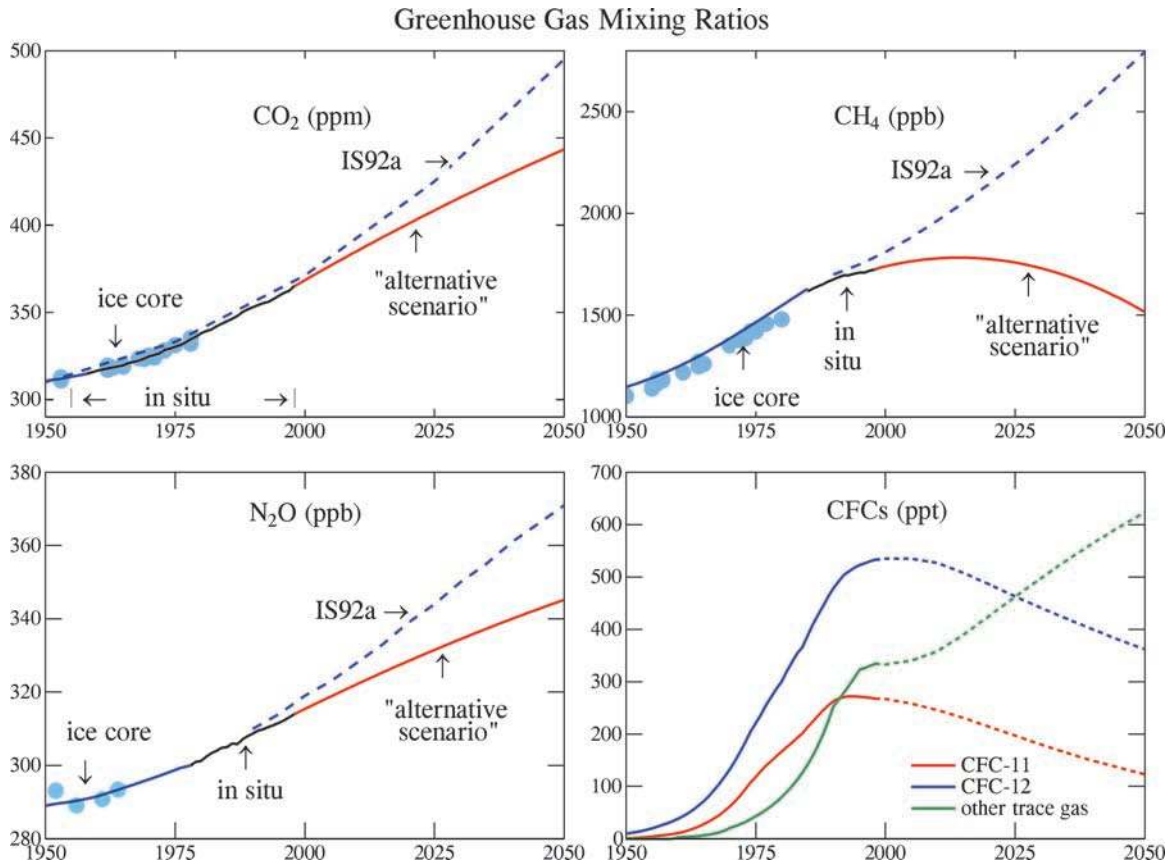

Figure 1. Measured greenhouse gas amounts and an extension to 2050 based on the "alternative scenario" of *Hansen et al.* [2000b]. The sum of the CFC and "other trace gas" forcings is constant after 2000. For comparison, we illustrate IS92a scenarios for CO_2, CH_4, and N_2O [*Intergovernmental Panel on Climate Change, IPCC*, 1992]. After 2000, "other trace gases" are assumed to increase so as to exactly compensate for predicted declines of CFC-11 and CFC-12.

quantitative and reliable, e.g., based on polar ice core data and improved chemical transport models.

[4] One consequence of continued improvement of forcing data is that current scenarios are sure to be replaced by more realistic ones. Nevertheless, there is reason to document our present scenarios. This is needed for interpretation of our climate simulations, and it will also allow other researchers to use the same forcings or at least make accurate comparisons.

[5] We use the radiative flux change at the tropopause as a primary measure of climate forcings. However, in some cases, especially for absorbing aerosols and ozone changes, this flux change can be a poor predictor of even the global mean climate response [*Hansen et al.*, 1997c] (hereinafter referred to as RF-CR). Therefore we also illustrate the simulated equilibrium climate response to each forcing using a climate model with a mixed layer ocean. This helps to characterize and compare the different forcings.

[6] We define in section 2 the scenarios for well-mixed greenhouse gases, stratospheric aerosols, solar irradiance, ozone, stratospheric water vapor, and tropospheric aerosols, and we compare the climate forcings for each of these mechanisms. In section 3 we discuss the SI2000 model and summarize the experiments that are being carried out with it. In section 4 we illustrate the equilibrium response of the climate model to each of these forcings. The transient model response to these forcings for the period 1951–2050 is presented in section 5 for simple representations of the ocean. Implications of the simulations are discussed in section 6.

2. Climate Forcings

[7] We consider a sequence of six climate forcings in order of how accurately we believe they can be defined: well-mixed greenhouse gases, stratospheric aerosols, solar irradiance, ozone, stratospheric water vapor, and tropospheric aerosols. This sequence, for the first five forcings, is also approximately the order of their importance for timescales of 1–100 years. The sixth forcing, tropospheric aerosols, is probably large, but it is complex with negative and positive components, and its history is uncertain, especially the critical black carbon component. A seventh forcing, the indirect effect of tropospheric aerosols on clouds, could be substantial, but it is even more uncertain. The indirect aerosol effect is being tested in the SI2000 model by S. Menon and A. Del Genio, as will be reported elsewhere. The forcing due to anthropogenic land surface alterations [*Sagan et al.*, 1979; *Henderson-Sellers and Gornitz*, 1984; *Hansen et al.*, 1998; *Govindasamy et al.*,

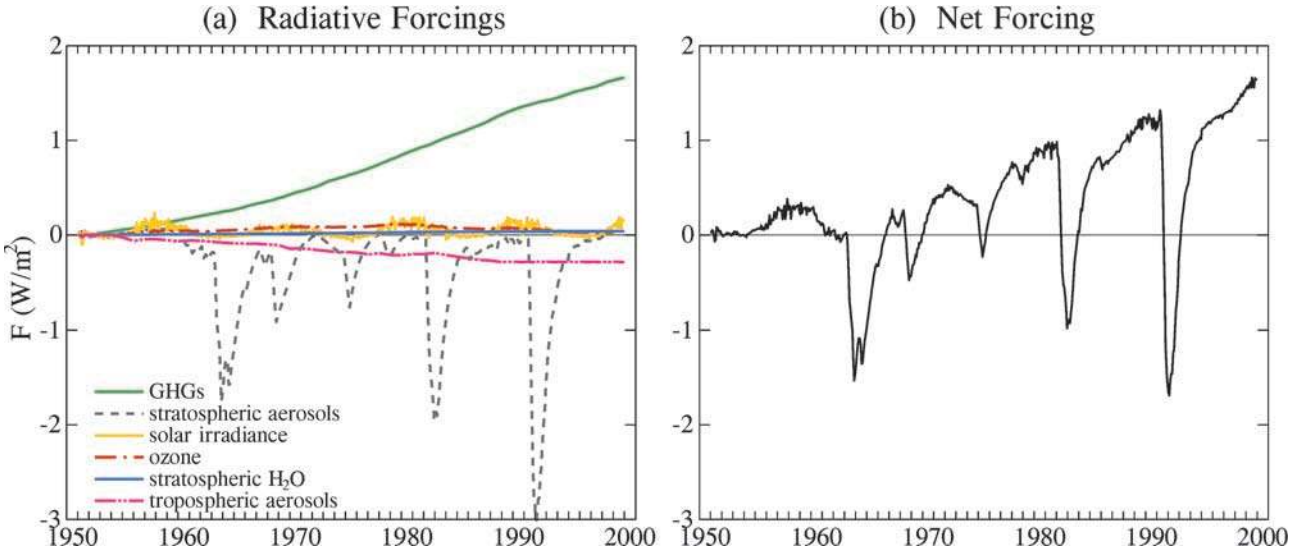

Figure 2. Adjusted climate forcings due to six mechanisms. (a) Global mean forcings and (b) their sum as a function of time.

2001] is not included in our present simulations, as its time dependence is not well defined and tests [*Henderson-Sellers and Gornitz*, 1984; *Hansen et al.*, 1998; *Govindasamy et al.*, 2001] suggest that its global variations in the past 50 years are $\lesssim 0.1$ W/m^2.

[8] We calculate both the instantaneous and adjusted forcings for most of the climate change mechanisms that we consider. The instantaneous forcing, F_i, is the flux change at the tropopause that occurs when the radiative constituent is changed, but the temperature is kept fixed throughout the atmosphere. The adjusted forcing, F_a, is the flux change after the stratospheric temperature has been allowed to adjust to a new radiative equilibrium profile. It has been shown that the adjusted forcing in general provides a better measure to judge the expected climate response [RF-CR], so we usually illustrate the adjusted forcing. We show only the global mean forcing here; global maps are shown in section 4, where they can be compared with global maps of the climate response. We consider only the period since 1950. The historical evolution of forcings since 1750 is discussed by *Myhre et al.* [2001].

[9] We calculate the instantaneous and adjusted forcings using a full annual cycle of the model control run for which the three-dimensional climate fields were saved at every time step. We define the tropopause the same as RF-CR have, varying from 100 hPa in the tropics to 300 hPa at the poles. We calculate the fluxes at the model levels just above and just below this tropopause level, averaging these results to obtain the flux at the tropopause.

2.1. Well-Mixed Greenhouse Gases

[10] The primary gases that we include (Figure 1) are CO_2, CH_4, N_2O, and the chlorofluorocarbons (CFCs). Data for recent decades are based on in situ observations available from the NOAA *Climate Monitoring and Diagnostics Laboratory* (*CMDL*) [1998]. The earlier data for CO_2 and CH_4 are based on ice core measurements [*Etheridge et al.*, 1996, 1998], as are the earlier N_2O data [*Machida et al.*, 1995]. The deviation of the estimated global mean CH_4 from the amount measured at the South Pole (Figure 1) is due to the pole-to-pole gradient of CH_4. CFC amounts prior to in situ measurements are estimated from industry production data, assuming atmospheric lifetimes of 50 and 100 years for CFC-11 and CFC-12, respectively [*Hansen et al.*, 1998]. We include an estimate for the other well-mixed trace gases, primarily halons [*Intergovernmental Panel on Climate Change* (*IPCC*), 1996, 2001; *Myhre et al.*, 1998; *Hansen et al.*, 1998; *Highwood and Shine*, 2000], which we specify as an additional amount of CFC-12. Annual amounts of the well-mixed greenhouse gases at 5-year intervals are given in Table 1. All annual data are available at www.giss.nasa.gov/data/si2000/ghgases.

[11] We calculate the climate forcing using the SI2000 version of the Goddard Institute for Space Studies three-dimensional climate model [*Hansen et al.*, 2000a], which uses the *Lacis and Oinas* [1991] correlated k distribution radiative transfer method. The updated absorption coefficients are based on fits to line-by-line radiative transfer calculations with current HITRAN [*Rothman et al.*, 1998] absorption line data. We estimate the possible error in the forcing for the sum of the well-mixed greenhouse gases as about 10%, because of uncertainties in gas amounts and absorption coefficients.

[12] The forcing by the well-mixed greenhouse gases (GHGs) has increased steadily over the past 50 years (Figure 2a). The increase of the GHG forcing in the period 1951–2000, more than 1.6 W/m^2, is about 70% of the increase during the Industrial Era, i.e., since 1850 [*Hansen et al.*, 1998]. Although it is barely perceptible in a cumulative graph such as Figure 2, the growth rate of the GHG forcing slowed significantly in the 1990s. This slowdown was mainly in the CFCs and CH_4, as illustrated for the individual gases by *Hansen et al.* [2000b] and *Hansen and Sato* [2001].

[13] We include for comparison two scenarios for future greenhouse gases in Figure 1: scenario IS92a of *IPCC* [1992, 1996] and the "alternative" scenario of *Hansen et al.* [2000b]. In the "alternative" scenario the CO_2 growth

Table 1. GHGs With "Alternative" Scenario for 2000–2050[a]

Year	CO_2, ppm	CH_4, ppb	N_2O, ppb	CFC-11, ppt	CFC-12, ppt	Others, ppt
1850	285.2	791	275.4	0	0	0
1900	295.6	879	279.8	0	0	0
1950	310.7	1147	289.0	0.7	9.3	0
1955	313.1	1192	290.1	4.1	19.7	0
1960	316.5	1247	291.6	10.7	38.1	2.9
1965	319.6	1312	293.8	27.8	72.0	6.4
1970	324.7	1386	296.2	61.7	133.0	20.5
1975	330.2	1465	298.8	118.0	220.9	43.1
1980	337.9	1547	301.2	166.6	300.3	79.9
1985	344.9	1618	305.0	213.3	387.4	141.5
1990	353.0	1676	308.7	262.7	478.7	253.4
1995	359.5	1709	311.6	271.4	522.8	322.8
2000	368.4	1740	315.4	267	535	333
2005	376.8	1765	318.8	258	535	340
2010	385.0	1779	322.1	246	527	358
2015	393.0	1783	325.4	231	508	389
2020	400.8	1776	328.5	214	486	425
2025	408.4	1759	331.5	197	463	462
2030	415.8	1731	334.5	180	441	498
2035	423.0	1693	337.3	164	420	532
2040	430.0	1644	340.0	149	400	564
2045	436.8	1585	342.7	136	380	595
2050	443.4	1515	345.2	123	362	624

[a] "Other" trace gases are radiatively equivalent CFC-12 amounts.

rate initially rises slightly but begins to decline after 2020. The CH_4 growth rate continues to decline slowly such that the CH_4 amount peaks in about 2015 at about 1785 ppm and declines to 1515 ppm in 2050 (13% less CH_4 than at present). The CH_4 forcing in 2050 is thus -0.1 W/m^2 relative to 2000. N_2O continues to increase through the period at a slowly declining rate, such that the additional forcing in 2050 is +0.1 W/m^2. The "other" well-mixed trace gases are assumed to increase so as to provide a forcing that balances expected decreases of CFC-11 and CFC-12. For computational purposes this is handled by keeping the CFCs and "other" well-mixed gases constant after 2000.

2.2. Stratospheric Aerosols

2.2.1. Aerosol properties

[14] Climate forcing by stratospheric aerosols depends mainly on the aerosol optical depth across the solar spectrum and in the thermal infrared [*Lacis et al.*, 1992; RF-CR]. The optical depth is thus required over almost 2 orders of magnitude of wavelength, which implies that the aerosol size distribution must be known well. This means that the effective radius of the size distribution, i.e., the area weighted mean radius [*Hansen and Travis*, 1974], must be known accurately. In addition, the effective variance of the size distribution is needed with reasonable accuracy for the sake of calculating infrared heating of the stratosphere.

[15] Accurate aerosol information can be derived for the period with multispectral measurements of atmospheric extinction obtained by the SAGE (Stratospheric Aerosol and Gas Experiment) instrument [*McCormick et al.*, 1995]. The four wavelengths of SAGE, from 0.385 μm to 1.02 μm, cover a range sufficient to define the effective radius of the size distribution. When combined with satellite data for aerosol extinction in the thermal infrared region, the effective variance of the size distribution is also constrained.

[16] One of us (AL) has used the SAGE data at all wavelengths to calculate the effective particle radius that fits the multispectral SAGE data most accurately, with the variance of the size distribution constrained by infrared occultation data [*Lambert et al.*, 1993], as summarized by *Hansen et al.* [1996]. The retrieval method is defined by *Lacis et al.* [2000]. The satellite data required for this analysis are available for the Pinatubo era, i.e., the 1990s, but not immediately after the El Chichon eruption of 1982. Thus for El Chichon we employed information extracted from aircraft, balloon, and ground-based observations by P. Russell and colleagues at Ames Research Center [*Russell et al.*, 1996; *Hansen et al.*, 1997d (hereinafter referred to as F-C)]. For still earlier times we used aerosol optical depths inferred from ground-based observations [*Sato et al.*, 1993]. Aerosols in the Mount Agung period, which had an optical depth similar to that of the El Chichon aerosols, were assumed to have the same size distribution as those after El Chichon, but the latitudinal distribution of sizes was reflected about the equator. Lesser volcanoes were assigned the size distribution of the background stratospheric aerosols.

[17] The optical depth at wavelength 550 μm and the effective radius of stratospheric aerosols for our resulting scenario are shown in Figures 3a–3d for the period 1951–2000. The vertical distribution of the aerosol optical depth is based on the SAGE data for Pinatubo, which showed an early injection or lifting of aerosols toward higher levels followed by subsidence. Aerosols from earlier major volcanoes were assumed to follow a similar altitude scenario (Figure 3e). Tabular data for our stratospheric aerosol parameters are available from www.giss.nasa.gov/data/strataer, including updates and minor improvements to the data file of *Sato et al.* [1993].

2.2.2. Radiative forcing

[18] Even with the aerosol properties known, there is uncertainty in their climate forcing. Using our SI2000 climate model to calculate the adjusted forcing for a

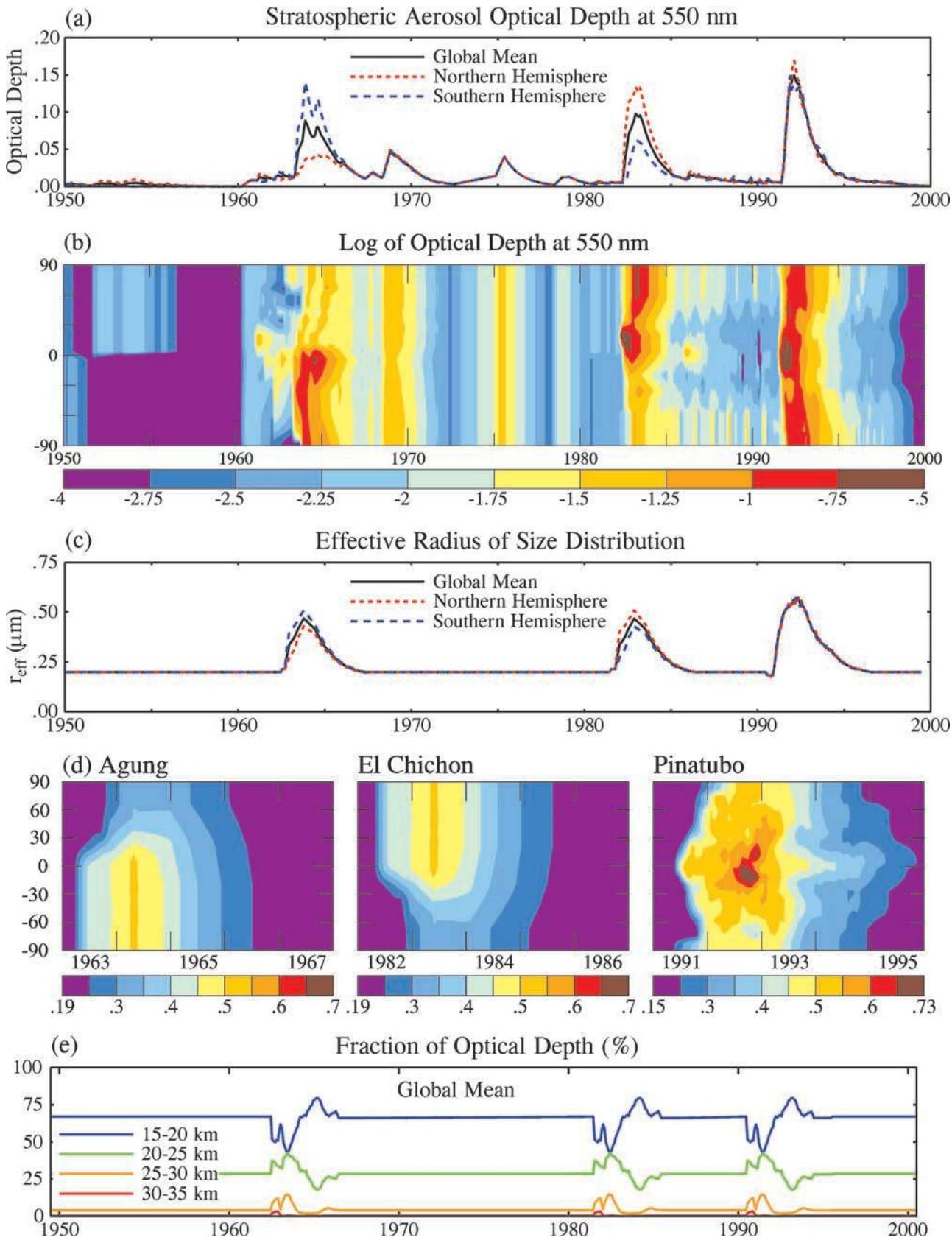

Figure 3. (a) Global and hemispheric mean stratospheric aerosol optical depth at wavelength 550 nm. (b) Variation of this optical depth with latitude. (c and d) Effective radius of the aerosol size distribution. (e) Altitude distribution of stratospheric aerosols employed in simulations with SI2000 model.

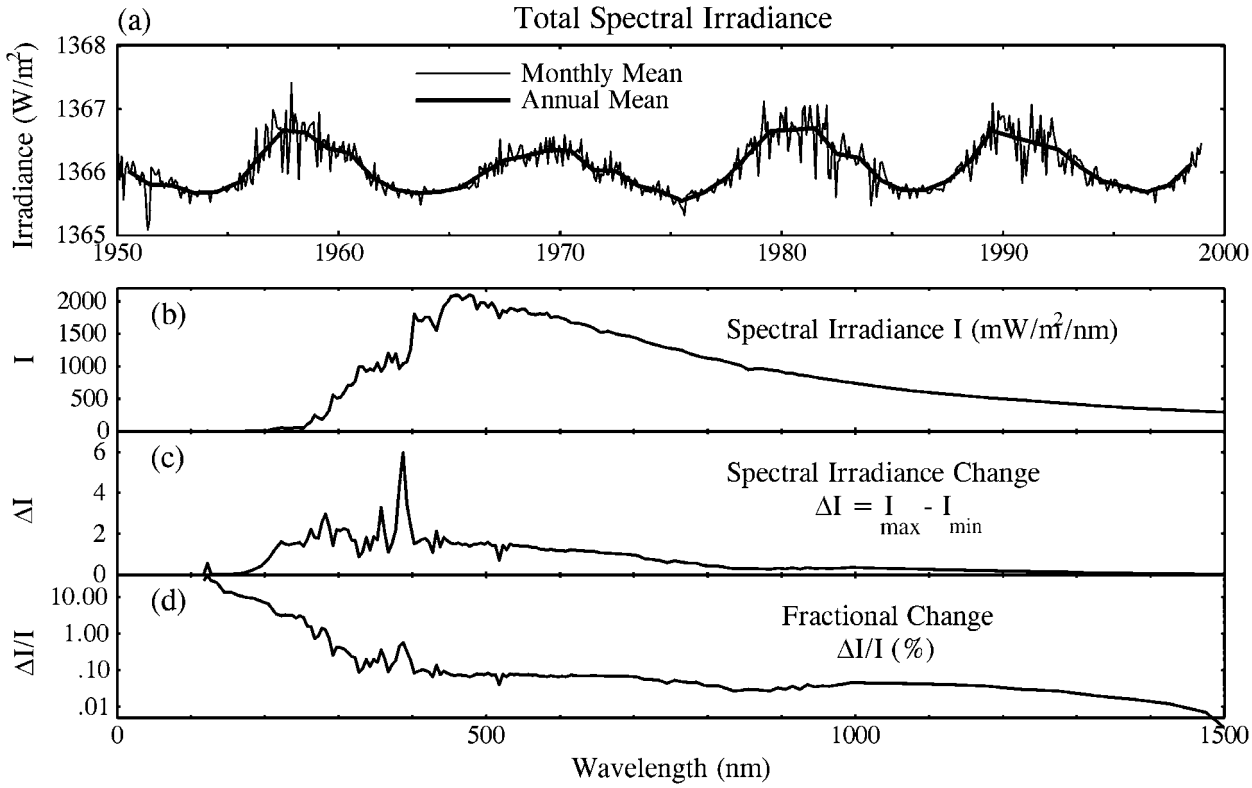

Figure 4. Solar irradiance characteristics based on data from analysis of J. Lean (1999): (a) total irradiance for the period 1950–1998, (b) spectral variation of irradiance, (c) spectral irradiance change between solar minimum (1996) and solar maximum (1989), and (d) the fractional irradiance change between solar maximum and solar minimum.

globally uniform stratospheric aerosol layer with optical depth $\tau = 0.1$ at wavelength $\lambda = 0.55$ μm yields a forcing of 2.1 W/m^2, and thus we infer that for small optical depths

$$F_a\left(\mathrm{W/m^2}\right) \sim -21\,\tau\,.$$

This is substantially smaller than values we estimated earlier ($-30\,\tau$ by *Lacis et al.* [1992] and $-26.8\,\tau$ by F-C [1997]). The smaller forcing in our current model may be due in part to increased vertical resolution in the stratosphere, greater warming of the stratosphere by the volcanic aerosols, and thus greater downward thermal radiation. In our earlier 9-layer model stratospheric warming after El Chichon and Pinatubo was about half of observed values (Figure 5 of F-C), while the stratospheric warming in our current model exceeds observations, as shown below. Our calculated forcing is smaller than the $-25.4\,\tau$ of *Andronova et al.* [1999], but it is larger than the $\sim -15\,\tau$ of *Ramachandran et al.* [2000]. This forcing is sensitive to the assumed aerosol size distribution.

[19] The adjusted forcing resulting from the stratospheric aerosol properties defined above is shown in Figure 2a. The peak global mean forcing was about -3 W/m^2 after Pinatubo and about -2 W/m^2 after both Agung and El Chichon. The geographical distribution of aerosols (and the aerosol forcing, which we illustrate in section 4) in the 12 months after Pinatubo peaks at low latitudes and is reasonably symmetric about the equator. The aerosols after Agung and El Chichon were greater in one hemisphere than in the other by a factor of 2–3, as shown in Figure 3a. On the basis of studies and comparisons in our several previous papers on stratospheric aerosols we subjectively estimate the uncertainty in the stratospheric aerosol forcing as 15% for the Pinatubo era, 20% for El Chichon, 30% for Mount Agung, and 50% for the large volcanoes in the period 1880–1915.

[20] Climate forcing by stratospheric aerosols is substantial after large volcanoes, even temporarily exceeding in magnitude the forcing by greenhouse gases, as shown in Figure 2. It is apparent that a clustering of volcanoes could be a significant contributor to long-term climate change. It has been suggested, for example, that volcanic aerosols were the principal cause of the "Little Ice Age" [*Lamb*, 1970; *Pollack et al.*, 1976]. *Free and Robock* [1999] carry out simulations of that period with both solar and aerosol forcings, and they argue that volcanoes were at least as important as solar irradiance in climate change of recent centuries.

[21] We note that the stratospheric aerosol optical depth inferred by *Andronova et al.* [1999] for the period after the Pinatubo eruption is about 50% larger than our value [*Andronova et al.*, 1999, Figure 14]. Their larger aerosol optical depth is the primary reason that they obtain a Pinatubo forcing of about -5 W/m^2, compared with our maximum forcing of about -3 W/m^2. (A secondary reason is that their calculated maximum instantaneous forcing of

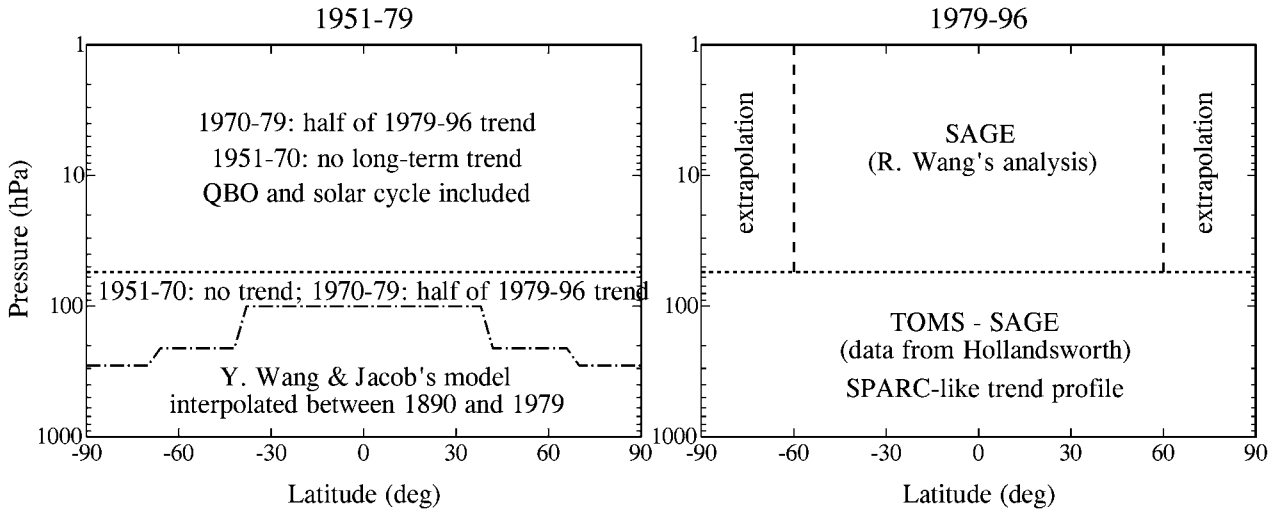

Figure 5. Data sources and assumptions used to construct the ozone change scenario $O_3{}^A$ for different regions in the atmosphere and different time intervals. $O_3{}^B$ is the same except that the 1979–1996 trends in the stratosphere are based on the analysis of *Randel and Wu* [1999].

-4.7 W/m^2 increases to -5.4 W/m^2 after thermal adjustment of the stratosphere. Our calculated forcing decreases with thermal adjustment (section 4.1), as the aerosols heat the stratosphere thus increasing downward longwave radiation.) The main reason for their larger optical depth may be their assumption of a fixed aerosol size distribution (log-normal with mean radius 0.2 μm). As discussed above, we obtain the aerosol size by finding the effective particle radius that fits the multispectral SAGE data most accurately. The estimated uncertainty of the optical depth in our multiple wavelength retrievals [*Lacis et al.*, 2000] using SAGE observations is typically several percent. There were situations after Pinatubo in which the SAGE observations were saturated and required aide from ground-based lidar observations [*McCormick et al.*, 1995] and other data sources [*Russell et al.*, 1996]. However, this saturation occurred only a small fraction of the time and affected mainly low altitudes. The large differences with *Andronova et al.* [1999] persist at times and places where there was no saturation. As part of our previous modeling study [F-C] we found that our Pinatubo aerosol properties, derived from SAGE, are in good agreement with analyses of multiple data sources by *Russell et al.* [1996]. We believe that our stratospheric aerosol climate forcing is accurate within about 15% during the Pinatubo era.

[22] We show in sections 4 and 5 that satellite measurements of the planetary radiation balance and ocean measurements of heat storage are consistent with a Pinatubo forcing of -3 W/m^2 but not with a forcing of -5 W/m^2. However, neither of these measures of aerosol forcing can provide an accuracy approaching that obtainable from the precise multispectral occultation measurements of SAGE. The SAGE extinction measurements are simple and precise, including calibration observations of the unocculted Sun. These data can be converted accurately to multispectral aerosol optical depths, and thus they should yield the most accurate available information on climate forcing by stratospheric aerosols.

[23] We assume in our "alternative scenario" that stratospheric aerosol amount in the period 2001–2050 will be comparable to that of the previous 50 years. Specifically, we duplicate the aerosol properties for 1951–2000. Thus a Mount Agung eruption occurs in 2013, an El Chichon eruption occurs in 2032, and a Pinatubo eruption occurs in 2041.

2.3. Solar Irradiance

[24] The total solar irradiance has been measured to a useful accuracy since 1979 [*Willson and Hudson*, 1991]. For earlier times we must rely on solar irradiance reconstructed from proxy measures of solar variability. Analysis of historical change of the total solar irradiance and its spectrum are described by *Lean et al.* [1995, 1997]. We use the solar spectral radiance reconstruction provided by J. Lean in 1999 (private communication). The data that we employ in our present total and spectral irradiance scenarios are available from our web site www.giss.nasa.gov/data/si2000/solar.irradiance) or from J. Lean.

[25] Lean's scenario for total solar irradiance is shown in Figure 4a. We also illustrate the mean spectral irradiance (Figure 4b), the spectral irradiance change, i.e., the difference between solar maximum and solar minimum (Figure 4c), and the corresponding fractional change at each wavelength (Figure 4d). The solar variability is largest in the ultraviolet, in the wavelength range where the solar energy is absorbed in the stratosphere. However, because the irradiance is small in the ultraviolet, only about 15% of the solar variability occurs at wavelengths that are absorbed in the stratosphere [RF-CR]. The other 85% of the solar variability is deposited below the tropopause, mainly at the Earth's surface.

[26] There are other, indirect, climate forcings caused by solar variability, in addition to the direct forcing from absorbed solar radiation. One indirect solar forcing that has been investigated is the change of ozone induced by solar irradiance variability [*Haigh*, 1994, 1999; RF-CR; *Shindell et al.*, 1999, 2001]. However, there is uncertainty about

the magnitude of this indirect forcing, and we caution that the ozone forcing provides a very poor measure of the surface temperature response, even regarding its sign (see section 4.2). The ozone change associated with the solar cycle almost certainly provides a positive amplification of the direct solar forcing, but it is complex and may depend significantly on the background state of the stratosphere [*Shindell et al.*, 2001]. *Haigh* [1994] points out that increased ultraviolet radiation should increase ozone throughout the stratosphere for today's atmospheric composition. The instantaneous forcing due to ozone increase at any altitude in the stratosphere is negative, but the adjusted forcing is positive for ozone increases at altitudes below about 30 km (Table 3 of RF-CR). *Shindell et al.* [2001] conclude that in the drier preindustrial stratosphere the temperature dependence of ozone chemistry would cause the indirect ozone forcing to be positive for both upper and lower stratosphere, and the effect on surface climate would be magnified by its influence on the phase of the Arctic Oscillation.

[27] Ozone change in the lower stratosphere (below 30 km) is much more effective in causing radiative forcing than changes at higher altitudes [RF-CR]. If the changes in the lower stratosphere are systematic, they are likely to be the dominant indirect forcing. In our previous [RF-CR] and present calculations the solar cycle ozone forcing are 0.05 and 0.02 W/m^2, respectively, both of these in phase with the direct solar forcing. The solar cycle ozone change, inferred in these two cases by S. Hollandsworth and R. Wang, respectively, are difficult to extract from a 2-decade record because of other causes of ozone change during that period and measurement errors.

[28] Study of these solar cycle ozone changes, even though the radiative forcing is small, should be pursued in more detail with a model that resolves the stratosphere well, because of possible dynamical indirect effects. *Stuber et al.* [2001] suggest that ozone perturbations may in turn amplify stratospheric water vapor changes, which raises the interesting possibility of a second-generation indirect forcing that might significantly amplify the solar forcing.

[29] Other possible amplifications of the solar forcing have long been discussed, usually involving mechanisms that alter cloud properties, for example, solar modulation of cosmic ray flux and thus atmospheric ionization [*Svensmark and Friis-Christensen*, 1997]. Marginal detection of a change in earthshine during the current solar cycle [*Goode et al.*, 2001] are not inconsistent with a larger cloud reflectivity during solar minimum, but the suggestion remains, at most, a hypothesis.

[30] The direct climate forcing due to solar irradiance variability has a peak-to-peak amplitude of about 0.2 W/m^2, over each of the recent solar cycles, as illustrated in Figure 2a. The geographical distribution of the solar irradiance forcing, which we illustrate in section 4, is of course largest at low latitudes. The trend in solar irradiance is near zero for the period 1951–2000. However, there is a long-term change of about 0.25% in the *Lean et al.* [1995] solar irradiance between 1700 and 1950, corresponding to a forcing of about 0.6 W/m^2. It has long been argued that the Sun is the likely cause of the "little ice age" [*Eddy*, 1976]. The simulations of *Shindell et al.* [2001] provide a plausible quantitative explanation of how a moderate global forcing may provide a substantial regional climate effect. It appears that volcanic aerosols and solar irradiance could be of comparable importance as climate forcings on century timescales.

[31] We include solar variability in our "alternative scenario" for 2000–2050 with 10-year periodicity, cyclically repeating the data for January 1989 to December 1998. Thus there is no long-term solar trend in our simulations. We argue elsewhere [*Hansen*, 2000] that solar irradiance could be a significant climate forcing in the next 50 years, but as yet we have no reliable way of predicting future solar changes.

2.4. Ozone

[32] We construct an ozone change scenario from several data sources, models and assumptions. For the presatellite era (until 1979) we use a model calculation to specify the tropospheric ozone change, and we include only cyclic (solar cycle and QBO) stratospheric ozone variations. After 1979 satellite data are the primary basis for both stratospheric and tropospheric ozone change. Because of uncertainties in the data, climate simulations using this scenario should be viewed as a sensitivity study. We hope that this straw man scenario may stimulate construction of a more precise ozone change data set. Indeed, as discussed below, we already include one optional change to the ozone trends in the polar stratospheric regions for the period after 1979, based on the analysis of *Randel and Wu* [1999].

[33] Figure 5 summarizes data sources employed in the first version of our O_3 data set, O_3^A. A key component is the "model" of ozone change constructed by R. Wang from SAGE measurements [*McCormick et al.*, 1992] for the altitudes (20–51 km), latitudes (60S-60N), and period (1979–1996) sampled by SAGE. The model includes seasonal, long-term trend, solar cycle, and quasi-biennial ozone changes. Solar cycle and QBO periodicities are based on proxy indicators (10.7 cm solar flux series for the solar cycle and Singapore zonal winds for the QBO) with O_3 amplitudes and phases inferred from the SAGE data. Our extrapolation back to 1951 is based on the assumption that the long-term trend of stratospheric ozone was zero in 1951–1970, and in 1970–1979 it was half as large as in 1979–1996. The assumption that there was some stratospheric ozone depletion in 1970–1979 is consistent with limited surface (Dobson) measurements [*World Meteorological Organization* (*WMO*), 1999, Tables 4–7] and ozone sonde data [*WMO*, 1998], as well as with the interpretation that ozone depletion of recent decades is caused by halocarbons. In scenario O_3^A ozone change at the altitude of SAGE data was extrapolated to the poles with reference to latitudinal variations in SBUV [*Hollandsworth et al.*, 1995] and TOMS [*WMO*, 1999] data. In scenario O_3^B this extrapolation is replaced by the analysis of *Randel and Wu* [1999] for the ozone trend during 1979–1996. O_3^B is presumed to be more realistic, but O_3^A is also defined here since it was used in some of our climate simulations reported below.

[34] At lower altitudes the ozone change for 1979–1996 is based on the difference between the column ozone change measured by TOMS, as analyzed by S. Hollandsworth, and the SAGE ozone change. The resulting ozone change is distributed with height according to a "SPARC-like" vertical profile [*WMO*, 1998]. Specifically, we assumed that the maximum ozone depletion occurred about 3 km above the tropopause, with a trend toward less negative or positive ozone

change closer to the ground. This procedure yielded ozone depletion in the upper troposphere at all latitudes, but ozone increase in the lower troposphere at latitudes 90N to 30S.

[35] For the period prior to 1979 our ozone change is based mainly on the model calculations of *Wang and Jacob* [1998]. They calculate the tropospheric ozone distributions for preindustrial and 1980 conditions, accounting for fuel combustion, industry, and biomass burning. We assume that the change between 1890 and 1980 occurs exponentially, as suggested by observations in Europe [*Marenco et al.*, 1994], at the rate (which varies from grid box to grid box) required to yield the *Wang and Jacob* [1998] change.

[36] Our present ozone scenario differs markedly from that employed by F-C. The main change is the omission of the large ozone depletion at 17–20 km in the tropics that earlier SAGE analyses had suggested, but which is omitted from *WMO* [1998] assessments. This has a large impact on the simulated change of vertical temperature profile, as discussed in sections 5 and 6. Also F-C used SBUV data above the 32 hPa level, but we now use SAGE because it is more consistent with ozone sonde data [*WMO*, 1998].

[37] We take stratospheric ozone change as being independent of longitude, because of the absence of adequate measurements. It is likely that there are correlations between decadal longitudinal temperature changes and ozone changes, so it is desirable to remove this limitation in the future. We include longitudinal dependence of tropospheric ozone change during the time prior to 1979, when the tropospheric ozone change was taken from the model of *Wang and Jacob* [1998].

[38] Figure 6 summarizes the resulting ozone history. Total ozone (Figure 6a) shows little trend prior to 1980, as stratospheric ozone depletion during 1970–1980 competes with the longer-term tropospheric ozone increase. Figures 6b–6d shows the ozone change in more detail for the periods 1970–1979 and 1979–1997, with the two alternatives for the latter period, O_3^A and O_3^B, both illustrated. Total ozone decreases in spring at high latitudes in both periods, but for 1970–1979 this result is in part an assumption justified by only limited data. Ozone in the lower troposphere increases at tropical and northern latitudes during 1979–1997 but decreases at high southern latitudes. This tropospheric ozone change for 1979–1997 is based on our combination of two satellite data sets, rather than upon any assumption about ozone sources or ozone change.

[39] The global mean ozone forcing is barely noticeable in Figure 2. The tropospheric ozone change by itself yields a positive forcing, but, on the global average, this tends to be balanced by the negative forcing due to recent stratospheric ozone depletion. This does not mean that the climate effect of ozone change is negligible. In fact, we show below that stratospheric ozone loss seems to be the largest cause of polar stratospheric cooling in recent decades, which in turn strengthens the polar vortex in zonal winds and affects the Antarctic and Arctic Oscillations [*Thompson and Wallace*, 1998; *Sexton*, 2001]. Over the Industrial Era, 1850–2000, the forcing that we estimate for tropospheric ozone change, 0.4 ± 0.15 W/m^2 [*Hansen et al.*, 1998], is third in magnitude to CO_2 and CH_4 among the greenhouse gases. Our tropospheric O_3 forcing is consistent with that estimated by several other groups [*IPCC*, 2001]; however, we note that *Mickley et al.* [2001] and D. T. Shindell (private communication, 2001) argue that the tropospheric O_3 forcing over the Industrial Era could be as large as 0.7–0.8 W/m^2. The negative forcing that we calculate due to stratospheric ozone depletion of recent decades, about -0.1 W/m^2, is less in magnitude than the forcing calculated by RF-CR, because the current reconstructions for ozone change do not include a large depletion near the tropical tropopause.

[40] We do not provide a detailed breakdown of the ozone climate forcing into contributions from the troposphere and stratosphere for different periods, because the forcing is relatively small. However, we note that our results seem to be consistent with other recent calculations. *Myhre et al.* [2000] find a global forcing of +0.05 W/m^2 for tropospheric ozone change over the period 1980–1996. *Shine and Forster* [1999] obtain -0.15 ± 0.12 W/m^2 for the forcing due to stratospheric ozone change in the same period. Our small positive forcing for ozone change over the period 1951–1997 occurs because the positive forcing from tropospheric ozone increase over the full period exceeds the negative forcing due to stratospheric ozone depletion in 1979–1997.

[41] We have zero long-term trend for future ozone in our "alternative scenario." (The zero trend begins with 1998 in all of our simulations; the rate of ozone change derived from 1979–1996 data was extended through 1997). We include QBO and solar cycle ozone variations with 26 month and 10-year periodicities for the sake of retaining such variability. In reality, a small positive climate forcing is expected because of stratospheric ozone recovery, but conceivably the global mean forcing could be countered by a decrease of tropospheric ozone pollution (or enhanced by an increase of pollution). In any case, our scenario with zero future ozone trend provides climate change results that can be compared with those for more detailed and realistic assumptions about future ozone change.

2.5. Stratospheric Water Vapor

[42] We include the climate forcing due to stratospheric H_2O produced by oxidation of increasing CH_4. The forcing is small, only about 0.1 W/m^2 for the CH_4 increase between 1850 and 2000. However, changing H_2O, along with changing O_3 and CO_2, has a significant effect on stratospheric temperature.

[43] Measurements of stratospheric H_2O change [*Rosenlof et al.*, 2001] reveal a larger trend, close to 1%/year, than CH_4 oxidation alone can account for. If this water vapor change were interpreted as a climate forcing it would yield a value greater than 0.1 W/m^2 [*de Forster and Shine*, 1999; *Oinas et al.*, 2001; *Shindell*, 2001; *Smith et al.*, 2001]. Although part of the excess stratospheric H_2O change could be a consequence of some climate forcing other than CH_4 oxidation, most of it is probably a climate feedback, i.e., a climatic response to forcings. Indeed, we find the profile of simulated H_2O change to be reasonably consistent with observations. The maximum increases are in the upper stratosphere and near the tropopause, with a minimum increase at 50–100 hPa. In our model, and we believe in the real world, the maximum in the upper stratosphere is from CH_4 oxidation and the maximum in the lower stratosphere is a positive climate feedback in response to tropo-

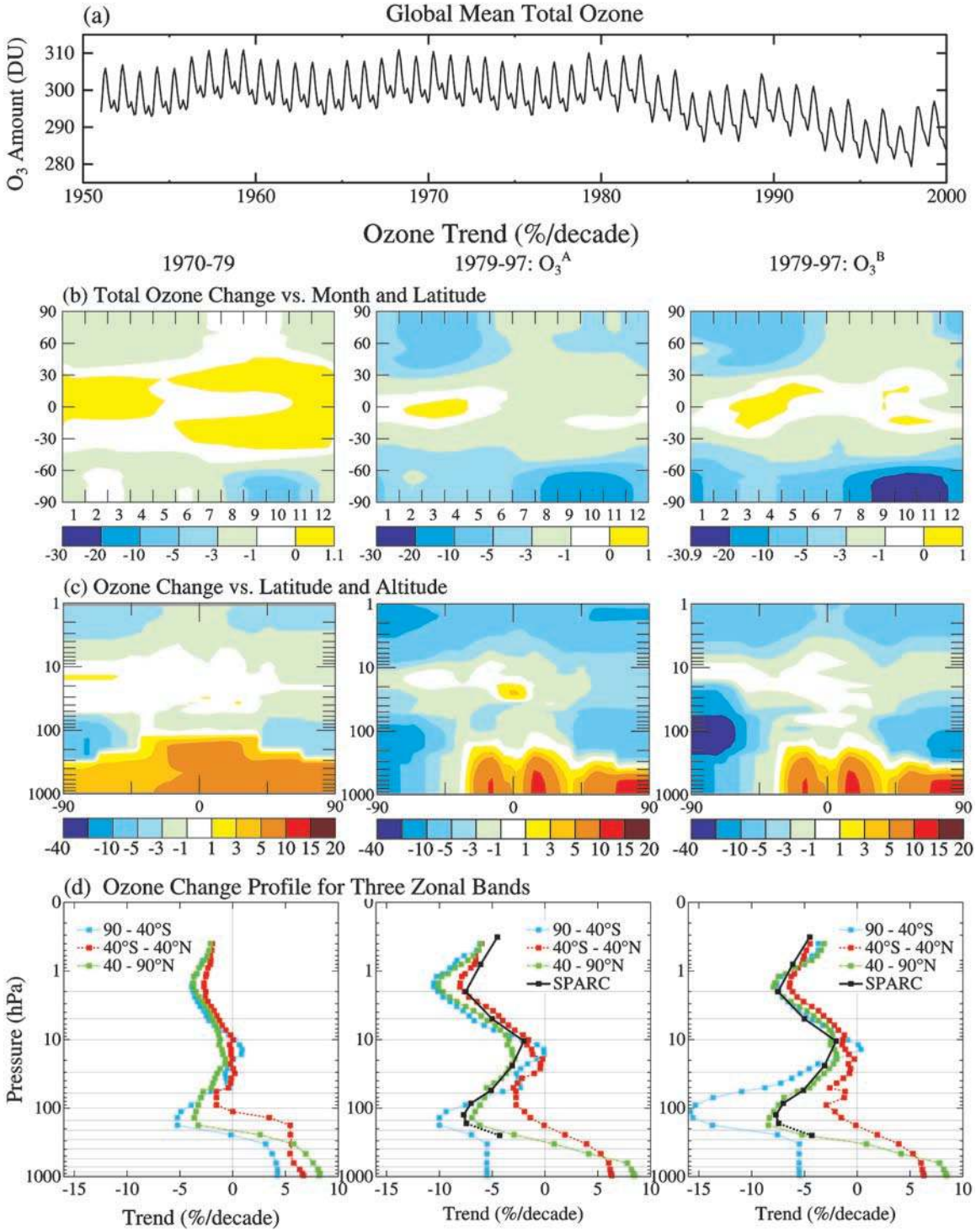

Figure 6. Ozone change in our scenario for 1951–1997: (a) total ozone versus time and (b–d) ozone trends in two time intervals as a function of month, latitude, and altitude. The third column in Figures 6b–6d shows the recommended alternative scenario O_3^B for 1979–1997 that incorporates stratospheric ozone change according to *Randel and Wu* [1999]. Dashes in Figure 6d delineate the 12 layers below 10 hPa and the three layers above 10 hPa employed in our model calculations.

spheric temperature increase. The simulated water vapor increase in the lower stratosphere occurs without any warming of the tropopause. (This increase may be caused by an increased flux from the troposphere, where the water vapor amount increases, but we defer quantitative examination until we include a more realistic representation of the stratosphere.)

[44] In our terminology the portion of the H_2O change that is a consequence of CH_4 oxidation is an indirect climate forcing; specifically, we include it is an indirect forcing

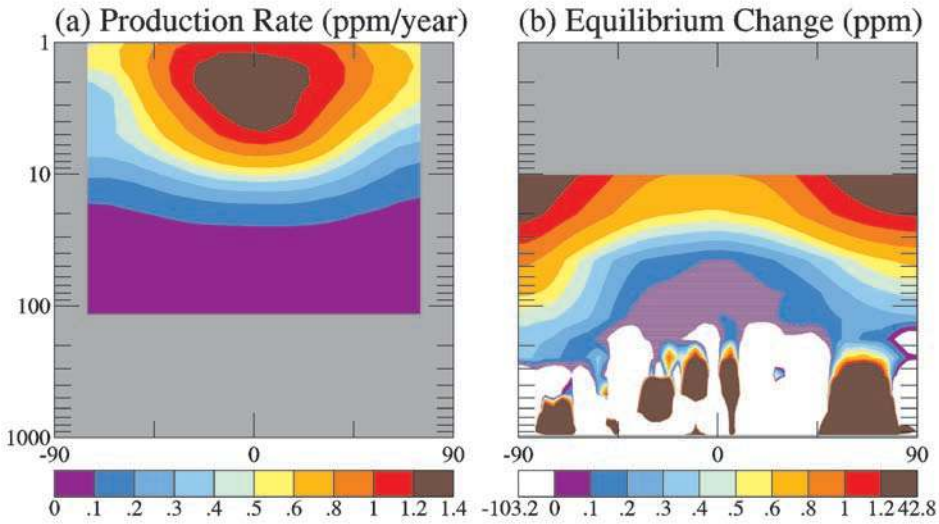

Figure 7. (a) Annual stratospheric H_2O production rate for a tropospheric CH_4 abundance of 1675 ppmv based on the two-dimensional model of I. Plumb. (b) Equilibrium increase of stratospheric H_2O in our 12-layer SI2000 model with fixed SST given the production rate in Figure 7a.

associated with anthropogenic CH_4 increase [*Hansen et al.*, 2000b]. The distinction between an indirect climate forcing and a climate feedback is that the indirect forcing occurs in response to a specific imposed change of atmospheric composition, rather than as a hydrologic response of the climate system to temperature change.

[45] We determine the CH_4-derived H_2O amount at levels below 10 hPa (i.e., in the part of the model with interactive dynamics, water vapor and radiation) by using the source strength for CH_4 oxidation as a function of latitude and height (Figure 7a) from a two-dimensional model [*Randeniya et al.*, 1997]. In our transient simulations the H_2O production is proportional to surface CH_4 at time $t - 5$ years. We include the 5-year delay because it requires several months for a surface CH_4 increase to be mixed through the tropopause, a few years for it to reach the 1–10 hPa level where most oxidation occurs, and some additional time for the H_2O to mix down into the top climate model layer (10–30 hPa). With H_2O added continuously at this rate and with the SST fixed, the 12-layer version of the SI2000 model yields the equilibrium increase of H_2O shown in Figure 7b. The mass of the equilibrium increase of stratospheric H_2O is 1.6 times the annual column-integrated production, implying an average lifetime in the lower stratosphere (below the 10 hPa level) of 1.6 years for the H_2O in our model. The H_2O in the model exits the stratosphere mainly via saturation in the winter hemisphere in the polar and midlatitude regions. Although this removal mechanism is perhaps realistic, the stratospheric lifetime of the injected H_2O is shorter than estimates based on tracers [*Hall and Waugh*, 2000]. The too rapid removal is not surprising, given the crude vertical resolution of the model and the low model top.

[46] In the three model layers above 10 hPa, which have only a radiative influence in our 12-layer model, we specify a temporal variation of H_2O proportional to surface CH_4 at time $t - 5$ years. The distribution of CH_4-derived H_2O for a specific amount of surface CH_4 was calculated by one of us (D.S.) using a 23-layer version of the GISS model [*Rind et al.*, 1988]. The H_2O above the 10 hPa level causes only a small forcing of the order of 0.01 W/m^2.

[47] Without any CH_4 source of H_2O, the lower stratosphere in the 12-layer SI2000 model is very dry, with about 1.9 ppm H_2O (average for layers 10–12, which corresponds to pressures 100-10 hPa or heights about 16–30 km) in the control run with 1951 boundary conditions. With the CH_4 source the stratospheric H_2O amount increases to about 2.4 ppm (in 1951), and in our transient simulations (section 5) the stratospheric H_2O increases to 2.7 ppm by 1998. However, this is still drier than recent observed values of about 4 ppm [*Nedoluha et al.*, 1998]. Part of this underestimate of stratospheric H_2O is likely to be caused by the too brief (1.6 years) lower stratospheric residence time of H_2O oxidized from CH_4. Another reason for the deficiency of stratospheric H_2O is likely to be the fact that the model troposphere is 1°–2°C cooler than recent observations. The cool troposphere is due in part to imprecision in the treatment of longwave absorption by H_2O in the SI2000 model, as discussed below.

[48] The lifetime of H_2O injected into the lower stratosphere by the CH_4 source increased about 20% in a test with the 23-layer version of the GISS model [*Rind et al.*, 1988] with top at 0.05 hPa. However, the 23-layer model also has a coarse vertical resolution, and we suspect that it still removes water vapor from the stratosphere too rapidly. We estimate that the climate forcing by CH_4-derived H_2O could be underestimated by 20–50% in our 12-layer model.

[49] The global mean climate forcing that we obtain for CH_4-derived H_2O is small, amounting to only 0.1 W/m^2 for the period 1850–2000 (790 ppb → 1700 ppb) and being hardly noticeable in Figure 2. Nevertheless, together with the indirect effect of CH_4 on tropospheric O_3, it is sufficient to make the climate forcing by CH_4 in the Industrial Era (0.7 W/m^2) half as large as the climate forcing by CO_2. As

illustrated in section 4, the forcing by CH_4-derived H_2O is relatively more effective than most forcings because it is concentrated at high latitudes.

2.6. Tropospheric Aerosols

[50] Tropospheric aerosols cause great uncertainty about anthropogenic climate forcing. The uncertainty is related to the variability and heterogeneity of aerosols, which makes it difficult to accurately characterize and monitor aerosols on a global basis. Improved understanding of the aerosol forcing may be brought about by a combination of global aerosol transport models, global composition-specific aerosol monitoring from satellites, ground-based and in situ observations that constrain the transport models and satellite retrievals, and compilations and analyses of historical emissions. In the mean time, we carry out a sensitivity study using an aerosol scenario derived from an aerosol transport model that employs simple assumptions about time-dependent aerosol emissions.

[51] Aerosols cause climate forcing in several ways: (1) the direct effect of aerosols on solar and infrared radiation, which has been studied extensively, (2) the semidirect-direct effect on clouds, as absorbing aerosols heat the atmosphere and thus tend to reduce large-scale cloud cover [RF-CR; *Ackerman et al.*, 2000], (3) indirect effects on clouds, as increased condensation nuclei lead to smaller cloud drops, which can increase cloud brightness [*Twomey*, 1974] and cloud lifetime and cloud cover [*Albrecht*, 1989], (4) cloud absorption of sunlight caused by black carbon nuclei in cloud drops, and (5) snow and ice albedo reduction due to black carbon deposition. The direct and semidirect-direct effects are included in our present climate simulations. The indirect (Twomey and Albrecht) effects are not included here, but they are being investigated in the SI2000 model by S. Menon and A. Del Genio (private communication, 2001). The dirty cloud and dirty snow forcings, which are perhaps smaller than the other aerosol forcings, are not included in our present transient climate simulations.

[52] There are a number of aerosol compositions that contribute significantly to the total atmospheric aerosol load [*Andreae*, 1995; *Penner et al.*, 1998; *Haywood and Boucher*, 2000; *IPCC*, 2001]. Moreover, these aerosols are often internally mixed and their characteristics change with humidity, aerosol age, and other factors. As a first approximation we treat the different aerosols individually, i.e., as an "external mixture" of distinct aerosol compositions; a discussion of the differences between these mixtures is given in Box 7.1 of *Harvey* [2000]. We can ameliorate the impact of the external mixture approximation when we assign aerosol optical properties and when we assess the results. For example, we can estimate the increased absorption by black carbon when it is internally mixed [*Fuller et al.*, 1999; *Jacobson*, 2000, 2001a, 2001b]. However, it is desirable to eventually employ explicit realistic representation of multiple composition aerosols.

[53] The aerosols that are included in the SI2000 model are listed in Table 2. The only tropospheric aerosols that are time-dependent in our present experiments, and thus the only ones providing a climate forcing, are sulfates (S), black carbon (BC), and organic carbon (OC) aerosols. The primary sources of these aerosols are associated with fossil fuel use. We do not include a long-term change of aerosols from biomass burning, of soil or desert dust, or of nitrates. There has probably been some increase of biomass burning over the past 50 years, but we do not have data that quantify the temporal variation. Soil dust has probably changed because of human activities, especially land use practices, and there is also a natural variability of airborne soil dust with drought cycles, but it is difficult to quantify these. Calculations by *Adams et al.* [2001] of climate forcing by nitrates suggest a forcing change of the order of -0.1 W/m^2 in the past 50 years. This is less than the uncertainties in some of the other aerosol forcings, so the omission may not be too important for our present simulations, but *Adams et al.* [2001] suggest that nitrates could become increasingly important in the future.

Table 2. Aerosol Optical Depth at Wavelength 0.55 μm and Shortwave Single Scattering Albedo for Standard Aerosols (in 1950 and 1990) in the SI2000 Model

Aerosol	Optical Depth 1950/1990	Single Scattering Albedo 1950/1990
Tropospheric sulfate		
Natural	0.004	1.00
Biomass burning	0.0006	1.00
Anthropogenic	0.0072/0.0184	1.00
Black carbon		
Biomass burning	0.0013	0.48
Industrial	0.0004/0.0016	0.31
Organic carbon		
Natural	0.0009	0.98
Biomass burning	0.0096	0.93
Industrial	0.0016/0.0056	0.96
Soil dust	0.0324	0.89
Sea salt	0.0267	1
Stratospheric sulfate	0.0065/0.0110	1
Total	0.0912/0.1121	0.942/0.944

[54] The sources of the aerosol distributions in our model that do not have a secular trend are as follows. The natural sulfate distribution was computed by one of us (D.K.) using the sources specified by *Koch et al.* [1999] in the transport model described below. The sulfates, black carbon and organic carbon aerosols from biomass burning are based on the transport modeling of *Koch et al.* [1999], with the carbonaceous aerosols employing the source distribution of *Cooke and Wilson* [1996]. Soil dust is based on *Tegen and Fung* [1995] and *Tegen and Lacis* [1996]. The sea salt distribution is based on *Tegen et al.* [1997], but it has been increased by a factor of four as suggested by *Quinn and Coffman* [1999] and *Haywood et al.* [1999].

[55] Our time-dependent aerosol distributions are based on aerosol transport model calculations carried out by one of us (D.K.) with a 9-layer version of the GISS GCM. We interpolate the results to the 12 layers of the SI2000 model. *Koch et al.* [1999] and *Koch* [2001] describe the transport calculations for S, BC, and OC distributions for current emissions. Koch used the same model to calculate the distributions in 1950, 1960, 1970, 1980, and 1990 that we employ in our present climate simulations. The global S emission scenario is from *Lefohn et al.* [1999]. The method of *Cooke and Wilson* [1996] was used to derive BC emissions from United Nations energy statistics [*Tegen et al.*, 2000; *Koch*, 2001]. The UN statistics distribute fuel use among countries, and emissions within countries are distributed in proportion to the population. The fuel data account for temporal changes in sulfur content, but not for changes of combustion technology

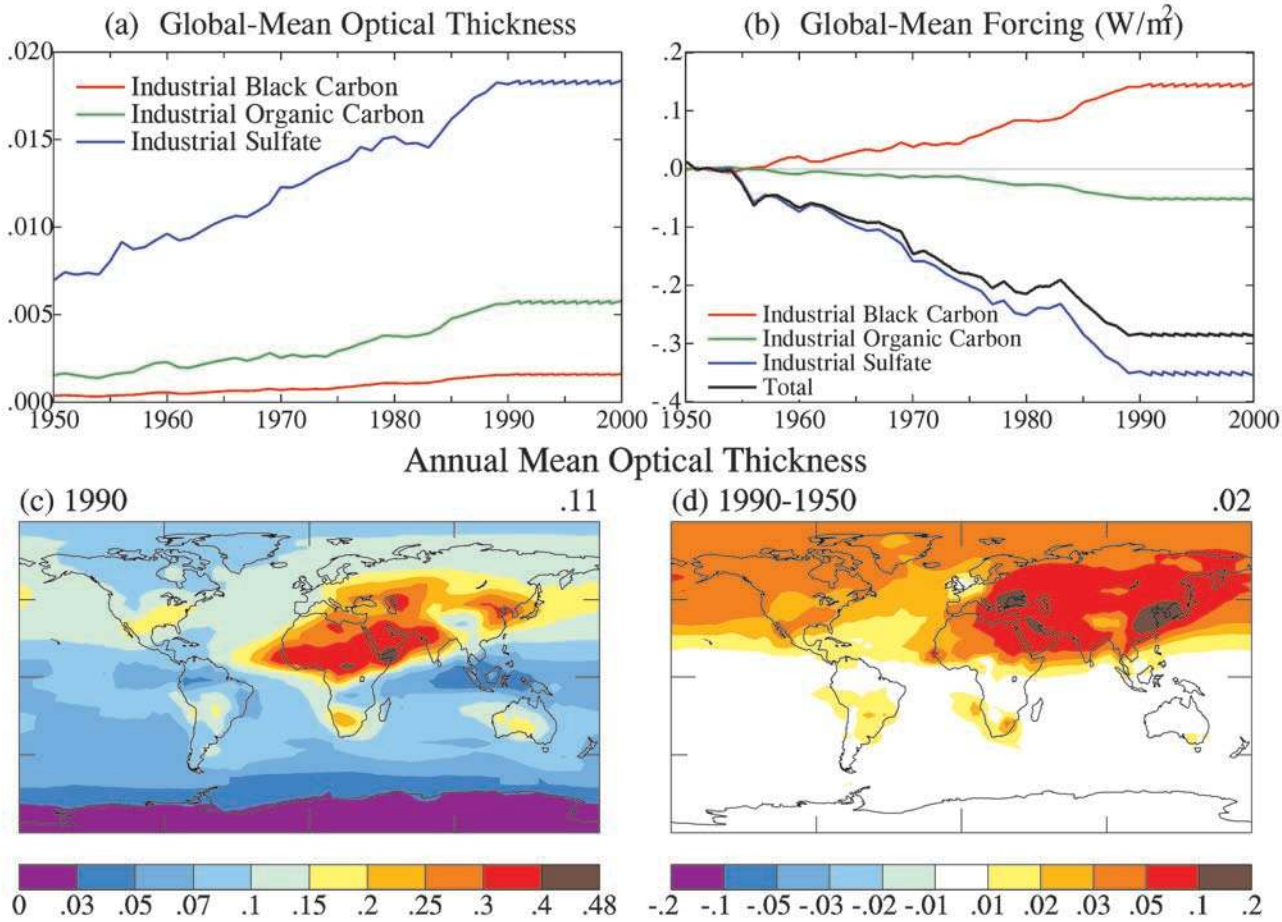

Figure 8. (a) Optical thickness at wavelength 0.55 μm and (b) climate forcing for the three time-dependent tropospheric aerosols in the GISS SI2000 model. Optical depth at wavelength 0.55 μm (c) for all aerosols in the SI2000 model in 1990 and (d) the change between 1950 and 1990.

that may affect carbon or sulfur emissions. BC global annual emissions are 6.4 Mt/yr in 1984, based on consumption of hard coal, brown coal and diesel [*Cooke et al.*, 1999]. OC fossil fuel emissions were assumed to be a factor of four larger than the BC emissions, following *Liousse et al.* [1996]. The aerosol distributions and global amounts after 1990 are kept fixed at the 1990 values.

2.6.1. Results

[56] The calculated changes of BC, OC, and S aerosol global-mean optical depths are shown in Figure 8a, and the climate forcings are shown in Figure 8b. The net change of the global aerosol forcing is about -0.3 W/m^2 over the period 1950–1990. Maps of the optical depth in 1990 and the change between 1950 and 1990 are given in Figures 8c and 8d.

[57] Table 2 summarizes the aerosol optical depths and single scattering albedos in the SI2000 model. The small absorption by OC, which is assumed to occur at ultraviolet wavelengths, is based on absorption measurements by one of us (T.N.). The variation of the spectrally integrated single scatter albedo for natural, industrial and biomass burning OC is due to their assumed effective radii of 0.3, 0.5, and 1.0 μm, respectively. The global mean aerosol optical depth (at wavelength 0.55 μm) for all aerosols in the SI2000 model is about 0.09 in 1950 and 0.11 in 1990. The global mean single scattering albedo is about 0.94. This shortwave albedo includes a full spectral integration for desert dust [*Tegen and Lacis*, 1996] and the mean effect of the small absorption by OC in the ultraviolet region.

2.6.2. Assessment

[58] *Koch* [2001] makes extensive comparisons of the simulated BC and OC distributions with observations. Although the observations are highly variable, if the measurements near urban locations are excluded the modeled BC and OC are in good agreement with observations on the average [*Koch*, 2001, Figures 3 and 4]. An exception is remote ocean regions, especially over the Pacific, where the model aerosol amount tends to be too small. One potentially serious problem for climate applications is that the BC does not fall off with height as rapidly as observed. The BC amount in the upper troposphere is about an order of magnitude greater than observed amounts [*Koch*, 2001, Figure 5], although the amounts there are quite small.

[59] Sulfates are nonabsorbing, so, as far as their direct climate effect is concerned, their vertical distribution is not crucial. The geographical distribution of our sulfate aerosols is similar to that of other investigators, and we believe that it is realistic. The total anthropogenic sulfate forcing (present

minus preindustrial) for our present model [*Koch*, 2001] is -0.65 W/m^2, in the middle of the range for other investigators [*Adams et al.*, 2001, Figure 1]. However, *Adams et al.* [2001] make a strong case that the anthropogenic sulfate forcing may be even larger (more negative), because the swelling of sulfate aerosols at high humidity is probably underestimated.

[60] The total aerosol amount in our model, with a current optical depth of 0.11, is probably less than in the real world. Likely reasons include too little S over the oceans because of a deficient dimethylsulfide (DMS) and insufficient hydration effects on S as mentioned above, the absence of nitrates, and the absence of a trend in biomass burning. For example, Figure 8 has very little aerosol over Indonesia, where recent satellite data [*Nakajima et al.*, 1999] show large aerosol amounts.

[61] The important factor for climate change is the temporal aerosol change. We consider our present aerosol scenario as providing only an initial aerosol sensitivity study. We believe that the time dependence of nonabsorbing and absorbing aerosols is qualitatively realistic, but we have few data to check against. We suspect that this scenario underestimates both negative and positive aerosol forcings, and the transport model may loft the aerosols too efficiently, as discussed above. It may be useful to have a sensitivity study in which the vertical profile of the BC is modified in accord with observations and the BC absorption is increased. One reason to increase absorbing aerosols is their present treatment as an external mixture, which underestimates their absorption [*Haywood and Shine*, 1995; *Fuller et al.*, 1999; *Jacobson*, 2001b]. Additional reasons are the evidence for deficient aerosol amount in remote regions and an impression that our single scattering albedos tend to fall toward the high side of typical field observations. Additional aerosol sensitivity studies might include enhancement of the nonabsorbing-absorbing aerosol opacities including a stronger amplification at high humidities, as well as a more complete representation of BC absorption effects (addition of dirty cloud and dirty snow). We suggest elsewhere [*Hansen and Sato*, 2001; *Hansen*, 2002] that the total BC forcing, including the albedo effects on clouds and on ice and snow surfaces may be as large as 0.8–1 W/m^2.

3. GISS SI2000 Model

[62] The GISS SI2000 atmospheric model is similar to predecessor versions that are documented in the literature for the $4^\circ \times 5^\circ$ resolution that we employ here. We summarize here recent model changes and model shortcomings that seem particularly relevant to the present applications. We also discuss the climate sensitivity of the model. Finally, we summarize the array of simulations that is underway with the SI2000 model.

3.1. Atmospheric Model

[63] The SI2000 atmospheric model is similar to the SI95 model described by F-C. The primary change is an increase of vertical resolution from 9 to 12 layers in the principal version of the model, with the added resolution in the upper troposphere and stratosphere (Figure 9). This vertical resolution allows stratospheric radiative forcings (e.g., volcanic aerosols and ozone change) to be defined more accurately. We find that the stratospheric thermal response to stratospheric aerosols and ozone changes is typically 50% larger in the 12-layer model than in the 9-layer version. We show in section 5 that the results with 12 layers are in closer agreement with observations. However, the 12-layer resolution is still inadequate for reliable simulation of stratospheric dynamics or stratosphere-troposphere interactions, as discussed below.

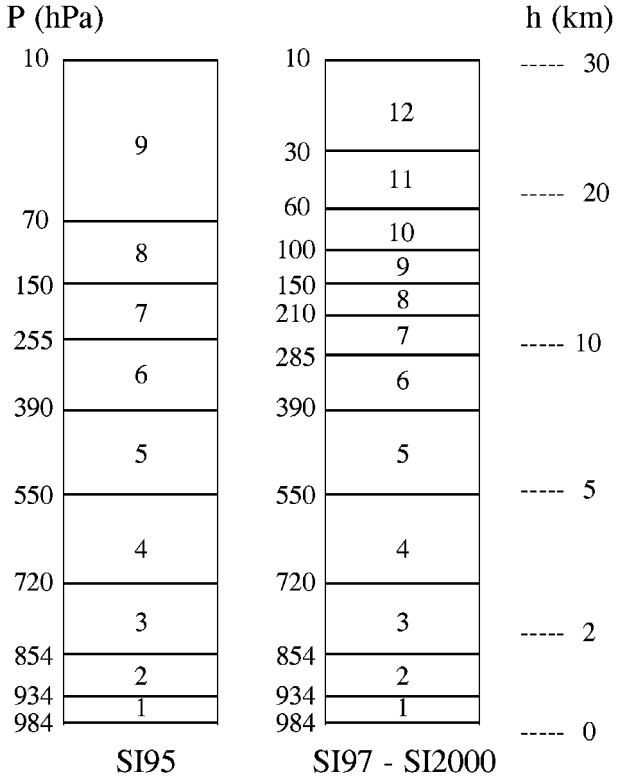

Figure 9. Global mean pressure levels (hPa) for 9-layer and 12-layer models. The 12-layer version is the minimum resolution in SI2000 model.

[64] The discrepancies in absorbed solar radiation in SI95 compared with ERBE data in regions of sea ice and near the South Pole, illustrated in Figure 1 of F-C, are reduced considerably in SI2000. The excessive absorption of solar radiation by sea ice puddling was found to be a result of a programming error that caused the albedo reduction to be in effect at all times, rather than when the surface of the sea ice reached the melting point. The excessive absorption in Antarctica near the South Pole in SI95 was found to occur when sublimation exceeded snowfall thus exposing dark bare ice. The resulting unrealistic reduction of surface albedo is avoided in SI2000 by fixing the albedo of interior Antarctica (and Greenland) at 0.80. Additional changes were made to the radiation routines in SI2000, as discussed below in conjunction with the model's climate sensitivity.

[65] The GISS atmospheric model is representative of state-of-the-art GCMs in a number of ways. In a comparison of GCM radiation results with line-by-line calculations [*Cess et al.*, 1993] the GISS model was among the more

accurate. This was also true in comparisons of cloudiness and its variability [*Weare et al.*, 1995] and in comparisons of seasonal changes in cloud radiative forcing [*Cess et al.*, 1996]. A comparison of hydrologic processes in 29 GCMs with observations ranked the GISS model in the upper quartile [*Lau et al.*, 1996]. Comparison among 30 GCMs of the amplitude and seasonality of precipitation over the United States showed the GISS model to be one of the most realistic, with a fidelity similar to that of the finer resolution 19-layer T42 model of the Max Planck Institute [*Boyle*, 1998]. Model shortcomings are summarized next.

3.2. Atmospheric Model Deficiencies

[66] The 12-layer version of SI2000 retains the simple top-layer drag formulation from GISS model II [*Hansen et al.*, 1983] designed to assure numerical stability. The model does not yield a well-defined polar night jet or realistic interannual variability of stratospheric zonal wind, and it is not anticipated that this version of the model can provide realistic dynamical interactions between the stratosphere and troposphere. An immediate strategy, summarized below, is to make trial simulations with a version of the GISS middle atmosphere climate model [*Rind et al.*, 1988], which has higher vertical resolution, a model top in the mesosphere, and a parameterized gravity wave drag representation. The computing time is several times greater with this middle atmosphere model, so in our climate model development we will also seek a model with the top at an intermediate level that can still yield a realistic representation of the lower stratosphere and its variability.

[67] Another continuing problem with the GISS model is inaccurate radiation balance in regions of stratus clouds over the ocean, specifically off the coasts of California, Peru, and southern Africa. There is a deficiency of cloud cover and an excess of absorbed solar radiation of the order of 50–75 W/m^2 in the summer in those regions. Although this problem is common among GCMs, the GISS model is among the models that have the largest discrepancy. Tests with higher vertical resolution in the PBL and an improved turbulence representation (Y. Cheng, private communication, 2001) yield some improvement. However, this inaccuracy in the fluxes delivered to the ocean surface by the SI2000 model, as it stands, presents a substantial problem for ocean models.

[68] The GISS model is generally too cool. The surface of SI2000 is about 1°C cooler than observed and the troposphere is typically 1–2°C too cool. In a perhaps related problem the troposphere tends to be too dry, especially at upper levels. Cirrus cloud cover is deficient.

[69] The radiation in the SI2000 model uses the correlated *k* distribution method of *Lacis and Oinas* [1991]. This allows explicit realistic representation of gaseous absorption and atmospheric scattering. The SI2000 version of the radiation has 33 *k* intervals in the thermal spectrum, which allows the climate forcing by the principal greenhouse gases to be calculated accurately. However, recent line-by-line tests [*Oinas et al.*, 2001] show that some adjustments are needed to the *k* distributions in regions of CH_4-N_2O-H_2O overlap. Radiation for the SI2001 model has not been completed, but tests with an improved parameterization yield a surface and tropospheric warming of about 1°C. The improved parameterization does not alter the model's sensitivity to CH_4-N_2O changes, which was already pegged to line-by-line results.

[70] The horizontal resolution and finite difference calculations in the GISS GCM are another concern. The "tracers" in the model, including heat and water vapor, use a quadratic upstream scheme [*Prather*, 1986], which is both accurate and stable. The momentum equation is more difficult. The SI95 model uses a fourth-order finite differencing scheme that moves storms realistically in the troposphere but is computationally slow and very noisy in the stratosphere. In the SI2000 model we allow the option of either second or fourth-order differencing for the momentum equation. As a test, we are also making simulations with 2° × 2.5° atmospheric resolution, which reduces the importance of the differencing scheme. It should be noted that because of the higher-order differencing schemes in the GISS model and the preservation of concentration gradients within grid boxes, the effective resolution of the GISS model is generally higher than that of other models with the same grid size.

3.3. Model Sensitivity

[71] The climate sensitivity of GISS model II [*Hansen et al.*, 1984] was 4.2°C for 2 × CO_2. The sensitivity of the SI95 model [F-C] was 3.6°C for 2 × CO_2. The sensitivity of the SI2000 model is about 3°C for 2 × CO_2. Specifically, it is 3.2°C for the version of SI2000 that uses second-order finite differencing and 2.9°C for the version that uses fourth-order differencing.

[72] A precise quantitative analysis of all the causes for changes in model sensitivity requires a new control run and a 2 × CO_2 experiment to be carried out for every model alteration. Although that is impractical, we can provide an indication of the main causes of the lesser sensitivity of the SI2000 model.

[73] Part of the reduced sensitivity to 2 × CO_2 is due to a smaller radiative forcing for 2 × CO_2, rather than to a change in the model's sensitivity to a forcing. The forcing for 2 × CO_2 was about 4.2 W/m^2 in both GISS model II and the SI95 model. The 2 × CO_2 forcing in SI2000 (for 311 ppm → 622 ppm) is 3.95 W/m^2. This 6% reduction of the forcing accounts for about 0.2°C of the reduced model response to 2 × CO_2. The smaller forcing results from higher spectral resolution in the SI2000 radiation, which is calibrated against line-by-line calculations. We estimate that the uncertainty in our present radiative forcing for 2 × CO_2 is $\lesssim$ 10%. The forcing in SI2000 falls within the range of results for 2 × CO_2 reported by *IPCC* [2001], which is 3.5 to 4.1 W/m^2.

[74] Changes of the model sensitivity, as opposed to changes of the forcing, are associated with climate feedbacks. The principal feedbacks involve changes of water vapor, clouds, and sea ice [*Hansen et al.*, 1984; *Held and Soden*, 2000]. Changes of the temperature lapse rate are also a factor, but lapse rate changes are usually associated with changes of the water vapor profile. The positive feedbacks feed off of each other, in the sense that they cause higher temperature thus increasing the other feedbacks [*Hansen et al.*, 1984]. We note that 2 × CO_2 experiments with the earlier GISS model tended to have a larger increase of water vapor, larger decrease of sea ice cover, larger increase of cirrus clouds, and larger decrease of low clouds. However,

this comparison does not identify the model changes that instigated the lesser sensitivity in SI2000.

[75] Among the changes between the SI95 and SI2000 models, prime candidates for affecting the climate sensitivity are changes in the sea ice parameterization and changes of the radiation that affected the clouds. The "aging" of snow on sea ice, which reduces the albedo, occurred in SI95 only when the surface temperature was above the freezing point. Snow on sea ice continuously ages in SI2000, regardless of the temperature. Thus the sea ice in SI2000 tends to be darker, and the reduced contrast in albedo between sea ice and ocean tends to lessen the sea ice feedback effect. It is also possible that several changes in the radiation could have affected the model sensitivity. One of these is the introduction of a parameterization for the effect of finite cloud size on shortwave albedo and on infrared emissivity [*Cairns et al.*, 2000]. However, we have not quantified the effect of the individual changes on model sensitivity.

[76] The difference in sensitivity between the two versions of the SI2000 model (second- or fourth-order differencing in the momentum equation), to at least a large degree, is related to the different amounts of sea ice in their control runs. The sea ice in the fourth-order model covers 4% of the globe, which is realistic. This compares with more than 6% sea ice cover in the second-order model. In retrospect, we should have made adjustments in the sea ice parameterizations in the second-order model control run in an attempt to achieve a realistic sea ice cover. However, that would not necessarily have yielded a model with the same sensitivity as the fourth-order model. Because the atmospheric energy transports are different in the two atmospheric models, the implied ocean heat transports are different and this may affect the climate sensitivity.

[77] The bottom line is that, although there has been some narrowing of the range of climate sensitivities that emerge from realistic models [*Del Genio and Wolf*, 2000], models still can be made to yield a wide range of sensitivities by altering model parameterizations. We suggest that the best constraint on actual climate sensitivity is provided by paleoclimate data that imply a sensitivity 3 ± 1°C for $2 \times CO_2$ [*Hansen et al.*, 1984, 1993, 1997b; *Hoffert and Covey*, 1992]. It is satisfying that the a priori sensitivity of the SI2000 model comes out near the middle of the empirical range of 2–4°C for $2 \times CO_2$. However, for the sake of interpreting observed climate change and predicting future change it is appropriate to consider climate sensitivity as an uncertain parameter that may, in fact, be anywhere within that range.

[78] Therefore we include the possibility of altering the model's climate sensitivity. We do this by adjusting an arbitrary cloud feedback as defined in the appendix of *Hansen et al.* [1997a]. Specifically, the cloud cover is multiplied by the factor $1 + c\Delta T$, where ΔT, computed every time step, is the deviation of the global mean surface air temperature from the long-term mean in the model control run at the same point in the seasonal cycle and c is an empirical constant. For the SI2000 second-order model we take $c = 0.04$ and -0.01 to obtain climate sensitivities of 2°C and 4°C for $2 \times CO_2$.

3.4. Ocean Representations

[79] Ocean A (observed SST) uses the SSTs and sea ice of HadISST1 (N. A. Rayner et al., Globally complete analyses of SST, sea ice, and night marine air temperature, 1871–2000, manuscript in preparation, 2002) (hereinafter referred to as Rayner et al., manuscript in preparation, 2002), which uses reduced-space optimum interpolation [*Kaplan et al.*, 1997, 1998] to fill in data sparse regions. SSTs at high latitudes have substantial uncertainties. The sea ice records in HadISST1 have been "homogenized" in an attempt to make the different components consistent, but considerable uncertainty remains in the sea ice record, especially in the presatellite era. Ocean A has severe limitations for climate studies, as discussed in sections 3.5 and 5.2.2.

[80] Ocean B (Q-flux ocean) includes a deep ocean with diffusive penetration of heat anomalies. The diffusion coefficient varies geographically as described by *Hansen et al.* [1984]. Ocean B, based on observed rates of ocean mixing of tracers, should provide a useful approximation of global heat uptake by the ocean for climate forcings that do not fundamentally alter the deep ocean circulation.

[81] Oceans C, D, and E are distinctly different dynamical ocean models. Ocean C, developed initially by *Russell et al.* [1995], uses a vertical coordinate related to pressure. Ocean D, the GFDL Modular Ocean Model (MOM), uses depth (z-level) [*Pacanowski and Griffies*, 1999]. Ocean E, the Hybrid Coordinate Ocean Model (HYCOM) of *Bleck* [1998], uses an isopycnic vertical coordinate in the deep ocean with a z level in the less stratified upper ocean.

[82] All of the ocean models are being attached to the same (B grid) version of the SI2000 atmospheric model. This should help to isolate the role of the ocean in the simulated climate response. The wide range of ocean models will provide an indication of the model dependence of any inferences about climate change.

[83] We report in this paper only results of simulations for ocean A (observed SST) and ocean B (Q-flux ocean). These simple ocean "models" allow us to characterize the efficacy of each radiative forcing when only limited dynamical interactions are permitted. (By "efficacy" we mean the effectiveness of a forcing for producing a climate response in a general sense. One specific measure of efficacy is the global climate sensitivity, the ratio of the global mean temperature response to the magnitude of the forcing, $\Delta T_s/F_a$ (see section 4.1 and Table 4).)

3.5. Model Experiments

[84] Table 3 summarizes model runs (climate simulations) carried out or planned. Our rationale is that we may be able to learn more from a systematic array of experiments in which we vary key factors one by one. The variable factors include the climate forcings, the ocean model, and the atmosphere model.

[85] Each atmosphere-ocean model has one long control run with the atmospheric composition fixed at 1951 conditions. The control runs each cover at least a few hundred years. A few of them are continuing to run and may be extended for thousands of years, if that appears to be useful.

[86] There are also two "long" (or "equilibrium") runs for each radiative forcing. The first equilibrium run is a 250-year run made with the Q-flux mixed layer ocean, without any attached deep ocean. The objective is to help characterize each radiative forcing. Weak forcings, e.g., stratospheric H_2O change, are exaggerated by a specified

Table 3. SI2000 Experiments[a]

Radiative Forcing	Ocean A (Varying SST)	Ocean A (Mean SST)	Ocean A (Stratospheric Model)	Ocean A (2° × 2.5° Atmosphere)	Ocean B (*Q*-Flux, 3°C Sensitivity)	Ocean B (2° and 4°C Sensitivity)	Ocean C (GISS Ocean)	Ocean D (GFDL MOM)	Ocean E (Bleck/Sun Isopycnal)
None	five runs[b]	long run	*long run*	*long run*	long run	*long run*	*long run*	*long run*	*long run*
GHGs		long run			long run				
Stratospheric aerosols		long run			long run				
Solar		long run			long run				
O_3		long run			long run				
Stratospheric H_2O		long run			long run				
Five forcings	five runs[b]				five runs				
Tropospheric aerosols		long run			long run				
Six forcings	five runs[b]		*five runs*	*five runs*	five runs[b]	*five runs*	*five runs*	*five runs*	*five runs*
Aerosol indirect					long run				

[a] The "long run" is a control or a run with time-independent forcing, while "five runs" is an ensemble of runs with transient forcings. Italicized runs are not included in present paper.

[b] Runs are made for both second- and fourth-order differencing of atmospheric momentum equation.

factor in the equilibrium runs, so that a reasonable signal-to-noise ratio can be obtained. The second equilibrium run is a 21-year run with ocean A using the mean (seasonally varying) SST for 1946–1955. A good signal-to-noise ratio is obtained with a 21-year run because of the fixed SST. These runs are used to define a fixed SST forcing (section 4).

[87] Ensembles of transient simulations, i.e., with time-dependent forcings, are carried out for the period 1951–2000 or 1951–2050. Ensembles presently completed all contain five runs. The ensembles are run with six forcings, and in some cases with five forcings (fixed 1951 aerosols).

[88] At least two different atmospheric models are also being coupled to certain of the ocean models, as summarized in Table 3. The middle atmosphere model of *Rind et al.* [1988] has been attached to ocean A and also may be attached to a dynamical ocean model. A 2° × 2.5° version of the SI2000 atmospheric model is being run with observed SSTs (ocean A).

[89] Simulations for ocean A (observed SST) and ocean B (*Q*-flux ocean) are presented in this paper. The inherent constraints in these models limit the degree of realism in the climate response. However, for just this reason the results provide a useful comparison and complement to simulations with more fully interactive coupled models.

[90] Ocean A, for example, has "correct" SSTs, but obviously will not yield realistic ocean-atmosphere fluxes in some cases of interest. A prime example is the North Atlantic Oscillation, a dynamical fluctuation in which the North Atlantic Ocean cools and in the process disgorges energy that warms Siberia. Ocean A, by specifying a cool North Atlantic, tends to cool Eurasia. This characteristic limits the merits of ocean A, even though it is a popular model for atmospheric data assimilation and reanalysis.

[91] Ocean B is useful for studying the global mean thermal response to forcings. It is most relevant to forcings of moderate size, for which heat anomalies are likely to penetrate the ocean like passive tracers. *Sokolov and Stone* [1998] showed that the transient global surface temperature response in a wide variety of ocean models can be matched with the *Q*-flux ocean by choosing the diffusion coefficient appropriately.

[92] Geographical patterns of climate change depend upon realistic representation of climate dynamics. Analysis will require use of a dynamically interactive ocean-atmosphere, including a realistic stratosphere. It has been suggested that even the global mean temperature is altered by dynamical fluctuations [*Wallace et al.*, 1995]. This is the sort of issue that can be examined with the full array of experiments in Table 3.

4. Equilibrium Simulations

4.1. Global Means

[93] We carry out here long ("equilibrium") GCM runs for each of the six climate forcings used later in our transient climate simulations (section 5). These long runs are made with both ocean A (fixed SST) and ocean B (*Q*-flux ocean). Control runs for oceans A (21 years) and B (250 years) have 1951 atmospheric composition. The fixed SST in ocean A is the mean of years 1945–1955 of the HadISST climatology (Rayner et al., manuscript in preparation, 2002). Individual runs are made for each forcing. The mean of years 2–21 for ocean A and years 51–250 for ocean B are taken as the equilibrium responses.

[94] Most of the six forcing mechanisms were included in our earlier study with the Wonderland model [RF-CR], but the new results are useful for several reasons. First, the forcings used here, including their global distributions, are more specific to our current 1951–2000 simulations and in some cases are more realistic. Second, the present 4° × 5° 12-layer SI2000 model is more realistic than the 8° × 10° 9-layer Wonderland (sector) model that employed the physics of our 1983 climate model. For example, the present model has state-of-the-art cloud modeling [*Del Genio and Yao*, 1993; *Del Genio et al.*, 1996], which may effect the "semidirect-direct" climate forcing found for absorbing aerosols [RF-CR].

[95] We compute several measures of each climate forcing, as summarized by the cartoon in Figure 10. F_i, the instantaneous forcing, is the flux change at the tropopause prior to any thermal response. F_a, the adjusted forcing, is the flux change at the tropopause (or any higher level) after the stratospheric temperature reaches radiative equilibrium with the tropospheric temperature held fixed. F_s, the fixed SST forcing, is the equilibrium energy flux change at the Earth's surface (and at all higher levels) with the sea surface temperature (SST) held fixed.

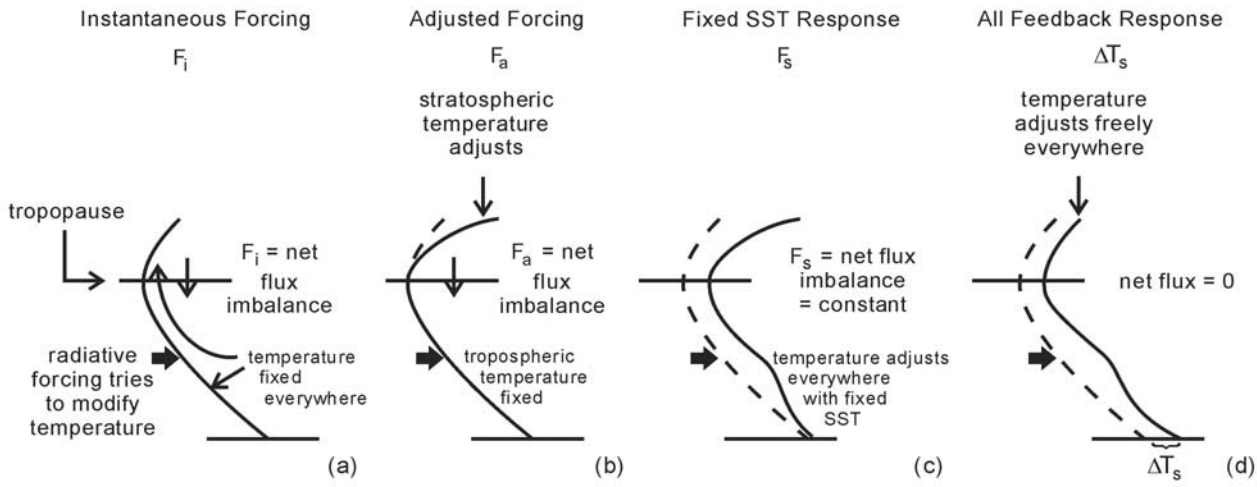

Figure 10. Cartoon defining (a) F_i, instantaneous forcing, (b) F_a, adjusted forcing, (c) F_s, fixed SST forcing, and (d) ΔT_s, equilibrium surface air temperature response.

[96] In a previous study [RF-CR] we concluded that for most radiative forcings the adjusted forcing, F_a, provides a reasonably good predictor of the equilibrium global-mean temperature response. However, there are notable relevant exceptions, specifically absorbing aerosols and ozone change. In one sense, F_s might be expected to provide a better measure than F_a of the flux perturbation that would beset the real world because the tropospheric lapse rate, as well as stratospheric temperature, can adjust rather quickly to a forcing. So can atmospheric temperature over a large continent, even though the magnitude of the response is limited by exchange of continental and marine air masses. The rationale for F_s is that the ocean's thermal inertia is the reason for sustained flux imbalance after the first transient atmospheric response to an imposed forcing. We find here, however, that F_s is no better than F_a as a predictor of global temperature change, as the latitude distribution of the forcing is apparently more critical than the vertical profile of temperature change. Therefore it seems better to use the conventional quantity, F_a, as our standard measure of climate forcing. However, F_s is the most relevant flux to estimate the initial rate of ocean heat storage and the response time of the climate system.

[97] We take F_s as the mean for years 2–21 of a 21-year GCM run with fixed SST. Although the need for a GCM to calculate F_s may seem to be a disadvantage, most climate studies are now made with GCMs and the run to obtain F_s only needs to be a few years if a precision of 0.1 W/m^2 for the global mean forcing is sufficient. F_s is simpler to compute in a consistent fashion than are the other forcings. For example, it removes the uncertainty associated with defining the tropopause level [*Harvey*, 2000, chapter 7.2]. Thus it is easy to compute F_s in conjunction with GCM studies. It would be informative if F_s were routinely reported as a quantification and verification of forcings actually employed by all models.

[98] Table 4 summarizes the forcings and equilibrium climate response for a large number of climate forcing mechanisms. ΔT_s is the equilibrium (years 51–250) global mean surface air temperature response. Several of the results in Table 4 warrant comment.

[99] We first compare the responses to the CO_2 and solar irradiance (S_O) forcings. *Manabe and Wetherald* [1975] and *Wetherald and Manabe* [1975] found that the responses of a swamp ocean model to similar forcings, specifically 2 × CO_2 and +2% S_O, were very similar. Our simulated responses to CO_2 and S_O forcings are consistent with their results.

[100] We obtain a climate sensitivity, $\Delta T_s/F_a$, between ¾°C and 1°C for each Watt of forcing for most of the forcing mechanisms in Table 4. The two apparent exceptions, O_3 and stratospheric H_2O, are explained by the geographical distribution of the forcings, as discussed in section 4.2. The change of tropospheric aerosols between 1950 and 1990 (or 2000), for the specific combination of S, BC and OC aerosols that we employ, yields a sensitivity of 1°C per W/m^2. However, this sensitivity is a strong function of the assumed amount of aerosol absorption [RF-CR], and it thus depends on the BC history and vertical distribution, which are very uncertain.

[101] We calculate the forcing by stratospheric aerosols for the specific aerosol distribution that existed for the 12-month period July 1991 through June 1992 and for a uniform distribution of aerosols with optical depth 0.1 at wavelength 0.55 μm. Note that although $F_i = -3$ W/m^2 for the first year after Pinatubo, $F_a = -2.6$ W/m^2 and $F_s = -2.4$ W/m^2. Thus, other things being equal, if the SST were truly fixed one would expect the ocean to pump heat into space after Pinatubo at a global rate of only 2.4 W/m^2. It is still less when the SST is allowed to respond partially to the forcing (section 5), as the SST would in the real world. One reason that the planet cools at a rate less than 3 W/m^2 even when the SST is fixed, i.e., one reason that $F_s < F_i$, is inefficiency of the ocean and atmosphere in pumping heat to the continents for radiation to space. In other words, despite exchange of continental and marine air masses the continents cool in response to the

Table 4. Radiative Forcings (W/m^2) and Equilibrium Responses (°C)[a]

Forcing Mechanism		F_i	F_a	F_s	ΔT_s	$\Delta T_s/F_a$
Doubled CO_2 (311.1–622.2 ppm)		4.46	3.95	3.94	3.2	0.81
Greenhouse gases (1951–1998)		1.75	1.62	1.65	1.55/1.21[b]	0.96/0.75[b]
Stratospheric aerosols						
Pinatubo (July 1991 to June 1992)		−2.97	−2.58	−2.40		
τ = 0.1 uniform		−2.35	−2.06	−1.80	−1.81	0.88
Solar irradiance		1.39	1.31	1.33	1.10	0.84
10×[b] (1951–1981)						
Ozone (1951–1998)						
O_3[A] data	stratosphere	0.08	−0.085			
	troposphere	0.16	0.135			
	entire atmosphere	0.23	0.05		−0.20	−4.00
O_3[B] data	stratosphere	0.06	−0.095			
	troposphere	0.15	0.125			
	entire atmosphere	0.21	0.03	0.05	−0.34	−11.00
Stratospheric water vapor (1951–1998)	0–10 hPa	0.005	0.007			
	10–150 hPa	0.037	0.029			
	all altitudes	0.041	0.036		0.00	
	10×[b] all altitudes	0.37	0.31	0.36	0.48	1.55
Tropospheric aerosols (1951–1990)		−0.29	−0.28	−0.13	−0.28	1.00

[a] F_i, F_a, and F_s, are the instantaneous, adjusted and fixed SST forcings, and ΔT_s is the equilibrium (years 51–250) GCM response. Stratospheric aerosol forcing is computed for Pinatubo aerosols (July 1991 through June 1992) and for a constant uniformly distributed aerosol with optical depth 0.1 at wavelength 0.55 μm. Solar irradiance and stratospheric water vapor changes are multiplied by a factor of 10 to magnify the response. Troposphere aerosol forcing is the change of sulfate, black carbon and organic aerosols between 1950 and 1990 in the model of *Koch* [2001].

[b] T_s is computed by the GCM with second-order differencing, except for the 1951–1998 GHG forcing, which is also computed with fourth-order differencing.

aerosols, and thus their rate of heat loss to space is less than 3 W/m^2.

4.2. Global Maps

[102] The global distribution of the forcings is shown in the first column of Figure 11. The greenhouse gas, stratospheric aerosol, and solar irradiance forcings are largest at low latitudes, decreasing by a factor of two or so toward the poles. The ozone forcing is positive at low latitudes but becomes negative in the polar regions because of ozone depletion there. The stratospheric water vapor forcing is largest in the polar regions. The tropospheric aerosol forcing is primarily in the Northern Hemisphere.

[103] The equilibrium surface air temperature change, Figure 11b, is computed with the mixed layer *Q*-flux ocean with second-order differencing. The global mean response is consistent with the global mean forcing, with a sensitivity of $\frac{3}{4}$–1°C per W/m^2, for all of the forcings except O_3 and stratospheric H_2O. As discussed above, the sensitivity of the second-order differencing model, which has excessive sea ice in the Southern Hemisphere, is higher than our best estimate. The sensitivity of the model with fourth-order differencing, which has realistic sea ice cover, is closer to the sensitivity of 0.75°C per W/m^2 that we estimate from empirical (paleoclimate) data.

[104] The unusual responses to O_3 and stratospheric H_2O are explained by the latitude variation of the forcing. The response of our models, and presumably of the real world, is larger for forcings at high latitudes than for forcings at low latitudes, typically by a factor of two [RFCR]. Thus, although the negative forcing from polar ozone depletion and the positive forcing from tropospheric O_3 approximately balance on global average, the polar forcing is more effective. The greater sensitivity to high-latitude forcings is due to the ice/snow positive feedback and the relatively stable atmospheric lapse rate at high latitudes. This effect may be exaggerated somewhat in the present model by the excessive sea ice in the control run.

[105] Note that there is some similarity in the geographical pattern of the equilibrium response to different forcings. Even the aerosol forcing, which is mainly in the Northern Hemisphere, evokes a global response. There is only a limited tendency toward a universal response, however. The Southern Hemisphere response to the aerosol forcing is not as intense as the Southern Hemisphere response to a globally uniform forcing. Also, the ozone forcing, which is concentrated near the South Pole, evokes a response that is restricted mainly to the Southern Hemisphere.

[106] The surface air temperature change with fixed SST is small on global average. However, several of the forcings yield a significant warming in Eurasia, which is largest in the winter. The winter warming is usually associated with an increased magnitude of the zonal wind (not illustrated).

4.3. Zonal Means and Altitude Profiles

[107] The equilibrium zonal-mean temperature response to the six forcings is given in Figure 11c for ocean A (fixed SST) and ocean B (*Q*-flux model). Figure 11c (right) gives the altitude profiles of the global mean responses.

[108] The GHGs (specifically CO_2) cause substantial stratospheric cooling that increases with altitude. When the SST is allowed to respond (ocean B), there is a relative maximum in the equilibrium warming at about the 300 hPa level in the tropics that is about 30% greater than the surface warming. The maximum in the equilibrium near-surface warming near the South Pole is probably exaggerated by the excessive sea ice in the control run.

[109] The volcanic aerosols cause warming in the lower stratosphere, with the warming concentrated at low latitudes even though the aerosols are uniformly distributed with latitude. The tropospheric thermal response is similar to that for greenhouse gases but with the opposite sign. The tropospheric response exceeds the surface response, con-

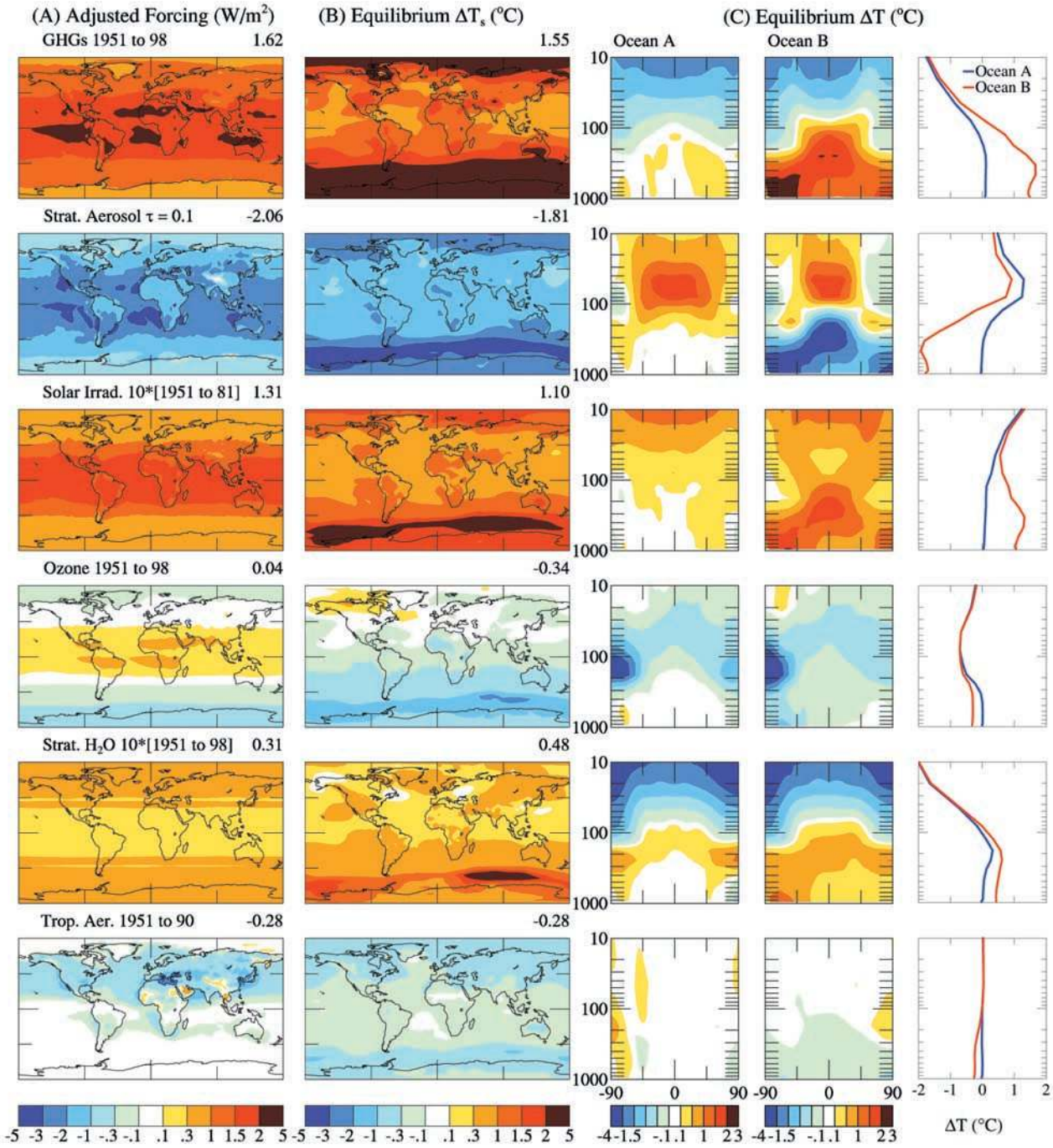

Figure 11. (a) Adjusted forcing for six climate forcing mechanisms. (b) Annual-mean equilibrium surface air temperature response for the *Q*-flux ocean, with the global means given on the upper right corner. (c) Annual-mean ΔT (°C) for both ocean A (fixed SST) and ocean B (*Q*-flux ocean). The SST is fixed in ocean A, so only the atmosphere and land surface can respond to the forcing.

sistent with empirical evidence after El Chichon and Pinatubo [*Santer et al.*, 2001].

[110] The solar irradiance forcing has been magnified by taking 10 times the difference between the solar irradiance near a solar maximum (1981) and near a solar minimum (1951), as estimated by J. Lean (section 2.3). No indirect forcings associated with solar irradiance changes are included. The solar irradiance increase warms the stratosphere, because of absorption of ultraviolet radiation, by an amount that increases with altitude. The spatial structure of the tropospheric temperature change is similar to that for other forcings.

[111] The ozone forcing includes the larger polar depletion estimated by *Randel and Wu* [1999], i.e., the $O_3{}^B$ data set (section 2.4). The ozone change causes substantial cooling in the lower stratosphere, particularly near the South

Pole. The tropospheric cooling that occurs when the SST is allowed to respond is associated with increased sea ice in the Southern Hemisphere.

[112] The stratospheric H_2O forcing is that for 10 times the 1951–1998 CH_4-derived H_2O increase in our 12-layer model. However, as discussed in section 2.5, the 12-layer model removes this H_2O from the stratosphere too rapidly, and thus we estimate that the forcing used here is only 6–8 times larger than the actual CH_4-derived H_2O increase in that 47-year period. This specified (magnified) H_2O source causes an equilibrium increase of 2.4 ppmv of H_2O in the 10–100 hPa layer. Reducing this by the factor 6–8 suggests that methane oxidation should have increased H_2O by 0.3–0.4 ppmv during 1951–1998. Indeed, in our transient simulations (section 5) we find an increase of stratospheric H_2O from 2.4 ppmv to 2.7 ppmv. Observations suggest that stratospheric H_2O may have increased in the past half century by of the order of 1 ppmv [*Rosenlof et al.*, 2001]. Thus either there are additional mechanisms causing H_2O to increase in the stratosphere or our simulation underestimates the CH_4 impact on H_2O, for example via climate feedbacks that are inadequately represented in our 12-layer climate model (transport of water vapor from the troposphere is probably underestimated in both the control run and perturbations because of the excessively dry upper troposphere in the SI2000 model). In either event, the H_2O increase employed in Figure 11 is only 2.4 times larger than the observed H_2O change during 1951–1998.

[113] The tropospheric aerosols cause a cooling that is rather uniform with height, as the sulfate aerosols are dominant in our current scenario. We mentioned in section 2.6 that BC aerosols are probably underrepresented in our present model, and they may be mixed too uniformly with height. The changes of aerosols that cause cooling are also probably understated. Although our global mean aerosol forcing probably has the right sign, and is perhaps even of the right order of magnitude, we do not have confidence in the vertical and temporal distributions of aerosol changes. Thus the nature of the aerosol forcing and simulated response may change with better aerosol information.

[114] Finally, we note the tendency for different forcings to produce similar spatial responses. This has obvious implications for studies aimed at identifying the causes of climate change based on comparison of modeled and observed spatial-temporal patterns of climate change, although it does not rule out identification and quantification of climate signatures, if the spatial-temporal distributions of the forcings are well known.

5. Transient Simulations

[115] We describe transient simulations for 1951–2000 using the simplest ocean representations, ocean A (observed SST) and ocean B (Q-flux ocean). The simulations are made for "five forcings" (GHGs, stratospheric aerosols, solar irradiance, O_3, and stratospheric H_2O) and for "six forcings," which adds the direct forcings by three tropospheric aerosols (sulfates, BC, and OC), all as defined in section 2. We extend the ocean B "six forcing" runs to 2050 for two distinct alternative scenarios of future climate forcings. The "business as usual" (BAU) scenario has a 1%/year CO_2 growth rate, which yields an added forcing of almost 3 W/m^2 in 2000–2050. The "alternative scenario," defined in section 2.1, has an added forcing of 1.1 W/m^2 in 2000–2050.

[116] We focus on the global mean response, as our aim is to investigate the global efficacy of the forcings. Study of the geographical distribution of climate change requires interactive ocean dynamics and a realistic representation of the stratosphere. Our present simple models are a useful prelude to such dynamical studies, especially if the latter employ the same forcings and atmospheric physics. Furthermore, for a crucial issue such as global ocean heat storage, the specified empirical mixing rates in the Q-flux ocean may provide as realistic an estimate as is possible at this time and, in any case, a standard for comparison. *Sokolov and Stone* [1998] have shown that heat uptake by the Q-flux ocean provides a good approximation to that by ocean general circulation models, providing that there is no change in the mode of deep circulation. This condition should be satisfied for timescales less than a century with the moderate forcings that we employ.

5.1. Global Mean Response

5.1.1. Period 1951–2000

[117] The global mean response to five forcings and six forcings is shown in Figures 12 and 13. The stratosphere (top row) cools as a result of O_3 depletion and CO_2 and H_2O increase, but it warms temporarily after large volcanoes as a result of thermal infrared and near-infrared heating by the aerosols. Such qualitative results have been reported in the literature many times. The quantitative agreement with MSU (microwave sounding unit) observations [*Christy et al.*, 2000] is better than that found by F-C or *Bengtsson et al.* [1999]. The increased stratospheric response in our model occurred when we increased the vertical resolution from 9 to 12 layers.

[118] We note that some of our models use a second-order finite differencing scheme for the momentum equation, while others use a fourth-order scheme. The second-order scheme is more diffusive, while the fourth-order scheme is much noisier in the stratosphere, as is apparent in the different levels of variability among the five-member ensembles. To ameliorate uncertainty about the effect of the numerical differencing scheme, we carried out some ocean A and ocean B calculations with both second-order and fourth-order differencing. The results were similar, as summarized in Table 5. We use the fourth-order results as our standard case, because that model has a more realistic sea ice area in its control run.

[119] The tropospheric temperature changes, weighted by the MSU channel 2 (MSU2) weighting function, are shown in the second row of Figures 12 and 13. The agreement with MSU2 data is good for ocean B, but the simulated warming trend with ocean A is larger than the observed warming (Figure 12 and Table 5). Discrepancies with the observed 1979–1998 temperature trend are greater for MSU2LT, which has a weighting function that peaks closer to the surface [*Christy et al.*, 1998]. Specifically, the lower troposphere with ocean B warms slightly (about 0.1°C) more than observed, and ocean A warms significantly (about 0.3°C) more than observed (MSU2LT is included in Table 5 but not in Figures 12 and 13.) The uncertainty in the MSU tropospheric temperature change for the 20-year interval 1979–1998 is probably at least 0.1°C; indeed, an alternative

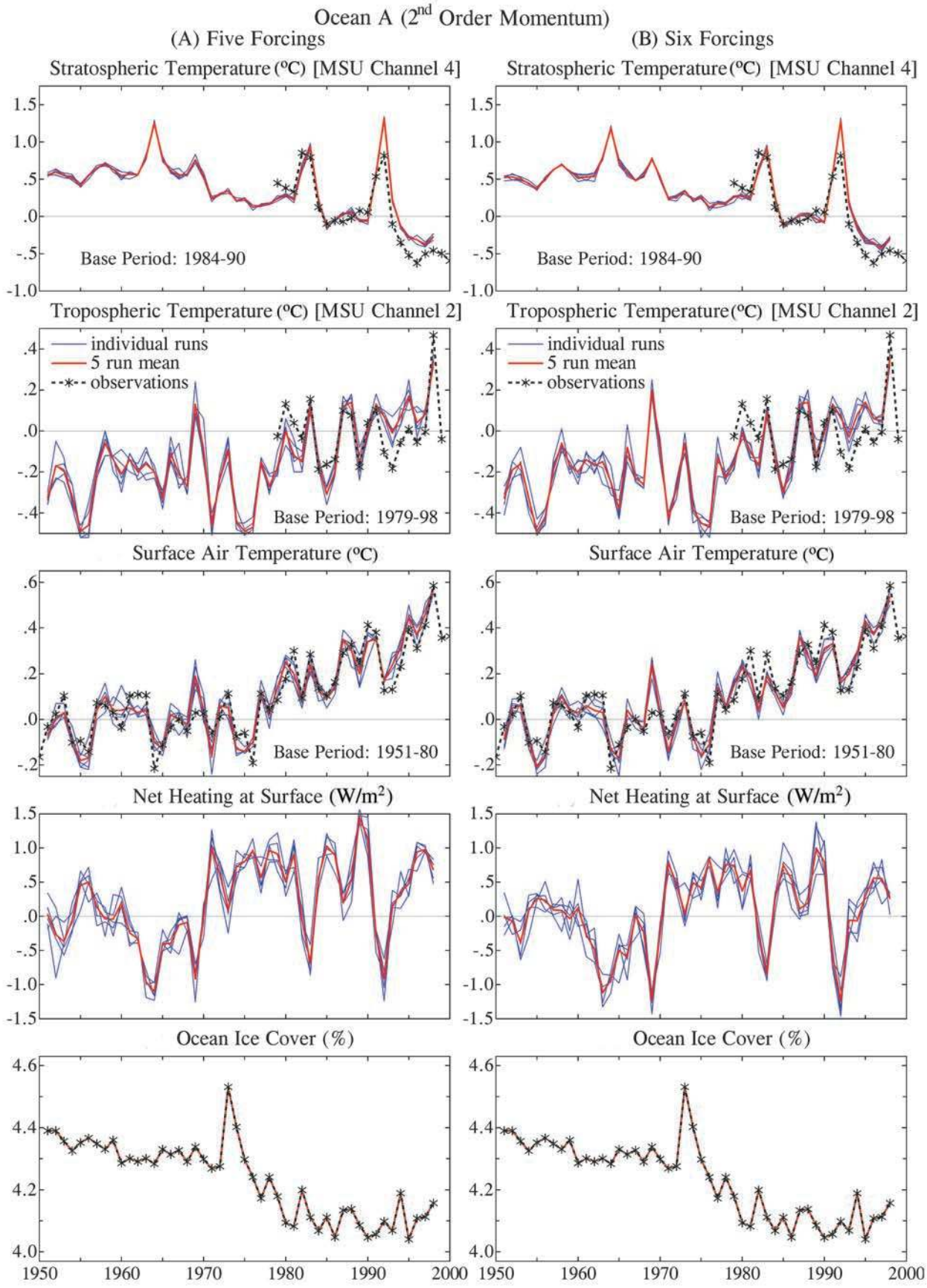

Figure 12. Transient response of SI2000 model with observed SST to (a) five forcings and (b) six forcings.

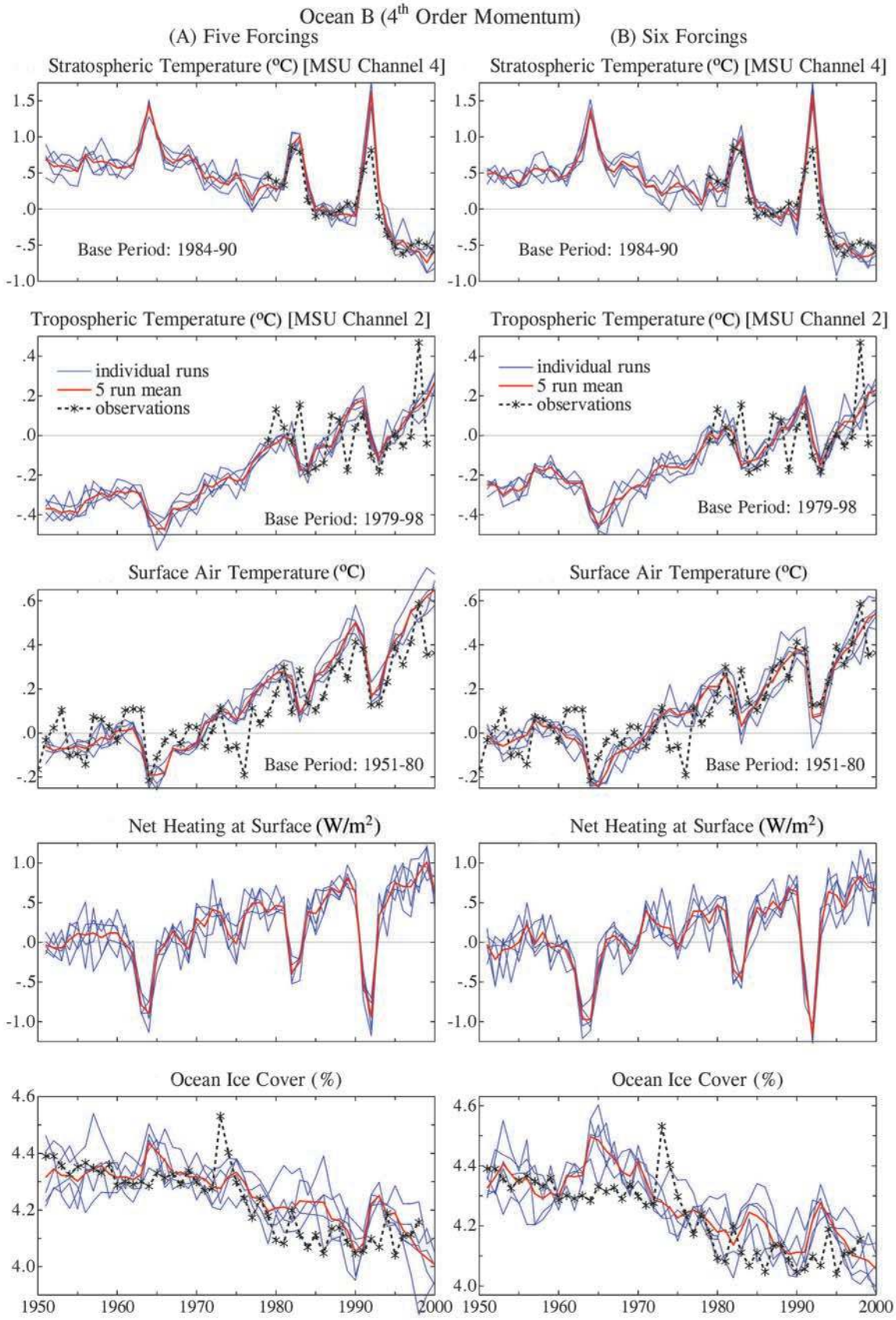

Figure 13. Transient response of SI2000 model with *Q*-flux ocean to (a) five forcings and (b) six forcings.

Table 5. Observed and Simulated Global Temperature Change at Several Levels Based on Linear Trends

Atmospheric Levels	Observations MSU/GISS[a]	Radiosondes	Ocean A (Second-Order)		Ocean B (Second-Order) Six Forcings	Ocean B (Fourth-Order)	
			Five Forcings	Six Forcings		Five Forcings	Six forcings
		HadRT2.0/2.1					
MSU channel 4							
1951–1998			−0.77	−0.74	−0.76	−0.94	−0.80
1958–1998		−1.58/−1.31	−0.83	−0.83	−0.82	−1.03	−0.94
1979–1998	−0.98	−1.46/−1.16	−0.57	−0.62	−0.72	−0.88	−0.93
MSU channel 2							
1951–1998			0.39	0.39	0.37	0.53	0.39
1958–1998		0.38/0.33	0.34	0.34	0.36	0.52	0.40
1979–1998	0.08	0.00/−0.09	0.32	0.31	0.07	0.18	0.11
MSU channel 2LT							
1951–1998			0.52	0.51	0.50	0.70	0.52
1958–1998		0.51/0.46	0.49	0.48	0.52	0.70	0.56
1979–1998	0.14	0.07/−0.02	0.42	0.41	0.20	0.32	0.25
Surface							
1951–1998	0.43		0.47	0.44	0.46	0.62	0.45
1958–1998	0.45		0.45	0.43	0.47	0.62	0.48
1979–1998	0.29		0.32	0.31	0.18	0.29	0.20

[a] Microwave Sounding Unit data for channels 4 (stratosphere), 2 (troposphere), and 2LT (lower troposphere). GISS surface analysis uses SST data of *Reynolds and Smith* [1994] over the ocean.

analysis by *Wentz et al.* [2001] suggests that the warming is 0.1°C/decade greater than reported by *Christy et al.* [1998]. We examine the height dependence of the temperature trends in more detail and discuss the differences between ocean A and ocean B in section 5.3. Note in Table 5 that the model results with six forcings agree well with the observed warming over the longer period, i.e., from the 1950s to the present.

[120] The surface temperature change, the third row in Figures 12 and 13, is in reasonable agreement with the observations. This is an expected result with ocean A, but it is a more meaningful test of the forcings with ocean B. The observed surface warming over the period 1951–1998 is about 0.4°C based on the linear trend. Ocean B yields a warming of about 0.6°C for five forcings and about 0.45°C for six forcings. Thus six forcings, i.e., the inclusion of aerosols, yields better agreement than five forcings. This conclusion becomes more solid on the basis of observations of ocean heat storage (section 5.2).

[121] The net heating at the Earth's surface is given in the fourth row of Figures 12 and 13. The units are W/m^2 averaged over the Earth's entire surface. Because heat storage in the atmosphere and land is small, the rate of heat storage through the ocean surface is obtained by multiplying our number by 1/0.7. The ocean A model, with fixed SST, would not be expected to be in precise energy balance with space in 1951, unlike the ocean B model, in which the SST of the control run is allowed to adjust until equilibrium (energy balance) is achieved. We evaluated the initial ocean A imbalance by running the model for 20 years with 1949–1953 mean SSTs, obtaining a global mean flux −0.18 W/m^2. We thus adjusted the zero point of the net heating by this amount. By 1999 both the ocean A and ocean B models are soaking up heat at a rate between +0.5 and +1.0 W/m^2. We integrate this time series of the net heat at the ocean surface over time and compare the result with observed ocean heat storage in section 5.2.

[122] Ocean ice cover is specified in the ocean A model, based on HadISST1 (Rayner et al., manuscript in preparation, 2002). Ocean ice cover decreases in the ocean B simulations. Although the magnitude of the simulated sea ice decrease is consistent with observations, the simulated decrease is primarily in the Southern Hemisphere while the observed decrease is mainly in the Northern Hemisphere. Realistic results for the spatial distribution of sea ice change are likely to require realistic representation of both ocean surface circulation and the full ocean dynamics and conceivably even a realistic stratosphere because of its influence on the Arctic Oscillation. We note also that it is possible that Southern Hemisphere sea ice has actually decreased since 1950, as some researchers have suggested [*de la Mare*, 1997]. The "homogenization" process included in the construction of the HadISST1 (Rayner et al., manuscript in preparation, 2002) data set removed a substantial (and probably unrealistically large) long-term trend that existed in prior versions of the data set, but there is considerable uncertainty in this adjustment process.

5.1.2. Period 2000–2050

[123] Simulations for ocean B were extended to 2050 for two greenhouse gas scenarios: CO_2 increasing at 1%/year (yielding a forcing of 2.95 W/m^2 in 50 years) and the "alternative" scenario for greenhouse gases illustrated in Figure 1 (yielding a forcing of 1.1 W/m^2 by 2050). The 1% CO_2 scenario had no other forcings for the sake of simplicity and to allow ready comparison with other climate models. The alternative scenario included stratospheric aerosols with the same sequence of optical depth in 2001–2050 as in 1951–2000.

[124] The rate of stratospheric cooling declines markedly after 2000 in the alternative scenario (Figure 14a). In fact, if anticipated recovery of stratospheric ozone is included, stratospheric temperature would tend to level out as the effects of increasing CO_2 and increasing O_3 approximately offset each other.

[125] Global warming over 2001–2050 is about 1.5°C and 0.75°C in the 1% CO_2 and alternative scenarios (Figure 14b). The response is only twice as large in the 1% CO_2 scenario as in the alternative scenario, despite the forcing being almost 3 times as large, because of the disequilibrium of about 0.75 W/m^2 in 2000. This planetary energy imbalance is the portion of the forcing to which the atmosphere has not yet responded; that is, this portion of the forcing has not yet

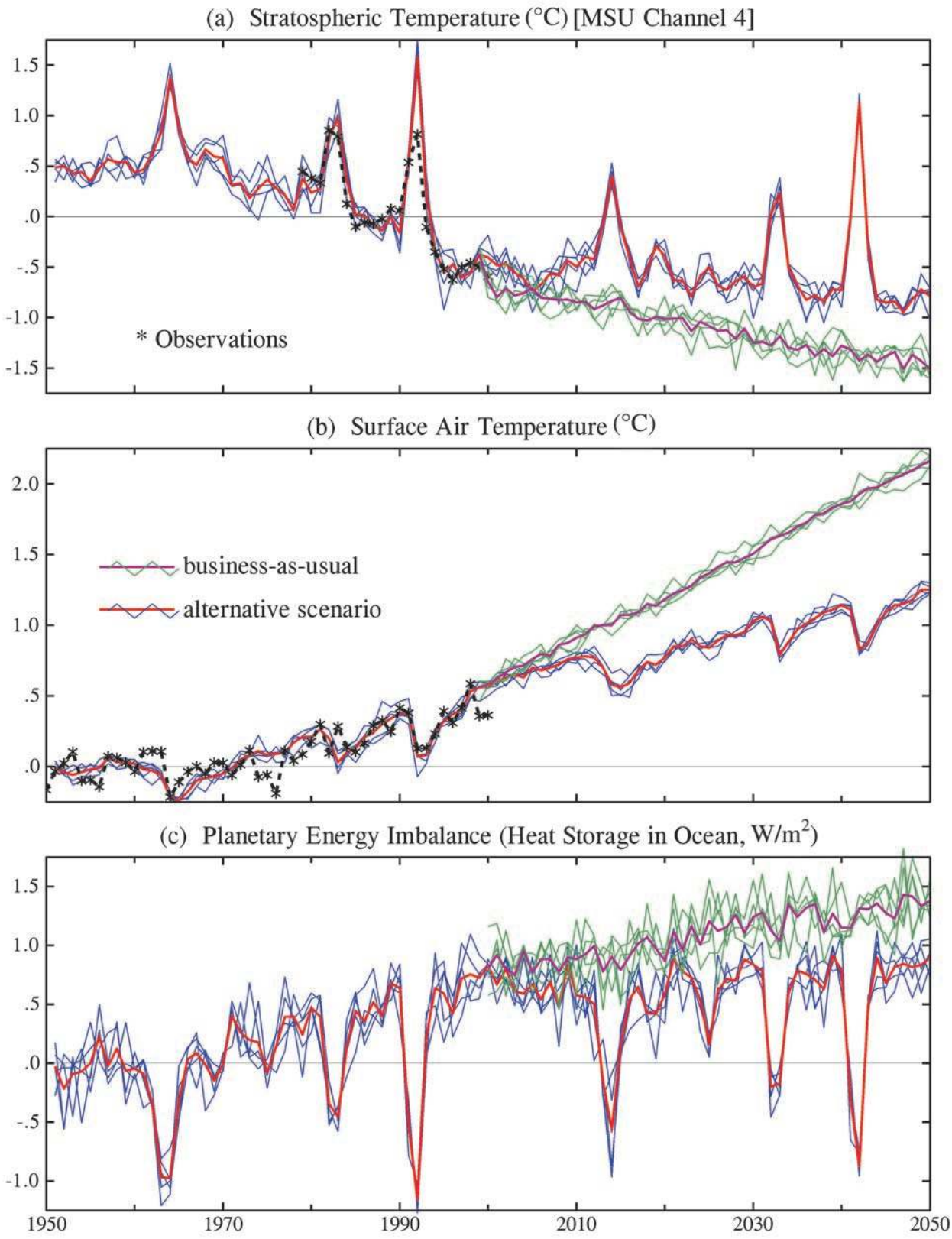

Figure 14. (a) Stratospheric temperature, (b) surface temperature, and (c) heat flux into the Earth's surface for SI2000 model with six forcings. "Business-as-usual" and "alternative" scenarios have added forcings of 2.9 and 1.07 W/m^2 in 2001–2050.

impacted the temperature. Thus the relevant forcing in the 1% CO_2 case is 2.95 + 0.75 = 3.7 W/m^2, while it is 1.1 + 0.75 = 1.85 W/m^2 in the alternative scenario.

[126] The planetary energy imbalance approximately doubles to 1.5 W/m^2 in the 1% CO_2 scenario. On the other hand, the imbalance is rather flat in the alternative scenario, perhaps increasing by 0.1–0.2 W/m^2. Thus the unrealized warming, i.e., the amount of warming "in the pipeline," hardly increases in the alternative scenario. In other words, if climate sensitivity is $\frac{3}{4}$°C per W/m^2, the 1% CO_2 scenario not only yields a warming of 1.5°C in the next 50 years, but it also leaves more than another 1°C warming in the pipeline. The alternative scenario produces a warming of about $\frac{3}{4}$°C and leaves about 0.5°C warming in the pipeline.

[127] These results depend not only on the climate forcing scenario but also on climate sensitivity. Our results are obtained from a model with sensitivity 3°C for doubled CO_2 ($\frac{3}{4}$°C per W/m^2). *Wetherald et al.* [2001] estimate that the present unrealized warming is 1°C, rather than $\frac{3}{4}$°C, at least in part because their model has a higher climate sensitivity (about 4.5°C for doubled CO_2). The measured rate of heat storage in the ocean should eventually help distinguish among models. However, unique interpretation will require quantitative information on climate forcings as well as accurate long-term data for heat storage.

5.2. Ocean Heat Storage

[128] A climate forcing, by definition, causes a planetary energy imbalance. An extended planetary energy imbalance must show up as a change of ocean heat content, because of the negligible heat conductivity of the continents and the small heat capacity of other heat reservoirs such as the atmosphere. We inferred previously [F-C] that the Earth had attained a positive rate of heat storage of 0.5–1 W/m^2 by the middle 1990s, and we argued that the best confirmation of this planetary disequilibrium would be measurements of ocean temperature adequate to define heat storage. Recent analysis of global ocean data [*Levitus et al.*, 2000] permits comparison of observations with the transient energy imbalance in climate scenarios. Model results for ocean B refer only to the upper 1000 m of the ocean, as the *Q*-flux model in our present simulations only extended to that depth.

[129] Figure 15a shows the observed heat content in the upper 500 m (top graph) and the upper 3000 m (middle and bottom graphs) of the ocean. The heat content is defined as anomalies relative to the mean for the period having both model results and observational data (1951–1994 in Figure 15a (top and middle graphs) and 1979–1994 in Figure 15a (bottom graph)). As done by F-C, we use the units W year/m^2 averaged over the entire Earth to allow ready comparison with global climate forcings (1 W year/m^2 = 1.61 × 10^{22} Joules). Note that the *Levitus et al.* [2000] data set has annual data through 1998 for the upper 500 m of the ocean. Because of sparse observations at greater depths, only a 5-year mean (through 1994) is provided for 500–3000 m, and no data are provided for greater depths. Thus in Figure 15a (middle) the heat content for years 1995–1998 includes annual heat gain at 0–500 m, but heat content at 500–3000 m is fixed at the mean value for 1992–1996.

[130] It is possible that the observed heat storage in the *Levitus et al.* [2000] analysis is an underestimate of the true value. In cases where no observations were available the procedure was to assign climatological values. Also no analysis is incorporated below 3000 m, where in at least some locations significant anomalies do occur [*Bindoff and Church*, 1992]. However, the vertical profile of the global ocean temperature trend (Figure 15b) suggests that the ocean beneath 3000 m would not contribute much to the full ocean value.

[131] The depth profile of ocean temperature change in Figure 15b is based on the linear trend for two alternative periods, which differ in their beginning date (1951 or 1955). The year 1951 corresponds to the beginning date of our climate model runs. However, the ocean heat content record since 1955 is considered to be more reliable because of a substantial expansion of the data sources that occurred in conjunction with global observing programs initiated in the mid 1950s.

[132] We discuss here possible relations between climate forcings and changes in the ocean heat content. We order the discussion according to timescale, from the brief perturbations (volcanoes) to the trend for the full period.

5.2.1. Volcanoes

[133] We mark in Figure 15a, with the symbol V + 2, the dates (2 years after large volcanoes) at which minima in the ocean heat content would be expected to occur because of large volcanic eruptions. By the third year after the eruption the aerosol forcing is small and tends to be overshadowed by trends in other forcings such as greenhouse gases. The observed ocean heat content shows evidence of cooling after all three large eruptions (Agung, El Chichon, and Pinatubo) since 1950, although the date of the minimum differs from that predicted by −1 year for El Chichon and +1 year for Pinatubo. It is unlikely that there are other short-term competing climate forcings comparable in magnitude to the volcanic aerosol forcings, so the discrepancies in timing are probably an indication of the level of "dynamic" variability of ocean heat uptake and/or the level of measurement uncertainty. By dynamic variability we refer to internal climate system mechanisms rather than global radiative forcings; these could involve, for example, fluctuations in heat transport by the ocean or atmospheric fluctuations including changes of cloud cover. The dynamic variability and measurement uncertainty issues may be related; for example, we have not subsampled the model with the time-varying coverage of the Levitus data, which may account for some of the higher frequency variability in the observations.

[134] The magnitude of the observed negative heat storage anomalies after the volcanoes is reasonably similar to the expected values. The climate simulations for both ocean A and ocean B yield decreases of 1–2 W years/m^2 in ocean heat content (ocean heat content is calculated in ocean A by integrating over time the heat flux at the ocean surface; see section 5.1.1). We discussed in section 4.1, in connection with Table 4, reasons that the ocean heat loss is less than would be estimated from instantaneous or even adjusted stratospheric aerosol forcing. In addition, the ocean heat uptake after a volcano is the net effect of the (negative) volcanic aerosol forcing and the (positive) portion of the greenhouse gas forcing that the climate system has not yet responded to. This disequilibrium greenhouse gas forcing was rather large by the time of the Pinatubo eruption.

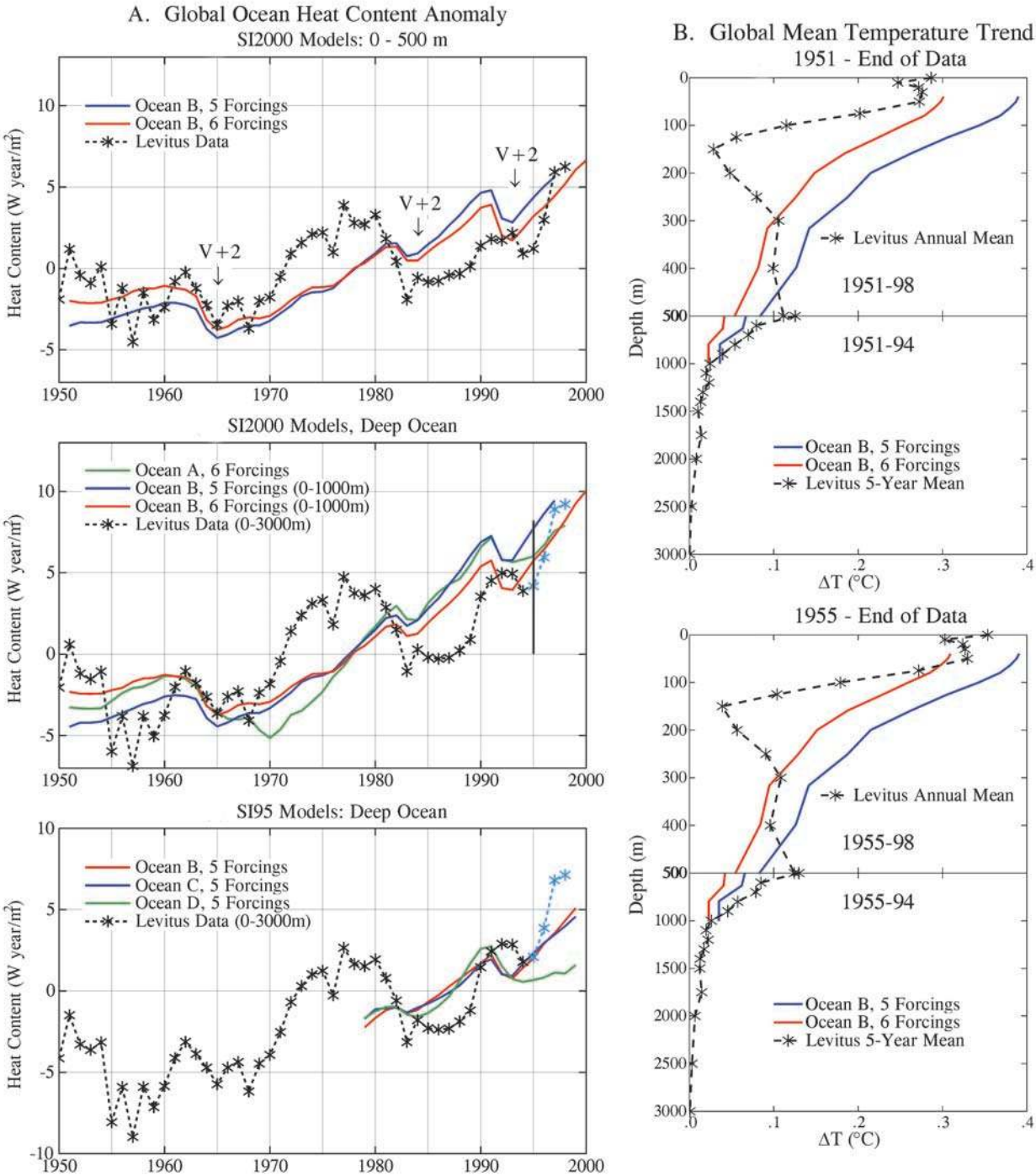

Figure 15. (a) Ocean heat content anomaly in units of W year/m^2 averaged over the entire surface of the Earth (1 W year/m^2 = 1.61 × 10^{22} Joules). The anomalies are relative to the common periods of data and simulations: 1951–1994 in top and middle graphs and 1979–1994 in bottom graph. Observed data are annual at 0–500 m (top graph), and the combination of this with 5-year mean data for depths 500–3000 m is shown (middle and bottom graphs). The combined data are repeated in the bottom graph to allow comparison with the SI95 simulations of F-C, which employed the *Q*-flux ocean model (ocean B) as well as two dynamic ocean models. The *Q*-flux model extends only to a depth of 1000 m. (b) Ocean temperature change versus depth based on the linear trend. Observations are annual and extend through 1998 in the upper 500 m. Below 500 m the data are 5-year mean and extend through 1994, which is the reason for the discontinuity in the model results. Note the scale change that occurs at 500 m. The full period is shown in the top graph, and the period of more reliable data, since 1955, is shown in the bottom graph.

(The planetary radiation imbalance probably was small at the time of El Chichon because of the 1976–1981 jump of global temperature, regardless of the (presumably dynamical, in part) cause of that jump.) Our prior modeling (Plate 5 of F-C, which included two dynamical ocean models) and our current results for oceans A and B (Figures 12 and 13) together suggest that the planetary radiative imbalance at the time of the Pinatubo eruption was 0.75 ± 0.25 W/m^2. This imbalance would reduce the 2-year (negative) heat storage after Pinatubo by 1–2 W year/m^2. Indeed, the fact that the ocean did not cool as much after Pinatubo as would have been expected if it were the only forcing, we suggest, could be because of an existing positive planetary energy imbalance at the time of the Pinatubo eruption.

[135] Verification of the negative planetary radiation imbalance that occurred after Pinatubo is provided by Earth Radiation Budget Experiment (ERBE) satellite measurements [*Minnis et al.*, 1993] as illustrated in Figure 12 of *Hansen et al.* [1996]. The ERBE data yield a radiation balance anomaly of -2.1 W year/m^2 in the two years after Pinatubo. The magnitude of our simulated ocean heat content anomaly (Figure 15) is reasonably consistent with, but somewhat larger than, the ERBE measured imbalance. The ERBE imbalance shifts back to positive in 1993, consistent with the climate model, but not with the observed ocean heat storage minimum in 1994. Finally, we note that both the ocean heat content anomaly and the ERBE data are inconsistent with a Pinatubo peak forcing as large as the -5 W/m^2 suggested by *Andronova et al.* [1999].

5.2.2. Decadal variations

[136] The observed ocean heat content (Figure 15a) has significant decadal variability. The warming from 1968 to 1977 and the cooling from 1977 to 1983, for example, are much larger than the year-to-year variability or the estimated uncertainty in observed year-to-year and decade-to-decade changes of heat content [*Levitus et al.*, 2000].

[137] These heat content changes do not appear to be caused by climate forcings. The simulations with a diffusive ocean model employing all of the known forcings, with and without the uncertain tropospheric aerosols, cannot produce the sharp increase of heat content in the early 1970s or a realistic representation of the cooling in the early 1980s. It is difficult to concoct a plausible underestimated forcing that might account for the observed variation. For example, if one suggested that solar cycle effects were underestimated by neglect of an indirect forcing (such as a forced cloud cover change), one would be faced with the contradiction that the time of minimum heat content in the mid 1980s and maximum heat content in the mid 1970s both occurred at the same phase of the solar cycle.

[138] It is more likely that the fluctuations are dynamical. However, they do not come about simply as a consequence of changing SST patterns that then alter fluxes to the atmosphere. This is shown by the simulation with ocean A (green line in Figure 10a (middle graph)), which used observed (HadISST1) SSTs for the period 1951–1999. On the basis of the energy fluxes at the ocean surface in this run the ocean heat storage is similar to that for the *Q*-flux ocean model. The failure of observed SSTs to produce the observed change of ocean heat content is not surprising. As discussed in section 3.4 in cases such as the North Atlantic Oscillation, specified SST calculations do not capture correctly the heat exchange between ocean and atmosphere associated with vertical motions in the ocean, and indeed that model (ocean A) can yield the wrong sign for the heat flux anomaly [*Bretherton and Battisti*, 2000]. That might also happen at low latitudes. For example, the west Indian Ocean warmed substantially over the past half century. It is possible that in reality the ocean warming in that region was associated with increased heat flux into the ocean surface; however, in ocean A the increasingly positive SST anomalies in that region yield an increased heat flux out of the ocean.

[139] Exploration of the decadal variations in ocean heat content will require use of dynamical ocean models, which are outside the scope of our present paper. We note that in previous simulations [F-C] with dynamical ocean models for the period beginning in 1979 (see Figure 15a (bottom)), one model had a variation in heat content in the 1990s that was unrelated to the climate forcings. However, that fluctuation was associated with unrealistic deep water formation in the North Pacific Ocean. Recent coupled model simulations by two different groups [*Levitus et al.*, 2001; *Barnett et al.*, 2001] do not capture the specific observed decadal variations, but *Barnett et al.* [2001] note that their model does produce decadal fluctuations of the magnitude and timescale of those observed.

5.2.3. Long-Term change

[140] The change in the ocean heat content over the past half century is in good agreement with the climate model driven by known climate forcings. The dominant forcing and the cause of the long-term increase in ocean heat content is the GHG forcing, as shown by Figure 2. The positive ocean heat storage, because it is so directly connected to the planetary energy balance, is probably the best confirmation of the sign of the net climate forcing that has been operating on the planet during the past half century.

[141] Observed temporal change of ocean heat content also has the potential to yield a good, perhaps the best, quantitative measure of the net global climate forcing. However, the rate of heat uptake by the ocean depends upon climate sensitivity and ocean mixing, as well as upon the net climate forcing [*Hansen et al.*, 1984, 1985]. If it were accepted that the mixing in ocean models is reasonably realistic, at least as it affects the global penetration of heat anomalies, and if it were accepted that climate sensitivity is about 3°C for doubled CO_2, then the observed ocean heat storage provides an indication that the net climate forcing is positive and of approximately the magnitude that we have assumed. In particular, under these assumptions, we find, as illustrated in Figure 15, that better agreement is obtained with a net climate forcing that includes the climate forcing by aerosols (six forcings) rather than the case without this negative aerosol forcing.

[142] Alternatively, if we knew the net global climate forcing, the rate of heat storage would provide an empirical measure of climate sensitivity. It is only if climate sensitivity is high that there is substantial "unrealized warming" due to the slow increase of greenhouse gases as the dominant climate forcing. Indeed, the recent positive trend of ocean heat storage and the fact that the ocean heat content dropped only slightly after Pinatubo are consistent with high climate sensitivity. However, there is such a large uncertainty in the indirect aerosol forcing that the ocean heat

storage does not provide a very helpful measure of climate sensitivity. Furthermore, all of these inferences are limited by poorly quantified but substantial uncertainty in the observed ocean heat storage, which potentially could be measured with high accuracy.

[143] *Barnett et al.* [2001] and *Levitus et al.* [2001] previously reported global climate model results for ocean heat storage, which they found to be reasonably consistent with the *Levitus et al.* [2000] data. *Barnett et al.* [2001] used the National Center for Atmospheric Research (NCAR) Parallel Climate Model (PCM) [*Dai et al.*, 2001], which has a sensitivity of 2.1°C for doubled CO_2, and forcing by greenhouse gases and sulfate aerosols, with a net forcing of 2 W/m^2 in 2000 relative to 1850. *Levitus et al.* [2001] used the Geophysical Fluid Dynamics Laboratory (GFDL) model [*Delworth et al.*, 2001], which has a of sensitivity 3.7°C for doubled CO_2, and a forcing similar to that of *Barnett et al.* [2001]. *Barnett et al.* [2001] found an ocean heat storage of 12×10^{22} J in the period 1955–1995, while *Levitus et al.* [2001] obtained 33×10^{22} J. The observed heat storage [*Levitus et al.*, 2000] is about 18×10^{22} J (this is reduced to $13–14 \times 10^{22}$ J if the data are first averaged over decades; *Barnett et al.* [2001] only report their model result after such averaging). When *Levitus et al.* [2001] added solar and volcanic aerosol forcings, the heat storage was reduced to 20×10^{22} J. The reduction in heat storage probably was due mainly to the volcanic aerosols. Their solar forcing was +0.18 W/m^2 over the interval 1865–2000. Their volcanic aerosol forcing averaged −0.54 W/m^2 over 1960–1999; it is based on the data of *Andronova et al.* [1999] and is thus larger than that which we employ, as discussed in section 2.2. The dependence of the simulated heat storage on the model sensitivity and the climate forcing in these studies is consistent with the discussion above. Their results are also consistent with the heat storage in our model over the same interval, which was 18×10^{22} J for five forcings and 14×10^{22} J for six forcings; our results refer just to the upper 1000 m of the ocean, because our present *Q*-flux ocean extended only to that depth.

5.3. Atmospheric Temperature Profile

[144] Climate forcings have a strong effect on the atmospheric temperature profile, as illustrated explicitly in Figure 6 of F-C and by *Ramaswamy et al.* [2001]. We do not attempt a comprehensive study here, which would require more realistic representations of the stratosphere and ocean as well as better information on the vertical profile of absorbing aerosols. However, our present simulations cover a longer period than those of F-C. This allows us to compare modeled and observed temperature profiles for both the era of satellite data and the longer period with radiosonde data.

[145] The satellite era begins in 1979 with the first MSU data, for which we use version d of *Christy et al.* [2000]. Radiosonde coverage was extensive by 1958, the International Geophysical Year, although the coverage is only considered to be reasonably global after 1964 [*IPCC*, 2001]. We use radiosonde data analysis of *Parker et al.* [1997]. The two radiosonde data sets, HadRT2.0 and HadRT2.1, differ in that the latter has been adjusted with the help of MSU data (version c) in an attempt to correct for bad radiosonde records. We illustrate both data sets, thus providing one indication of data uncertainty.

[146] We present two views of the temperature profile. Figure 16 compares line graphs of observed and modeled temperature profiles for the global mean and for northern latitudes, low latitudes, and southern latitudes. We define low latitudes as 40N-40S, which is the latitude range at which the tropopause extends to about the 100 hPa level. Figure 17, the zonal mean temperature change versus latitude, provides a more pictorial view of the nature of the zonal temperature change.

[147] Qualitatively, there is reasonable agreement between the simulated and observed temperature changes, particularly for the longer time period. However, Figure 16 reveals that the model warms more than observed in the upper troposphere, and the model cools less than observed in the stratosphere. The discrepancies occur primarily in the latter period, 1979–1998, the period with more complete observations of climate forcings. Agreement is best at southern latitudes. The simulated upper tropospheric warming is especially excessive at low latitudes. Simulated stratospheric cooling is too little at northern latitudes and low latitudes. The discrepancies are significant based on the standard deviation among the ensemble members, as illustrated at three pressure levels in Figure 16.

[148] Among the climate forcings, ozone, stratospheric water vapor, and aerosols probably are the best candidates for contributing to the discrepancies in simulated temperature profiles. Ozone should be considered first because it changed dramatically during 1979–1998, yet it was poorly measured in the lower stratosphere and troposphere. Indeed, much closer agreement with the observed change in temperature profile would have been obtained if we had employed the ozone change that was used by F-C. The ozone change of F-C had large ozone depletion near the 100 hPa level at all latitudes, including the tropics, based on the then available analysis of SAGE observations. The SPARC ozone trend assessment [*WMO*, 1998] excluded SAGE data below the 20-km level because of its uncertainties, but they did not replace it with any other estimate. As a result our current estimate for ozone change, as discussed in section 2.4, has a maximum ozone depletion rate near the tropical tropopause of only about 2% per decade. However, recent analyses of SAGE II data for October 1984 to April 2000 (J. Zawodny, private communication, 2000) yield an ozone depletion of more than 5% per decade with maximum depletion near 20 km altitude. This is less depletion than assumed by F-C, but it is substantial. Furthermore, the SAGE II period of data, beginning in late 1984, misses the period of rapid depletion of column-integrated ozone that occurred in 1980–1985 (Figure 6). Although column-integrated ozone amount does not show much depletion at low latitudes (Figure 6), this could be a result of increases in tropospheric ozone as suggested in the recent SAGE II analyses of J. Zawodny (private communication, 2000). Therefore it seems possible that the ozone depletion rate in the tropopause region for the full period 1979–1998 was larger than that in our current scenario. As shown in Figure 6 of F-C, ozone depletion near the tropopause could cause significant cooling in the upper troposphere and lower stratosphere.

[149] Stratospheric water vapor probably contributes to the discrepancy between the observed and modeled temperature profile change. The positive trend of stratospheric water vapor in the model is less than the observed trend, as

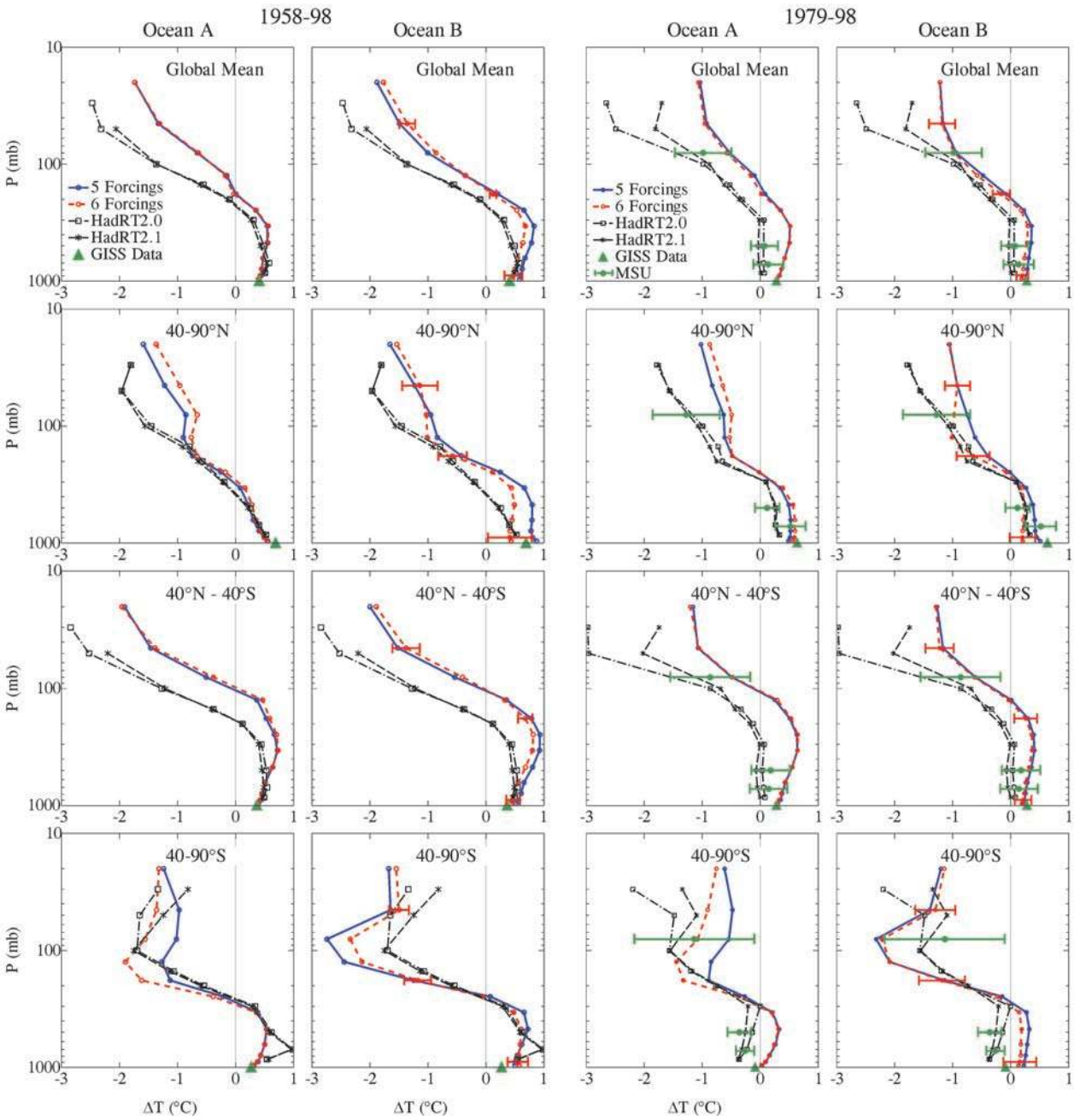

Figure 16. Change of annual-mean temperature profile for 1958–1998 and 1979–1998 based on linear trends. Model results are for oceans A and B, with five and six forcings. Surface observations are the land-ocean data of *Hansen et al.* [1999], with SSTs of *Reynolds and Smith* [1994] for ocean areas. The bars on the MSU satellite data [*Christy et al.*, 2000] are twice the standard statistical error adjusted for autocorrelation [*Santer et al.*, 2000]. Radiosonde profiles become unreliable above about the 100-hPa level. Twice the ensemble standard deviation is shown at three pressure levels for ocean B with six forcings.

discussed in section 2.5. Water vapor change at the rate reported by *Rosenlof et al.* [2001] would increase stratospheric cooling slightly, of the order of 0.1°C in 20 years [*Oinas et al.*, 2001]. However, this can account for only a small fraction of the discrepancy.

[150] Tropospheric aerosols cool the surface but have only modest impact on the temperature profile in our present simulations. However, suspected inaccuracies in the aerosol vertical distribution and temporal change may cause the upper troposphere to warm relative to the near surface layers in the simulations. As discussed in section 2.6, the black carbon aerosols are mixed too high in the troposphere compared with limited available observations, with the amount of black carbon in the upper troposphere

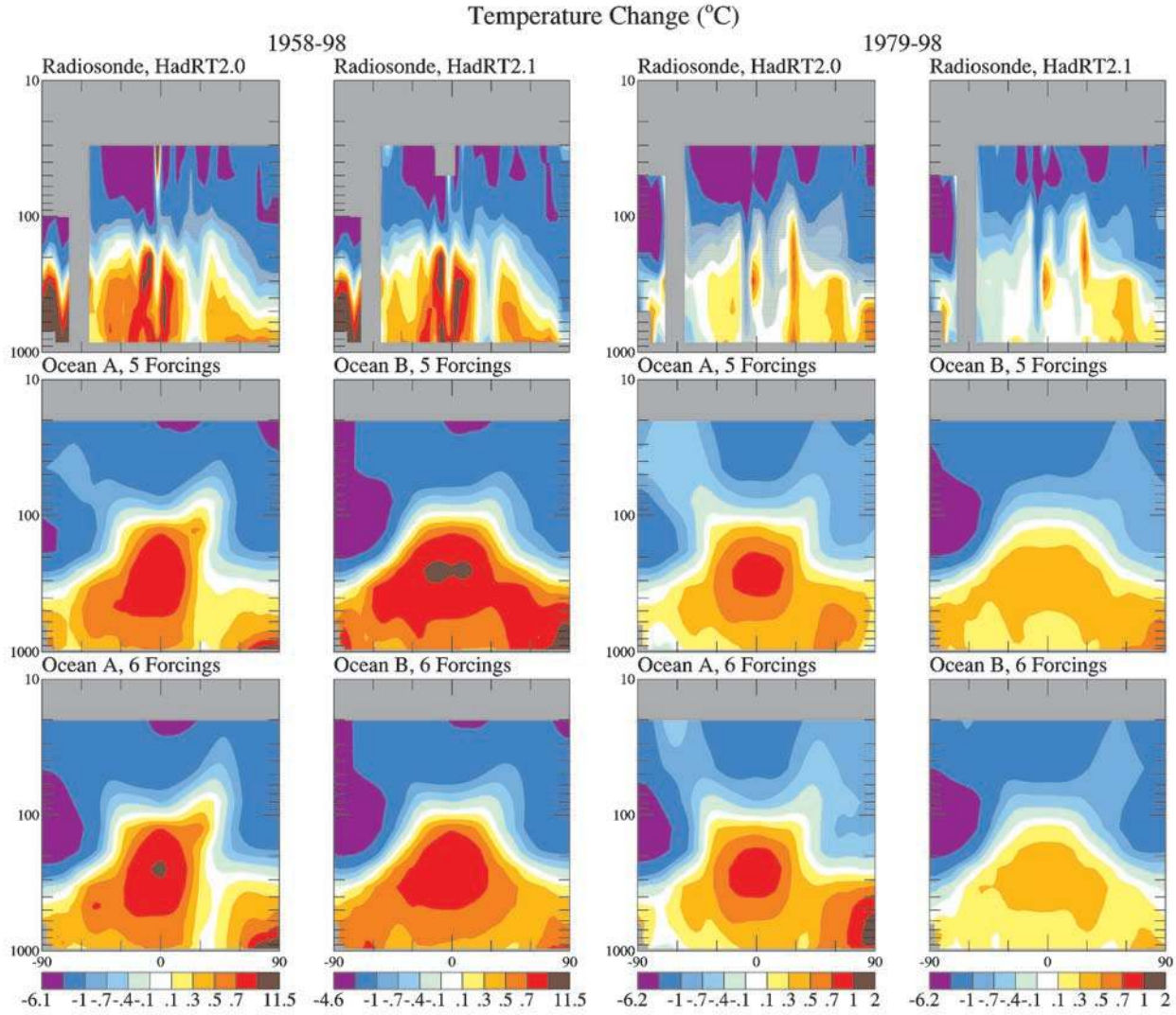

Figure 17. Change of zonal-mean annual-mean temperature for 1958–1998 and 1979–1998 based on linear trends. Radiosonde data in the top row are for versions 2.0 and 2.1 of the HadRT analysis [*Parker et al.*, 1997]. Model results are for oceans A and B, with five and six forcings. Note that ocean A with five forcings employs the ozone $O_3{}^A$ data set, while the others use $O_3{}^B$ (the latter has greater ozone depletion in the South Pole region).

perhaps as much as a factor of 10 too large. The temporal issue arises because black carbon (and sulfates and organic carbon) aerosols are taken as proportional to fossil fuel use. However, T. Novakov (private communication, 2001) argues that the proportion of black carbon aerosols has decreased in recent decades in developed countries because of a decrease in inefficient coal burning in domestic and commercial sectors as well as improved efficiency of diesel engines, at least in the United States. Thus it is plausible that more realistic vertical and temporal distributions of black carbon would cause less warming of the troposphere relative to the surface. Quantitative analysis requires better knowledge of aerosol distributions and their temporal change. This topic is discussed further in section 6.

[151] In the period 1979–1998 the discrepancy between model and observations is primarily at low latitudes, and it is larger in ocean A than ocean B. This is most apparent in Figure 17, as the bulls-eye warming in the tropical upper troposphere. Excessive warming at this level did not occur in our previous simulations [F-C], because of greater ozone depletion near the tropopause, as discussed above. Ocean B has slightly less warming at the surface than ocean A at low latitudes during 1979–1998, and this difference increases in the middle to upper troposphere in the way temperature anomalies are observed to change with height in the tropics [*Hurrell and Trenberth*, 1998; *Wentz and Schabel*, 2000; *Santer et al.*, 2001]. As shown in Table 5, the discrepancy between MSU lower tropospheric temperature change and the ocean B model results for six forcings is small, although the discrepancy is substantial for ocean A. The discrepancy with radiosonde temperature change for 1979–1998 is larger (Figure 17 and Table 5), but the radiosondes suffer from poor spatial sampling and temporal discontinuities [*Gaffen et al.*, 2000], suggesting that in this case MSU may provide the

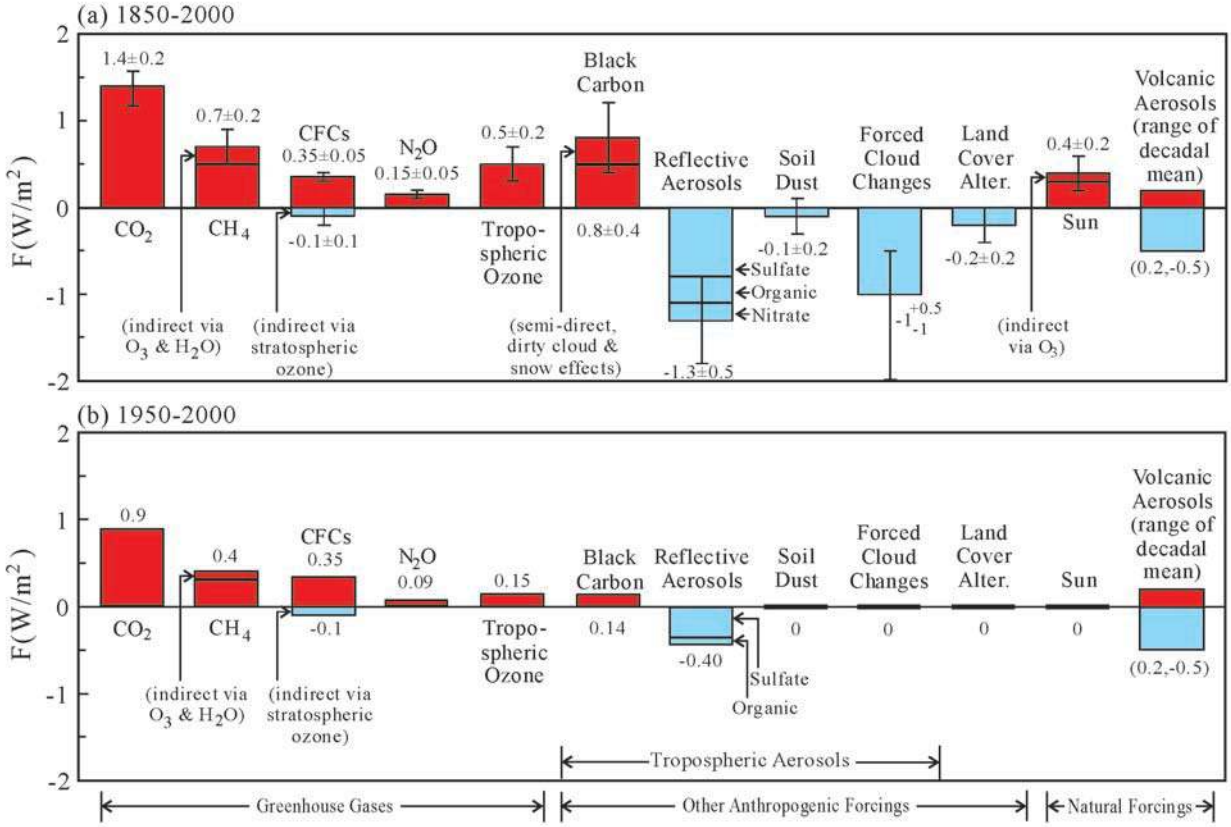

Figure 18. (a) Climate forcings estimated for 1850–2000 [*Hansen and Sato*, 2001] and (b) forcings for 1951–2000 included in present simulations.

more reliable result. However, there are also significant sources of potential error in the MSU temperature trends [*Santer et al.*, 1999; *Hurrell et al.*, 2000; *Wentz et al.*, 2001].

[152] There are several possible interpretations of these results. Perhaps there is an error in the observed trend of low latitude SSTs, as only a small error (about 0.2°C over 2 decades) in the SST is required to explain the tropospheric temperature change. Such an error would be consistent with the smaller warming of tropical nighttime marine air temperature (NMAT) found by *Christy et al.* [2001] for the period after 1979; that is, it would remove the difference between the NMAT and SST trends. Alternatively, the observed SST temperature trends may be accurate, and the difference between the NMAT and SST trends may be real, but the heat flux anomalies from the ocean to the troposphere may be inaccurately simulated. Given a positive SST anomaly, the model faithfully delivers a larger anomaly to the midtroposphere, but the model could be flawed in its simulated dynamical or thermodynamical energy fluxes or in the forcings that influence those fluxes.

[153] There are also real differences between the model and radiosonde observations for the longer period 1958–1998 at the tropical and northern latitudes, and on the global average, as summarized in Figure 16. We believe that these discrepancies are meaningful and probably related, at least in part, to inaccurate or incomplete representations of the three climate forcings' ozone, water vapor, and aerosols, as discussed above. Ozone depletion near the tropopause is probably understated in our scenario. We know that the measured stratospheric water vapor increase was larger than in our model. Suspected flaws in the BC aerosol scenario are in the sense to partially account for the discrepancies.

6. Discussion

6.1. Climate Forcings

[154] We have defined six radiative forcings, nominally from first principles, for the period 1951–2000. These forcings, when inserted in a climate model having sensitivity 3°C for doubled CO_2 and an ocean mixing rate for heat based on empirical data from ocean tracers, yield remarkably good agreement with observed global mean surface temperature change over that period. It may seem tempting to take this close agreement as evidence that these forcings accurately reflect the true forcings that influenced climate during this period. We suggest, however, that the close agreement could be, to a substantial degree, fortuitous, with omissions and errors in some forcings countering errors of the opposite sign in other forcings. Nevertheless, we argue that the net forcing has sufficient significance that, together with observed ocean heat storage, we can draw some conclusions about the present state of planetary energy imbalance, as discussed in section 6.2.

[155] We discuss the forcings with the aid of Figure 18. Figure 18a is the estimate of *Hansen and Sato* [2001] for the

change of climate forcings between 1850 and 2000. The greenhouse gas forcings are known with reasonably good accuracy. CO_2 (1.4 W/m^2) has the largest forcing, but the CH_4 forcing is half as large when its indirect effects on stratospheric H_2O and tropospheric O_3 are included, and the sum of non-CO_2 greenhouse gas forcings exceeds the CO_2 forcing. Recent studies [*Mickley et al.*, 2001; D. T. Shindell, private communication, 2001] suggest that the tropospheric O_3 forcing may be as large as 0.7–0.8 W/m^2. We take 0.1 W/m^2 of the O_3 forcing as an indirect effect of CH_4 for a total O_3 forcing of 0.6 W/m^2, with a large uncertainty.

[156] Aerosol forcings are still more uncertain. *Adams et al.* [2001] suggest that the sulfate forcing is −0.95 W/m^2 when the swelling of sulfate aerosols at high humidities is fully accounted for, and they suggest that the forcing due to anthropogenic nitrate aerosols is about −0.2 W/m^2. IPCC has a smaller estimate for sulfates and does not consider nitrates. We estimate the sum of the sulfate and nitrate forcings as −1 ± 0.25 W/m^2. Forcing by black carbon is estimated by *IPCC* [1996] as +0.1 W/m^2 and by *IPCC* [2001] as +0.25 W/m^2, but *Jacobson* [2000a, 2000b] estimates the black carbon forcing at about 0.5 W/m^2, and *Hansen et al.* [2000b] suggest that the total black carbon forcing might be closer to +1 W/m^2 when indirect effects are included. It should be noted, however, that the surface thermal response to forcing by absorbing aerosols is a strong function of the vertical distribution of the aerosols [RF-CR]. The greatest uncertainty, however, is the indirect effects of aerosols on clouds. We estimate these forced cloud changes to cause a forcing of the order of −1 W/m^2 with an uncertainty of at least a factor of two.

[157] Figure 18b is the change of forcings between 1951 and 2000 that were used for the simulations in this paper. The net increase in the forcing over this half century was about 1.6 W/m^2. Perhaps this net forcing, fortuitously, is reasonably realistic even though the assumed scenario probably underestimates several negative forcings, with the omission of forced cloud changes, nitrates, biomass burning, soil dust, and land cover alterations. These omissions could be at least partially compensated by underestimates of the tropospheric O_3 and black carbon forcings. Also, the vertical distribution of black carbon that we employed, being weighted too much toward high altitudes, probably reduced the efficacy of that positive forcing. There may also have been a positive initial disequilibrium forcing in 1951, perhaps as much as 0.1 to 0.2 W/m^2, representing the unrealized warming due to the history of forcings in the period 1850–1950. Figures 15 and 16 suggest that a slightly smaller net forcing for 1951–2000 would have yielded closer agreement with observed temperature change.

[158] This unsatisfactory knowledge of the true forcings could be improved in years to come. Measurements of current aerosol distributions, their relation to sources, and their influence on clouds may permit an improved understanding that can be used with chemical transport models to construct improved histories of many of these forcings. Success in this endeavor would require global satellite monitoring of aerosol and cloud particle microphysical properties, global surface monitoring stations, field campaigns, aerosol and cloud modeling, directed laboratory measurements, and the integration of information from all of these into global chemical transport and climate models.

6.2. Heat Storage: Planetary Disequilibrium

[159] The good fit that we obtain between simulated and observed atmospheric and surface temperature changes and the consistency with measured ocean heat storage suggest that the observed climate change in the past 50 years is primarily a response to the radiative forcings. However, it would be possible to obtain a comparably good fit to the observed temperatures with a larger (smaller) positive trend of the net forcing by employing a model with smaller (larger) climate sensitivity. Even the limited range for climate sensitivity that we infer from paleoclimate data, 3 ± 1°C for doubled CO_2, allows a substantial range of forcings. We are examining this topic further using versions of the *Q*-flux model with sensitivities 2°C and 4°C for doubled CO_2. More realistic ocean circulation models will also be needed for a full investigation.

[160] Using our present reconstruction of climate forcings for 1951–2000, and assuming that climate sensitivity is near 3°C for doubled CO_2, leads to a planetary disequilibrium in 2000, with the planet soaking up energy at a rate of about ¾ W/m^2. The same assumptions imply additional future global warming of about ½°C, even without any additional forcing. The amount of warming "in the pipeline," however, is a function of climate sensitivity, and, in principle, it could vary by almost a factor of two in either direction for the range of climate sensitivities from 2 to 4°C for doubled CO_2 [*Hansen et al.*, 1985]. The fact that the model with sensitivity 3°C for doubled CO_2 yields ocean heat storage comparable to observations tends to favor that sensitivity, but the examples given in section 5 illustrate that there is some latitude in the forcings and climate models that yield reasonable agreement with observed ocean heat storage. However, if the trend of ocean heat storage is established more accurately with a longer record, and if the forcings are defined more precisely, it should be possible to narrow the uncertainty in the unrealized warming.

6.3. Temperature Profile

[161] The simulated global-mean surface temperature change is in good agreement with observations. However, there seem to be significant discrepancies between the modeled and observed changes in the temperature profile. There are uncertainties in the observed temperature profile change, and we have not sampled the model at radiosonde locations, but these factors cannot fully account for the discrepancies. Model inadequacies, especially in our current representations of the stratosphere and ocean, may be partly responsible. However, we suggest that the discrepancies between the observed and modeled profiles are due at least partly to inaccuracies in the histories of some of the forcings, specifically, BC aerosols, O_3, and stratospheric H_2O.

[162] Perhaps the most important observational need is for composition-specific aerosol monitoring. The vertical profile of absorbing aerosols is especially important, but measurements are needed for all aerosols that can influence cloud cover and cloud properties. Troposphere O_3 needs to be monitored, especially near the tropopause level, where even small changes have a noticeable impact on the temperature profile. Stratospheric H_2O is in part a modeling problem that can probably be solved with higher vertical resolution, but continued monitoring of stratospheric H_2O is also important.

6.4. Strategy for Further Experiments

[163] Our strategy of investigation, described in section 2 of F-C, tries to balance the need for systematic experiments using fixed models and well-defined forcings with the need to improve the realism of both the climate model and the forcings that drive it. We want a structured set of simulations to allow comparisons but without inhibiting alternative ideas and initiative. We need to optimize use of limited human and computer resources.

[164] The simulations of F-C, carried out on desktop IBM RISC 6000 workstations, were 17-year runs. The present simulations, carried out on a Silicon Graphics 2000 system, focus on the past 50-year period and include additional forcings and models. Some of the experiments now being carried out for 1951 to present (see Table 3) are using a version of the model reprogrammed, documented, and optimized for parallel computations but nominally with the same physics as in SI2000. The aim is to find a practical path leading to a prompt new round of experiments for a longer period, 1850–2000, including improvements in the realism of both forcings and models.

[165] **Acknowledgments.** We thank Ian Plumb for providing model results on methane production of water vapor, David Randel for stratospheric ozone change data, Urs Baltensperger for aerosol data prior to publication, David Rind for comparative studies of water vapor in his middle atmosphere model, Tony Broccoli for comparative data from the GFDL model, Joe Zawodny for SAGE ozone data, Mark Chandler, Ralph Cicerone, Jos Lelieveld, Michael Oppenheimer, and Jonathan Overpeck for discussions, and two anonymous referees for helpful reviews. This research was supported by the NASA Earth Science Research Division.

References

Ackerman, A. S., O. B. Toon, D. E. Stevens, A. J. Heymsfield, V. Ramanathan, and E. J. Welton, Reduction of tropical cloudiness by soot, *Science*, *288*, 1042–1047, 2000.

Adams, P. J., J. H. Seinfeld, D. Koch, L. Mickley, and D. Jacob, General circulation model assessment of direct radiative forcing by the sulfate-nitrate-ammonium-water inorganic aerosol system, *J. Geophys. Res.*, *106*, 1097–1111, 2001.

Albrecht, B. A., Aerosols, cloud microphysics, and fractional cloudiness, *Science*, *245*, 1227–1230, 1989.

Andreae, M. O., Climatic effects of changing atmospheric aerosol levels, in *World Survey of Climatology*, vol. 16, in *Future Climates of the World*, edited by A. Henderson-Sellers, pp. 341–392, Elsevier Sci., New York, 1995.

Andronova, N. G., E. V. Rozanov, F. Yang, M. E. Schlesinger, and G. L. Stenchikov, Radiative forcing by volcanic aerosols from 1850 to 1994, *J. Geophys. Res.*, *104*, 16,807–16,826, 1999.

Barnett, T. P., D. W. Pierce, and R. Schnur, Detection of anthropogenic climate change in the world's oceans, *Science*, *292*, 270–274, 2001.

Bengtsson, L., E. Roeckner, and M. Stendel, Why is the global warming proceeding much slower than expected?, *J. Geophys. Res.*, *104*, 3865–3876, 1999.

Bindoff, N. L., and J. A. Church, Warming of the water column in the southwest Pacific Ocean, *Nature*, *357*, 59–62, 1992.

Bleck, R., Ocean modeling in isopycnic coordinates, in *Ocean Modeling and Parameterization*, edited by E. P. Chassignet and J. Verron, pp. 423–448, Kluwer Acad., Norwell, Mass., 1998.

Boyle, J. S., Evaluation of the annual cycle of precipitation over the United States in GCMs: AMIP simulations, *J. Clim.*, *11*, 1041–1055, 1998.

Bretherton, C. S., and D. S. Battisti, An interpretation of the results from atmospheric general circulation models forced by the time history of the observed sea surface temperature distribution, *Geophys. Res. Lett.*, *27*, 767–770, 2000.

Cairns, B., A. A. Lacis, and B. E. Carlson, Absorption within inhomogeneous clouds and its parameterization within general circulation models, *J. Atmos. Sci.*, *57*, 700–714, 2000.

Cess, R. D., et al., Uncertainties in carbon dioxide radiative forcing in atmospheric general circulation models, *Science*, *262*, 1252–1255, 1993.

Cess, R. D., et al., Comparison of the seasonal change in cloud-radiative forcing from atmospheric general circulation models and satellite observations, *J. Geophys. Res.*, *101*, 12,791–12,794, 1996.

Christy, J. R., R. W. Spencer, and E. Lobl, Analysis of the merging procedure for the MSU daily temperature time series, *J. Clim.*, *11*, 2016–2041, 1998.

Christy, J. R., R. W. Spencer, and W. D. Braswell, MSU tropospheric temperatures: Data set construction and radiosonde comparisons, *J. Atmos. Oceanic Technol.*, *17*, 1153–1170, 2000.

Climate Monitoring and Diagnostics Laboratory (CMDL), Summary report number 24, 1996–1997, edited by D. J. Hoffman, J. T. Peterson, and R. M. Rosson, report, 166 pp., Environ. Res. Lab., Natl. Oceanic and Atmos. Admin., Boulder, Colo., 1998.

Cooke, W. F., and J. N. Wilson, A global black carbon aerosol model, *J. Geophys. Res.*, *101*, 19,395–19,409, 1996.

Cooke, W. F., C. Liousse, H. Cachier, and J. Feichter, Construction of a $1^\circ \times 1^\circ$ fossil fuel emission data set for carbonaceous aerosol and implementation and radiative impact in the ECHAM4 model, *J. Geophys. Res.*, *104*, 22,137–22,162, 1999.

Dai, A., T. M. L. Wigley, B. A. Boville, J. T. Kiehl, and L. E. Buja, Climates of the twentieth and twenty-first centuries simulated by the NCAR climate system model, *J. Clim.*, *14*, 485–519, 2001.

De Forster, P.-M., and K. P. Shine, Stratospheric water vapor changes as a possible contributor to observed stratospheric cooling, *Geophys. Res. Lett.*, *26*, 3309–3312, 1999.

de la Mare, W. K., Abrupt mid-twentieth-century decline in Antarctic sea-ice extent from whaling records, *Nature*, *389*, 57–60, 1997.

Del Genio, A. D., and A. B. Wolf, The temperature dependence of the liquid water path of low clouds in the southern Great Plains, *J. Clim.*, *13*, 3465–3486, 2000.

Del Genio, A. D., and M. S. Yao, Efficient cumulus parameterization for long-term climate studies: The GISS scheme, in *Cumulus Parameterization, AMS Meteorol. Monogr.*, vol. 46, edited by K. Emanuel and D. Raymond, pp. 181–184, Am. Meteorol. Soc., Boston, Mass., 1993.

Del Genio, A. D., M. S. Yao, W. Kovari, and K. W. Lo, A prognostic cloud water parameterization for global climate models, *J. Clim.*, *9*, 270–304, 1996.

Delworth, T. L., R. J. Stouffer, K. W. Dixon, M. J. Spelman, T. R. Knutson, A. J. Broccoli, P. J. Kushnir, and R. T. Wetherald, Simulation of climate variability and change by the GFDL R30 coupled climate model, *Clim.*, in press, 2001.

Eddy, J., The Maunder minimum, *Science*, *192*, 1189–1202, 1976.

Etheridge, D. M., L. P. Steele, R. L. Langenfields, R. J. Francey, J. M. Barnola, and V. I. Morgan, Natural and anthropogenic changes in atmospheric CO_2 over the last 1000 years from air in Antarctic ice and firn, *J. Geophys. Res.*, *101*, 4115–4128, 1996.

Etheridge, D. M., L. P. Steele, R. J. Francey, and R. L. Langenfelds, Atmospheric methane between 1000 AD and present: Evidence of anthropogenic emissions and climatic variability, *J. Geophys. Res.*, *103*, 15,979–15,993, 1998.

Free, M., and A. Robock, Global warming in the context of the Little Ice Age, *J. Geophys. Res.*, *104*, 19,057–19,070, 1999.

Fuller, K. A., W. C. Malm, and S. M. Kreidenweis, Effects of mixing on extinction by carbonaceous particles, *J. Geophys. Res.*, *104*, 15,941–15,954, 1999.

Gaffen, D. J., M. A. Sargent, R. E. Habermann, and J. R. Lazante, Sensitivity of tropospheric and stratospheric temperature trends to radiosonde data quality, *J. Clim.*, *13*, 1776–1796, 2000.

Goode, P. R., J. Qiu, V. Yurchyshyn, J. Hickey, M. C. Chu, E. Kolbe, C. T. Brown, and S. E. Koonin, Earthshine observations of the Earth's reflectance, *Geophys. Res. Lett.*, *28*, 1671–1674, 2001.

Govindasamy, B., P. B. Duffy, and K. Caldeira, Land use changes and Northern Hemisphere cooling, *Geophys. Res. Lett.*, *28*, 291–294, 2001.

Haigh, J. D., The role of stratospheric ozone in modulating the solar radiative forcing of climate, *Nature*, *370*, 544–546, 1994.

Haigh, J. D., Modelling the impact of solar variability on climate, *J. Atmos. Sol. Terr. Phys.*, *61*, 63–72, 1999.

Hall, T. M., and D. W. Waugh, Stratospheric residence time and its relationship to mean age, *J. Geophys. Res.*, *105*, 6773–6782, 2000.

Hansen, J. E., A brighter future, *Clim. Change*, *52*, 435–440, 2002.

Hansen, J. E., and M. Sato, Trends of measured climate forcing agents, *Proc. Natl. Acad. Sci. U.S.A.*, *98*, 14,778–14,783, 2001.

Hansen, J. E., and L. D. Travis, Light scattering in planetary atmospheres, *Space Sci. Rev.*, *16*, 527–610, 1974.

Hansen, J., G. Russell, D. Rind, P. Stone, A. Lacis, S. Lebedeff, R. Ruedy, and L. Travis, Efficient three-dimensional global models for climate studies: Models I and II, *Mon. Weather Rev.*, *111*, 609–662, 1983.

Hansen, J., A. Lacis, D. Rind, G. Russell, P. Stone, I. Fung, R. Ruedy, and J. Lerner, Climate sensitivity: Analysis of feedback mechanisms, in *Climate Processes and Climate Sensitivity, Geophys. Monogr. Ser.*, vol. 29,

edited by J. E. Hansen and T. Takahashi, pp. 130–163, AGU, Washington, D.C., 1984.
Hansen, J., G. Russell, A. Lacis, I. Fung, D. Rind, and P. Stone, Climate response times: Dependence on climate sensitivity and ocean mixing, *Science*, *229*, 857–859, 1985.
Hansen, J., A. Lacis, R. Ruedy, M. Sato, and H. Wilson, How sensitive is the world's climate?, *Natl. Geogr. Res. Explor.*, *9*, 142–158, 1993.
Hansen, J., et al., A Pinatubo climate modeling investigation, in *Global Environment Change*, edited by G. Fiocco, D. Fua', and G. Visconti, *NATO ASI Ser., Ser. 1*, *42*, 233–272, 1996.
Hansen, J., R. Ruedy, A. Lacis, G. Russell, M. Sato, J. Lerner, and D. Rind, Wonderland climate model, *J. Geophys. Res.*, *102*, 6823–6830, 1997a.
Hansen, J., M. Sato, A. Lacis, and R. Ruedy, The missing climate forcing, *Philos. Trans. R. Soc. London, Ser. B*, *352*, 231–240, 1997b.
Hansen, J., M. Sato, and R. Ruedy, Radiative forcing and climate response, *J. Geophys. Res.*, *102*, 6831–6864, 1997c.
Hansen, J., et al., Forcings and chaos in interannual to decadal climate change, *J. Geophys. Res.*, *102*, 25,679–25,720, 1997d.
Hansen, J. E., M. Sato, A. Lacis, R. Ruedy, I. Tegen, and E. Matthews, Climate forcings in the Industrial Era, *Proc. Natl. Acad. Sci. U.S.A.*, *95*, 12,753–12,758, 1998.
Hansen, J., R. Ruedy, J. Glascoe, and M. Sato, GISS analysis of surface temperature change, *J. Geophys. Res.*, *104*, 30,997–31,022, 1999.
Hansen, J., R. Ruedy, A. Lacis, M. Sato, L. Nazarenko, N. Tausnev, I. Tegen, and D. Koch, Climate modeling in the global warming debate, in *General Circulation Modeling: Past, Present and Future*, edited by D. Randall, Academic, San Diego, Calif., 2000a.
Hansen, J. E., M. Sato, R. Ruedy, A. Lacis, and V. Oinas, Global warming in the twenty-first century: An alternative scenario, *Proc. Natl. Acad. Sci. U. S. A.*, *97*, 9875–9880, 2000b.
Harvey, L. D. D., *Global Warming: The Hard Science*, 336 pp., Prentice-Hall, Old Tappan, N. J., 2000.
Haywood, J., and O. Boucher, Estimates of the direct and indirect radiative forcing due to tropospheric aerosols: A review, *Rev. Geophys.*, *38*, 513–543, 2000.
Haywood, J. M., and K. P. Shine, The effect of anthropogenic sulfate and soot aerosol on the clear sky planetary radiation budget, *Geophys. Res. Lett.*, *22*, 603–606, 1995.
Haywood, J. M., V. Ramaswamy, and B. J. Soden, Tropospheric aerosol forcing in clear-sky satellite observations over the oceans, *Science*, *283*, 1299–1303, 1999.
Held, I. M., and B. J. Soden, Water vapor feedback and global warming, *Annu. Rev. Energy Environ.*, *25*, 441–475, 2000.
Henderson-Sellers, A., and V. Gornitz, Possible climatic impacts of land cover transformations, with particular emphasis on tropical deforestation, *Clim. Change*, *6*, 231–257, 1984.
Highwood, E. J., and K. P. Shine, Radiative forcing and global warming potentials of 11 halogenated compounds, *J. Quant. Spectrosc. Radiat. Transfer*, *66*, 169–183, 2000.
Hoffert, M. I., and C. Covey, Deriving global climate sensitivity from paleoclimate reconstructions, *Nature*, *360*, 573–576, 1992.
Hollandsworth, S. M., R. D. McPeters, L. E. Flynn, W. Planet, A. J. Miller, and S. Chandra, Ozone trends deduced from combined Nimbus 7 SBUV and NOAA 11 SBUV/2 data, *Geophys. Res. Lett.*, *22*, 905–908, 1995.
Hurrell, J. W., and K. E. Trenberth, Difficulties in obtaining reliable temperature trends: Reconciling the surface and Microwave Sounding Unit records, *J. Clim.*, *11*, 945–967, 1998.
Hurrell, J. W., S. J. Brown, K. E. Trenberth, and J. R. Christy, Comparison of tropospheric temperatures from radiosondes and satellites: 1979–1998, *Bull. Am. Meteorol. Soc.*, *81*, 2165–2178, 2000.
Intergovernmental Panel on Climate Change (IPCC), *Climate Change 1992*, edited by J. T. Houghton, B. A. Callander, and S. K. Varney, Cambridge Univ. Press, New York, 1992.
Intergovernmental Panel on Climate Change (IPCC), *Climate Change 1995*, edited by J. T. Houghton et al., Cambridge Univ. Press, New York, 1996.
Intergovernmental Panel on Climate Change (IPCC), *Climate Change 2001*, edited by J. T. Houghton et al., Cambridge Univ. Press, New York, 2001.
Jacobson, M. Z., A physically based treatment of elemental carbon optics: Implications for global direct forcing of aerosols, *Geophys. Res. Lett.*, *27*, 217–220, 2000.
Jacobson, M. Z., Global direct radiative forcing due to multicomponent anthropogenic and natural aerosols, *J. Geophys. Res.*, *106*, 1551–1568, 2001a.
Jacobson, M. Z., Strong radiative heating due to the mixing state of black carbon in atmospheric aerosols, *Nature*, *409*, 695–697, 2001b.
Kaplan, A., Y. Kushnir, M. Cane, and M. Blumenthal, Reduced space optimum analysis for historical data sets: 136 years of Atlantic sea surface temperatures, *J. Geophys. Res.*, *102*, 27,835–27,860, 1997.
Kaplan, A., M. A. Cane, Y. Kushnir, A. C. Clement, M. B. Blumenthal, and B. Rajagopalan, Analyses of global sea surface temperature 1856–1991, *J. Geophys. Res.*, *103*, 18,567–18,589, 1998.
Koch, D., Transport and direct radiative forcing of carbonaceous and sulfate aerosols in the GISS GCM, *J. Geophys. Res.*, *106*, 20,311–20,332, 2001.
Koch, D., D. Jacob, I. Tegen, D. Rind, and M. Chin, Tropospheric sulfur simulation and sulfate direct radiative forcing in the Goddard Institute for Space Studies general circulation model, *J. Geophys. Res.*, *104*, 23,799–23,822, 1999.
Lacis, A. A., and V. Oinas, A description of the correlated k-distribution method for modeling nongray gaseous absorption, thermal emission, and multiple scattering in vertically inhomogeneous atmospheres, *J. Geophys. Res.*, *96*, 9027–9063, 1991.
Lacis, A., J. Hansen, and M. Sato, Climate forcing by stratospheric aerosols, *Geophys. Res. Lett.*, *19*, 1607–1610, 1992.
Lacis, A. A., B. E. Carlson, and J. E. Hansen, Retrieval of atmospheric N_2O, O_3, aerosol optical depth, effective radius and variance information from SAGE II multi-spectral extinction measurements, *Appl. Math. Comput.*, *116*, 133–151, 2000.
Lamb, H. H., Volcanic dust in the atmosphere, *Philos. Trans. R. Soc. London, Ser. A*, *266*, 425–533, 1970.
Lambert, A., R. G. Grainger, J. J. Remedios, C. D. Rodgers, M. Corney, and F. W. Taylor, Measurements of the evolution of the Mt. Pinatubo aerosol cloud by ISAMS, *Geophys. Res. Lett.*, *20*, 1287–1290, 1993.
Lau, K. M., J. H. Kim, and Y. Sud, Intercomparison of hydrologic processes in AMIP GCMs, *Bull. Am. Meteorol. Soc.*, *77*, 2209–2227, 1996.
Lean, J., J. Beer, and R. Bradley, Reconstruction of solar irradiance since 1610: Implications for climate change, *Geophys. Res. Lett.*, *22*, 3195–3198, 1995.
Lean, J. L., G. J. Rottman, H. L. Kyle, T. N. Woods, J. R. Hickey, and L. C. Puga, Detection and parameterization of variations in solar mid- and near-ultraviolet radiation (200–400 nm), *J. Geophys. Res.*, *102*, 29,939–29,956, 1997.
Lefohn, A. S., J. D. Husar, and R. B. Husar, Estimating historical anthropogenic global sulfur emission patterns for the period 1850–1990, *Atmos. Environ.*, *33*, 3435–3444, 1999.
Levitus, S., J. I. Antonov, T. P. Boyer, and C. Stephens, Warming of the world ocean, *Science*, *287*, 2225–2229, 2000.
Levitus, S., J. I. Antonov, J. Wang, T. L. Delworth, K. W. Dixon, and A. J. Broccoli, Anthropogenic warming of Earth's climate system, *Science*, *292*, 267–270, 2001.
Liousse, C., J. E. Penner, C. Chuang, J. J. Walton, H. Eddleman, and H. Cachier, A global three-dimensional model study of carbonaceous aerosols, *J. Geophys. Res.*, *101*, 19,411–19,432, 1996.
Machida, T. T., T. Nakazawa, Y. Fujii, S. Aoki, and O. Watanabe, Increase in the atmospheric nitrous oxide concentration during the last 250 years, *Geophys. Res. Lett.*, *22*, 2921–2924, 1995.
Manabe, S., and R. T. Wetherald, The effects of doubling the CO_2 concentration on the climate of a general circulation model, *J. Atmos. Sci.*, *32*, 3–15, 1975.
Marenco, A., H. Gouget, P. Nedelec, and J. P. Pages, Evidence of a long-term increase in tropospheric ozone from Pic du Midi data series—Consequences: Positive radiative forcing, *J. Geophys. Res.*, *99*, 16,617–16,632, 1994.
McCormick, M. P., R. E. Viega, and W. P. Chu, Stratospheric ozone profile and total ozone trends derived from the SAGE I and SAGE II data, *Geophys. Res. Lett.*, *19*, 269–272, 1992.
McCormick, M. P., L. W. Thomason, and C. R. Trepte, Atmospheric effects of Mt. Pinatubo eruption, *Nature*, *373*, 399–404, 1995.
Mickley, L. J., D. J. Jacob, and D. Rind, Uncertainty in preindustrial abundance of tropospheric ozone: Implications for radiative forcing calculations, *J. Geophys. Res.*, *106*, 3389–3399, 2001.
Minnis, P., E. F. Harrison, L. L. Stowe, G. G. Gibson, F. M. Denn, D. R. Doelling, and W. L. Smith, Radiative climate forcing by the Mount Pinatubo eruption, *Science*, *259*, 1411–1415, 1993.
Myhre, G., E. J. Highwood, K. P. Shine, and F. Stordal, New estimates of radiative forcings due to well mixed greenhouse gases, *Geophys. Res. Lett.*, *25*, 2715–2718, 1998.
Myhre, G., S. Karlsdottir, I. S. A. Isaksen, and F. Stordal, Radiative forcing due to changes in tropospheric ozone in the period 1980 to 1996, *J. Geophys. Res.*, *105*, 28,935–28,942, 2000.
Myhre, G., A. Myhre, and F. Stordal, Historical evolution of radiative forcing of climate, *Atmos. Environ.*, *35*, 2361–2373, 2001.
Nakajima, T., A. Higurashi, N. Takeuchi, and J. R. Herman, Satellite and ground-based study of optical properties of 1997 Indonesian forest fire aerosols, *Geophys. Res. Lett.*, *26*, 2421–2424, 1999.
Nedoluha, G. E., R. M. Bevilacqua, R. M. Gomez, D. E. Siskind, B. C. Hicks, J. M. Russell, and B. J. Conner, Increases in middle atmospheric water vapor as observed by the Halogen Occultation Experiment and the

ground-based Water Vapor Millimeter-wave Spectrometer from 1991 to 1997, *J. Geophys. Res.*, *103*, 3531–3543, 1998.
Oinas, V., A. A. Lacis, D. Rind, D. T. Shindell, and J. E. Hansen, Radiative cooling by stratospheric water vapor: Big differences in GCM results, *Geophys. Res. Lett.*, *28*, 2791–2794, 2001.
Pacanowski, R. C., and S. W. Griffies, *Modular Ocean Model 3.0 Manual*, Geophys. Fluid Dyn. Lab., Princeton, N. J., 1999.
Parker, D. E., M. Gordon, D. P. N. Cullum, D. M. H. Sexton, C. K. Folland, and N. Rayner, A new global gridded radiosonde temperature database and recent temperature trends, *Geophys. Res. Lett.*, *24*, 1499–1502, 1997.
Penner, J. E., C. C. Chuang, and K. Grant, Climate forcing by carbonaceous and sulfate aerosols, *Clim. Dyn.*, *14*, 839–851, 1998.
Pollack, J. B., O. B. Toon, C. Sagan, A. Summers, W. Van Camp, and B. Baldwin, Stratospheric aerosols and climatic change, *Nature*, *263*, 551–555, 1976.
Prather, M. J., Numerical advection by conservation of second-order moments, *J. Geophys. Res.*, *91*, 6671–6680, 1986.
Quinn, P. K., and D. J. Coffman, Comment on "Contribution of different aerosol species to the global aerosol extinction optical thickness: Estimates of model results" by I. Tegen et al., *J. Geophys. Res.*, *104*, 4241–4248, 1999.
Ramachandran, S., V. Ramaswamy, G. L. Stenchikov, and A. Robock, Radiative impact of the Mount Pinatubo volcanic eruption: Lower stratospheric response, *J. Geophys. Res.*, *105*, 24,409–24,429, 2000.
Ramaswamy, V., et al., Stratospheric temperature trends: Observations and model simulations, *Rev. Geophys.*, *39*, 71–122, 2001.
Randel, W. J., and F. Wu, A stratospheric ozone trends data set for global modeling studies, *Geophys. Res. Lett.*, *26*, 3089–3092, 1999.
Randeniya, L. K., P. F. Vohralik, I. C. Plumb, and K. R. Ryan, Heterogeneous $BrONO_2$ hydrolysis: Effect on NO_2 columns and ozone at high latitudes in summer, *J. Geophys. Res.*, *102*, 23,543–23,557, 1997.
Reynolds, R. W., and T. M. Smith, Improved global sea surface temperature analyses, *J. Clim.*, *7*, 929–948, 1994.
Rind, D., R. Suozzo, N. K. Balachandran, A. Lacis, and G. L. Russell, The GISS global climate/middle atmosphere model, I, Model structure and climatology, *J. Atmos. Sci.*, *45*, 329–370, 1988.
Rosenlof, K. H., et al., Stratospheric water vapor increases over the past half-century, *Geophys. Res. Lett.*, *28*, 1195–1198, 2001.
Rothman, L., et al., The HITRAN molecular spectroscopic database and HAWKS (HITRAN Atmospheric WorKStation): 1996 edition, *J. Quant. Spectrosc. Radiat. Transfer.*, *60*, 665–710, 1998.
Russell, G. L., J. R. Miller, and D. Rind, A coupled atmosphere-ocean model for transient climate change studies, *Atmos. Ocean*, *33*, 683–730, 1995.
Russell, P. B., et al., Global to microscale evolution of the Pinatubo volcanic aerosol derived from diverse measurements and analyses, *J. Geophys. Res.*, *101*, 18,745–18,763, 1996.
Sagan, C., O. B. Toon, and J. B. Pollack, Anthropogenic albedo changes and the Earth's climate, *Science*, *206*, 1363–1368, 1979.
Santer, B. D., J. J. Hnilo, J. S. Boyle, C. Doutriaux, M. Fiorino, D. E. Parker, K. E. Taylor, and T. M. L. Wigley, Uncertainties in observationally based estimates of temperature change in the free atmosphere, *J. Geophys. Res.*, *104*, 6305–6333, 1999.
Santer, B. D., T. M. L. Wigley, J. S. Boyle, D. J. Gaffen, J. J. Hnilo, D. Nychka, D. E. Parker, and K. E. Taylor, Statistical significance of trends and trend differences in layer-average atmospheric temperature time series, *J. Geophys. Res.*, *105*, 7337–7356, 2000.
Santer, B. D., T. M. L. Wigley, C. Doutriaux, J. S. Boyle, J. E. Hansen, P. D. Jones, G. A. Meehl, E. Roeckner, S. Sengupta, and K. E. Taylor, Accounting for the effects of volcanoes and ENSO in comparisons of modeled and observed temperature trends, *J. Geophys. Res.*, *106*, 28,033–28,059, 2001.
Sato, M., J. Hansen, M. P. McCormick, and J. B. Pollack, Stratospheric aerosol optical depths, 1850–1990, *J. Geophys. Res.*, *98*, 22,987–22,994, 1993.
Sexton, D. M. H., The effect of stratospheric ozone depletion on the phase of the Antarctic Oscillation, *Geophys. Res. Lett.*, *28*, 3697–3700, 2001.
Shindell, D. T., Climate and ozone response to increased stratospheric water vapor, *Geophys. Res. Lett.*, *28*, 1551–1554, 2001.
Shindell, D., D. Rind, N. Balachandran, J. Lean, and P. Lonergan, Solar cycle variability, ozone, and climate, *Science*, *284*, 305–308, 1999.
Shindell, D. T., G. A. Schmidt, M. E. Mann, D. Rind, and A. Waple, Solar forcing of regional climate change during the Maunder Minimum, *Science*, *294*, 2149–2152, 2001.
Shine, K. P., and P. M. Forster, The effect of human activity on the radiative forcing of climate change: A review, *Global Planet. Change*, *20*, 205–225, 1999.
Smith, C. A., J. D. Haigh, and R. Toumi, Radiative forcing due to trends in stratospheric water vapor, *Geophys. Res. Lett.*, *28*, 179–182, 2001.
Sokolov, A. P., and P. H. Stone, A flexible climate model for use in integrated assessments, *Clim. Dyn.*, *14*, 291–303, 1998.
Stuber, N., M. Ponater, and R. Sausen, Is the climate sensitivity to ozone perturbations enhanced by stratospheric water vapor feedback?, *Geophys. Res. Lett.*, *28*, 2887–2890, 2001.
Svensmark, H., and E. Friis-Christensen, Variations of cosmic ray flux and global cloud coverage, a missing link in solar-climate relationships, *J. Atmos. Sol. Terr. Phys.*, *59*, 1225–1232, 1997.
Tegen, I., and I. Fung, Contribution to the mineral aerosol load from land surface modification, *J. Geophys. Res.*, *100*, 18,707–18,726, 1995.
Tegen, I., and A. A. Lacis, Modeling of particle size distribution and its influence on the radiative properties of mineral dust aerosol, *J. Geophys. Res.*, *101*, 19,237–19,244, 1996.
Tegen, I., P. Hollrigl, M. Chin, I. Fung, D. Jacob, and J. Penner, Contribution of different aerosol species to the global aerosol extinction optical thickness: Estimates from model results, *J. Geophys. Res.*, *102*, 23,895–23,915, 1997.
Tegen, I., D. Koch, A. A. Lacis, and M. Sato, Trends in tropospheric aerosol loads and corresponding impact on direct radiative forcing between 1950 and 1990: A model study, *J. Geophys. Res.*, *105*, 26,971–26,989, 2000.
Thompson, D. W. J., and J. M. Wallace, The Arctic Oscillation signature in the wintertime geopotential height and temperature fields, *Geophys. Res. Lett.*, *25*, 1297–1300, 1998.
Twomey, S., Pollution and the planetary albedo, *Atmos. Environ.*, *8*, 1251–1256, 1974.
Wallace, J. M., Y. Zhang, and J. A. Renwick, Dynamic contribution to hemispheric and mean temperature trends, *Science*, *270*, 780–783, 1995.
Wang, Y., and D. J. Jacob, Anthropogenic forcing on tropospheric ozone and OH since preindustrial times, *J. Geophys. Res.*, *103*, 31,123–31,135, 1998.
Weare, B. C., et al., Evaluation of total cloudiness and its variability in the atmospheric model intercomparison project, *J. Clim.*, *8*, 2224–2238, 1995.
Wentz, F. J., and M. Schabel, Precise climate monitoring using complementary satellite data sets, *Nature*, *403*, 414–416, 2000.
Wentz, F. J., M. Schabel, C. Mears, and D. Seidel, Lower tropospheric air temperature derived from a blended analysis of MSU, SSM/T1, SSM/I, NCEP/NCAR reanalysis, and Reynolds SST, *RSS Tech. Rep. 062801*, 46 pp., Remote Sens. Syst., Santa Rosa, Calif., 2001.
Wetherald, R. T., and S. Manabe, The effects of changing the solar constant on the climate of a general circulation model, *J. Atmos. Sci.*, *32*, 2044–2059, 1975.
Wetherald, R. T., R. J. Stouffer, and K. W. Dixon, Committed warming and its implications for climate change, *Geophys. Res. Lett.*, *28*, 1535–1538, 2001.
Willson, R. C., and H. S. Hudson, The Sun's luminosity over a complete solar cycle, *Nature*, *351*, 42–44, 1991.
World Meteorological Organization (WMO), Ozone change as a function of altitude, in *SPARC Assessment of Trends in the Vertical Distribution of Ozone*, edited by N. Harris, R. Hudson, and C. Phillips, *WMORep. 43*, pp. 67–87, Global Ozone Res. and Monit. Proj., Geneva, Switzerland, 1998.
World Meteorological Organization (WMO), Ozone variability and trends, in *Scientific Assessment of Ozone Depletion: 1998, WMO Rep. 44*, pp. 4.1–4.55, Global Ozone Res. and Monit. Proj., Geneva, Switzerland, 1999.

J. Antonov and S. Levitus, National Oceanographic Data Center, NOAA, Silver Spring, Maryland 20910, USA. (John.Antonov@noaa.gov; slevitus@nodc.noaa.gov)

L. Bishop, Honeywell International, Buffalo, New York 14210, USA. (lane.bishop@alliedsignal.co)

J. Christy, Earth System Science Center, University of Alabama, Huntsville, Alabama 35899, USA. (christy@atmos.uah.edu)

J. Hansen, T. Hall, D. Koch, A. Lacis, L. Nazarenko, R. Ruedy, M. Sato, and D. Shindell, NASA Goddard Institute for Space Studies, New York, New York 10025, USA. (jhansen@giss.nasa.gov; thall@scrapple.giss.nasa.gov; alacis@giss.nasa.gov; lnazarenko@giss.nasa.gov; dshindell@giss.nasa.gov)

S. Hollandsworth, NASA Goddard Space Flight Center, Greenbelt, Maryland 20771, USA.

D. Jacob and J. Logan, Department of Earth and Planetary Sciences, Harvard University, Cambridge, Massachusetts 01238, USA. (djj@io.harvard.edu)

J. Lean, E. O. Hulbert Center for Space Research, Naval Research Laboratory, Washington, D. C. 20375, USA. (lean@demeter.nrl.navy.mil)

T. Novakov, Lawrence Berkeley National Laboratory, Berkeley, California 94720, USA. (tnovakov@lbl.gov)

D. Parker and N. Rayner, Meteorological Office Hadley Centre for

Climate Prediction and Research, Bracknell, Berkshire RG12 2SY, U.K. (deparker@meto.gov.uk; nrayner@meto.gov.uk)

B. Santer, Lawrence Livermore National Laboratory, Livermore, California 94550, USA. (santer1@llnl.gov)

P. Stone, Center for Meteorology, Massachusetts Institute of Technology, Cambridge, Massachusetts 02139, USA. (phstone@mit.edu)

I. Tegen, Max-Planck-Institute for Biogeochemistry, D-07701, Jena, Germany. (itegen@bgc-jena.mpg.de)

L. Thomason, NASA Langley Research Center, Hampton, Virginia 23681, USA. (l.w.thomason@larc.nasa.gov)

R. Wang, School of Earth and Atmospheric Sciences, Georgia Institute of Technology, Atlanta, Georgia 30332, USA. (raywang@eas.gatech.edu)

Y. Wang, Department of Environmental Sciences, Rutgers University, New Brunswick, New Jersey 08901, USA. (yhw@envsci.rutgers.edu)

R. Willson, Center for Climate Systems Research, Columbia University, New York, New York 10025, USA.